AN EXPERIMENTAL INVESTIGATION
OF
DETACHED SHOCK WAVES

Thesis by

John H. Altseimer

In Partial Fulfillment of the Requirements

For the Degree of

Aeronautical Engineer

California Institute of Technology

Pasadena, California

1948

ACKNOWLEDGMENTS

The guidance and advice throughout the course of this work of Mr. Henry Nagamatsu is gratefully acknowledged. Thanks must also go to Mr. Allen E. Puckett for his assistance and advice on the operational and design problems.

Mr. Bernard W. Marschner and the author worked together to take and reduce the data herein presented.

Summary

Using the Galcit $2\frac{1}{2}$ inch Supersonic Tunnel equipment, surface pressure measurements were taken on cylindrical models with cone-shaped noses. The total included angle of the cones was 75° . The Mach number range covered was from 1.41 to 1.99 which for 75° cones covers most of the range from detached to attached shock waves. Stagnation pressure measurements were also taken by means of blunt cylindrical models.

Schlieren pictures were taken of the 75° cones and blunt models throughout the velocity range. Additional pictures of shock waves of 45°, 60° and 90° cones at some of the velocities used were also obtained. From the Schlieren pictures the traces of the shock waves were obtained and plotted on graph paper. Shock wave angles vs. distance from the model centerlines are also presented as well as the distribution of "M_2", the Mach number directly behind the wave.

Appendix #1 shows "Blocking" data for the $2\frac{1}{2}$ inch Galcit Tunnel.

Hand adjusted flexible nozzle walls were used for most of the work. Satisfactory flow through the tunnel was obtained with these nozzle blocks. However, design improvements are possible and Appendix #2 recapitulates the problems encountered and offers suggestions for future use.

TABLE OF CONTENTS

Page

Introduction

The problems of supersonic flow at or below the speed of attachment to conically shaped bodies have been and are being attacked theoretically. Extensive treatments above the speed of attachment have been made but again mostly from a theoretical approach. To complement the theory it has become apparent that experimental data is necessary for the detached shock wave studies. The data presented here for detached shock waves is the result of an effort to supply basic information needed to close the gap between theory and experiment.

A secondary objective was to determine the feasibility of using a simple flexible nozzle for similar future studies in the Galcit 2½" Supersonic Tunnel. Blocking data for this tunnel was also obtained for all of the Mach numbers used to obtain the pressure data.

Description of Test Facilities

The tunnel used was the Galcit $2\frac{1}{2}$" x 2 9/16" Supersonic Tunnel. Two flexible nozzle blocks were used (Fig. #1 and #2) which are adjustable by means of hand screws. To adjust the blocks to the desired contour, a small surface plate (see Fig. #3) with its length equal to the length of the blocks was set up on the tunnel frame next to the blocks. A sliding dial gage straddled the surface plate, the distance parallel to the tunnel axis being measured by a steel scale attached to the side of the surface plate. The vertical position of the nozzle walls was indicated on the dial gage by means of the overhanging arm as shown in Figure #3. The figure shows the dial gage set up to read the lower nozzle block wall location. To read the position of the upper nozzle block, the dial gage holder is rotated sideways 180° so that the upper saddle rides on the surface plate.

The models used (for pressure model details, see Fig. **5**) were circular in cross section with conically shaped noses. Except for the blocking models, the cylindrical sections were all 0.250 inches in diameter. The total included cone angles were 45°, 60°, 75°, 90° and 180°. Blocking models were 60° cones with cylindrical diameters ranging from 0.250 to 0.812 inches in increments of 0.062 inches. All of the surface pressure measurements were made with 75° cones except stagnation pressures, for which the 180° model was used. It was found that with models of 0.250 inches in diameter, the tunnel could not be operated much below $M = 1.4$ without having the blocking phenomenon take place. Therefore, to produce a shock wave which was detached reasonably far enough from the model, a cone angle as large as 75° was necessary.

One 0.013 inch diameter surface pressure tap hole was used per model. The pressure lines ran back through the base of the models, through the stinger and out to the manometer board. Five different pressure holes were located along the surface of the cones and two were located behind the line of intersection of cylinder and cone (see Fig. #5). Pressure tight joints of model to stinger were obtained simply by a small application of non-hardening "Permatex" cement to the threads. Mercury and acetylene tetrabromide manometers were used to measure pressures.

The standard Schlieren system and photographic equipment built for this tunnel were used. Photographic exposure time was 3×10^{-6} seconds on "Ansco Triple S Pan" film.

It was not possible to operate the tunnel at a relative humidity less than approximately 21%. However, the humidity did not change from that figure appreciably at any time. The difficulty apparently was that the drying material in the tunnel air-dryer was "worn-out".

Testing Procedures

The nozzle expansion shapes were drawn by means of the graphical method described in reference #1. For boundary layer corrections linear divergences of 0.0013 to 0.004 inches/inch were used. Some experimentation was necessary in each case to secure the correct configuration. A Mach number variation in the test section of less than 1% was maintained. See figure #4 for an example of the Mach number variation in the test section. The velocity distribution was obtained by measuring pressures at the two flexible walls and also down the tunnel centerline. Centerline data was obtained by means of a hyperdermic tube suspended in the tunnel from supports at the upstream and downstream ends of the nozzle.

It was found that due to slight differences in direction of threads, clearances, etc., all of the models did not screw onto the stinger at exactly the same angle of attack. To overcome this, each model was mounted once with the pressure hole on top and once with it on the bottom. For each of these two positions the angle of attack was varied and pressures recorded at three or four different angles. Then, by plotting pressures vs. angles to get the intersection of the two curves, the exact zero angle of attack pressure was obtained. Since each model had only one pressure hole, this procedure had to be repeated for each model.

To increase the accuracy of the manometer readings, the following procedure was followed: A convenient wall pressure, "p_w", Testing Procedures - Cont.

was chosen and read against the atmosphere on a mercury manometer. Since the difference here was large, the accuracy was good. The stagnation pressure, "p_o", was read against the atmosphere on an acetylene tetrabromide manometer. p_w vs. "p_x", the pressure on the surface of the cone were also read on an acetylene tetrabromide manometer. Then, in any one series of pressure runs at least 15 readings of p_o and p_w were taken and a very accurate value of p_w/p_o could be obtained. The desired ratio p_x/p_o could then be obtained from the relation:

$$\frac{p_x}{p_o} = \frac{p_w}{p_o} - \frac{p_w - p_x}{p_o}$$

All of the manometers used could be read to 0.5 mm.

Test Results

The following notations were used to represent the data:

p_x = abs. pressure at location being investigated.

p_o = stagnation pressure before the shock wave.

p_o' = stagnation pressure after the shock wave.

S' = distance of shock wave ahead of model.

θ_W = angle of shock wave to horizontal.

D = model diameter.

M or M_1 = Mach number before shock wave.

M_2 = Mach number after shock wave.

x', x, y, S are defined on Fig. #5.

Models were tested at Mach numbers of 1.41, 1.49, 1.58, 1.71, 1.83 and 1.99. Examination of Fig. #65 indicates what the theoretical conditions are on the cone. This figure was obtained for the 75° cone by cross plotting data obtained from Reference #2. From this figure, then, the Mach number at which the shock wave attaches to the cone is 1.80. The free stream Mach number at which the Mach number behind the cone is unity is 1.93. The free stream Mach number at which the surface of the cone is first supersonic is $M = 2.07$. Therefore, the data herein presented covers the range from completely detached conditions to attached conditions with subsonic flow on the cone surface. The flexible nozzle blocks were used to obtain all the above-mentioned Mach numbers except for $M = 1.99$ for which a solid steel block was used.

Test Results - Cont.

The method of drawing the pressure curves of Figs. #6 to #21 needs some explanation. For M = 1.41, 1.49, 1.58 and 1.71 the p_o' value used to obtain the p_x/p_o' curves is that obtained from the normal shock wave relations. For M = 1.41 and 1.49, an inspection of Figs. #23, #24 and #54 shows that the shock wave angle at the cone axis is very near 90°. Therefore, it was assumed that for these two velocity conditions, the cone nose pressure was equal to that obtained from the normal shock wave relations. Using this nose pressure the corresponding p_x/p_o' curves were dash-faired from the nose to the first experimental point.

For the two highest Mach numbers, 1.83 and 1.99, the p_o' used was that obtained from oblique shock wave relations. The wave inclination used can be read from the observed wave angle plots or directly from Fig. #65 since the two check very closely. For these two Mach numbers the nose pressures were faired in as if conical conditions existed there. This was felt to be a justifiable procedure since surface pressures calculated in the M.I.T. Report (Ref. #2) are in close agreement with those observed.

Neither the M = 1.58 nor M = 1.71 pressure ratio curves were faired to the nose since it was felt that neither of the aforementioned arguments used for the two lowest and two highest velocity conditions were applicable.

Test Results - Cont.

Using p_o' as outlined above, the variation of p_x/p_o' with Mach number has a discontinuity at the attachment Mach number. This is brought out in Fig. #21. Since there is considerable uncertainty about this method of calculating p_o', the region of discontinuity is shown dashed in Fig. #21.

Fig. #22 shows the p_o'/p_o vs. Mach number comparison of theoretical to experimental. The p_o's here are for normal shock waves since the pressures were measured with the blunt model.

Schlieren pictures taken during the runs are presented on Fig. #23 to #39. These pictures were enlarged approximately 6½ times for purposes of measurement of distances and wave angles. The accuracy of the wave angle measurements is approximately ± 1 degrees. From the measured wave angles the calculated Mach number M_2 could be obtained. θ_w and M_2 vs. y/D are presented on Fig. #40 to Fig. #53.

For reference purposes shock wave traces have been plotted on Figs. #54 to #58. Traces at 1.71, 1.83 and 1.99 are shown for all five of the cones used, i.e. 45°, 60°, 75°, 90°, 180°. Complete sets of pictures at the three lower Mach numbers were not taken and are therefore not shown.

For the 75° cone and the blunt model curves of S'/D vs. M_1 and vertical location on the shock wave of the $M_2 = 1.00$ point are also shown.

Conclusions

Examination of the summary curves of pressure distribution vs. position on the cone shows a gradual rotation of the curves counter-clockwise, i.e., the pressure becomes more nearly constant on the cone's surface. Below the speed of attachment the pressure ratio is high at the nose and drops off as the corner, i.e., the intersection of cone and cylinder is approached. The location of the sonic line on the surface of the cone is indicated from this data for detached conditions to be in the immediate vicinity of the corner. This sonic line location for detached shock wave cases in in agreement with previously reported results (Ref. 4).

Of interest, in this regard, is the location of $M = 1.00$ directly behind the shock waves (Fig. #61). This data, plus the fact that sonic velocity occurs at the corner for detached conditions, gives a portion of the subsonic region boundary.

Investigations of pressures at conditions of free stream flow above $M_1 = 2.07$ would have been desirable here but were not done due to lack of time. As mentioned in the "Test Results" section of this report, above $M_1 = 2.07$ would theoretically give supersonic flow on the cone surface.

The comparison of the experimental p_o' / p_o to theoretical shows excellent agreement. The maximum deviation from theoretical occurred at $M_1 = 1.83$ where a deviation of only $2\frac{1}{2}\%$ occurred.

On Fig. #59, S'/D vs. M_1 was plotted in an attempt to check

Conclusion - Cont.

the theoretical speed of attachment which equals $M_1 = 1.80$ (Ref. #2 and #3, and Fig. #65). The points obtained show considerable scatter and a definite conclusion cannot be reached. However, no radical deviation from theory is apparent and the data roughly checks it. The scatter in the points is due to the difficulty of accurately measuring very small distances from photographs.

An examination of the shock wave traces checks one conclusion also arrived at from the pressure ratio curves. That is, on the cone's surface back of the nose region, the transition from detached to attached shock waves takes place in a smooth and gradual manner. The pressures directly at the nose could, as was mentioned previously, only be estimated. Procurement of values at this point could be one of the objectives of future investigations.

REFERENCES

1. Puckett, A.E., "Supersonic Nozzle Design", Journal of Applied Mechanics, December, 1946.

2. Kopal, Z., "Supersonic Flow Around Cones", M.I.T. Center of Analysis, Report #1.

3. Taylor, G. I. & Maccoll, J. W., Proceedings of the Royal Society of London, Vol. 139, pages 278-311, 1933.

4. Maccoll, J. W. & Codd, J., "Theoretical Research Report #17/45" (Confidential.), September, 1945.

APPENDIX #1

Blocking Data

Figure #64 graphically shows the results of the blocking tests. The one dimensional curve is shown for comparison. This was calculated by means of the relation;

$$P_{10} A_1^* = P_{20} A_2^*$$

where, P_{10} = throat equivalent reservoir pressure

P_{20} = test section equivalent reservoir pressure

A_1^* = throat area

A_2^* = test section area - model area

This relation was obtained assuming the section at the model is the second throat and that a normal shock is standing ahead of the model.

It was found that by building up pressure on one side of the tunnel and suddenly releasing it to give a large initial pressure difference across the nozzle a flow could be sustained past a larger model than was possible otherwise. This procedure was used to obtain the data shown. Table I tabulates the data. Two views illustrating typical blocking behavior are shown on Figures #62 and #63.

TABLE I

BLOCKING DATA

GALCIT $2\frac{1}{4}$" x 2 9/16" SUPERSONIC TUNNEL

Mach No.	Test Area (In.^{2})	Model Dia. (In.)	Model Area (In.^{2})	$\frac{\Delta A}{A}$
1.41	6.31	.500	.196	.0311
1.49	6.41	.562	.248	.0387
1.58	6.43	.625	.307	.0478
1.71	6.39	.750	.442	.0692
1.83	6.35	.812	.518	.0815

APPENDIX #2

Commentary on the Flexible Nozzle

The flexible nozzle as used for this work was not altogether satisfactory and it is felt that design improvements should be incorporated if further use of it is attempted. The nozzles used were salvaged from some older nozzles and as a result, the jacks extend only to a point $3\frac{1}{4}$" away from the downstream end. Of this distance $2\frac{1}{2}$" is made up of a fixed block (see Sketch #1).

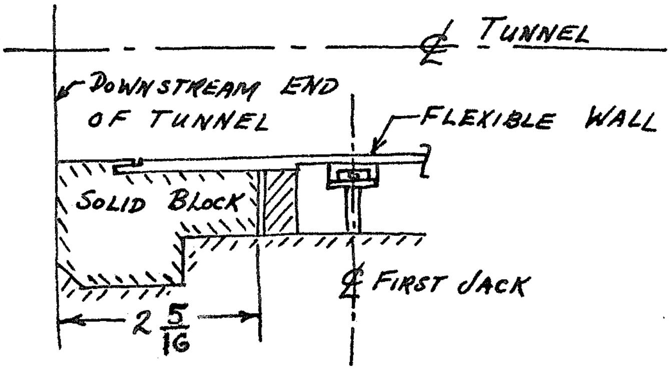

Sketch #1

This block is at present necessary for purposes of assembly. Removal of a screw allows the block to be slid out sideways. Enough space is then available to skew the nozzle sideways to pull it out. The junction of block and wall also serves as an expansion joint to allow for the longitudinal movement which occurs when the nozzle shape is changed. The end of the stinger also occurs at $2\frac{1}{2}$" from the downstream end and a model mounted directly on the stinger is thus only a small distance ahead of the block. The difficulty with the block is that no boundary

Appendix #2 - Cont.

layer correction can be incorporated in that section. This made itself consistently apparent in the velocity survey and produced a decrease in Mach number in that region as is illustrated in Sketch #2. To eliminate this condition at least two more jacks need to be incorporated into the design in place of the solid block.

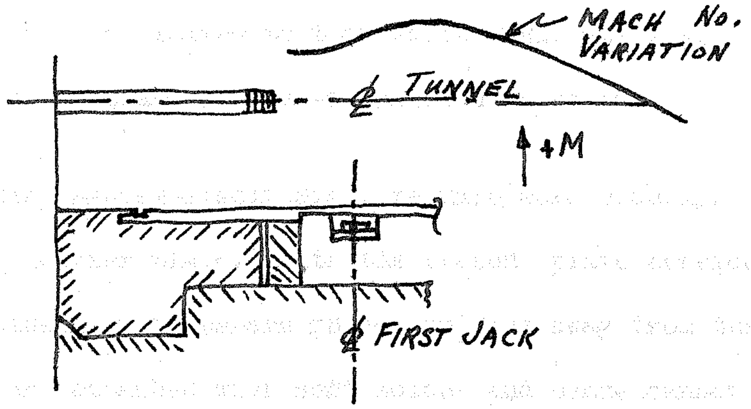

Sketch #2

Sealing between the flexible walls and the vertical tunnel walls was very satisfactory using the design illustrated in Figure #1. However, the "Pliobond" cement used to cement the rubber seal to the metal walls does have the one disadvantage of requiring several days to cure which causes considerable delay when repairs are necessary.

The flexible wall thickness now being used is 0.031 inches. The material is phosphor bronze. The stiffness of this wall is not sufficient to completely eliminate waviness. Small dips of the order of 0.005 to 0.010 inches were present. This waviness is enough to cause noticeable disturbances in the flow especially at the higher Mach numbers. With patience and considerable experimentation, it is possible to obtain uniform conditions. However, this is a time-consuming and undependable process. It is felt that a wall-thickness of at least 0.050 inches would be more desirable. The thickness would, of course, be limited to that which would still allow the wall to be bent by means of hand-actuated jack screws.

The jacking system itself might require some redesign to accommodate a heavier plate. With the present plate considerable delays were caused by cross-arm guides pulling away from the wall. These guides are attached with soft solder and hence cannot withstand much stress. Soldering is itself not a good method of attachment since the heat tends to warp the plate. Another disadvantage is that attempts to resolder the guides with the rubber seals attached to the walls tends to loosen the seals which in turn means more delay while recementing them. A more positive means of attachment can be and should be used to avoid delays in the future such as were experienced while taking data for this thesis.

GRAPHS

AND

PICTURES

LIST OF FIGURES

List of Figures - Cont.

List of Figures - Cont.

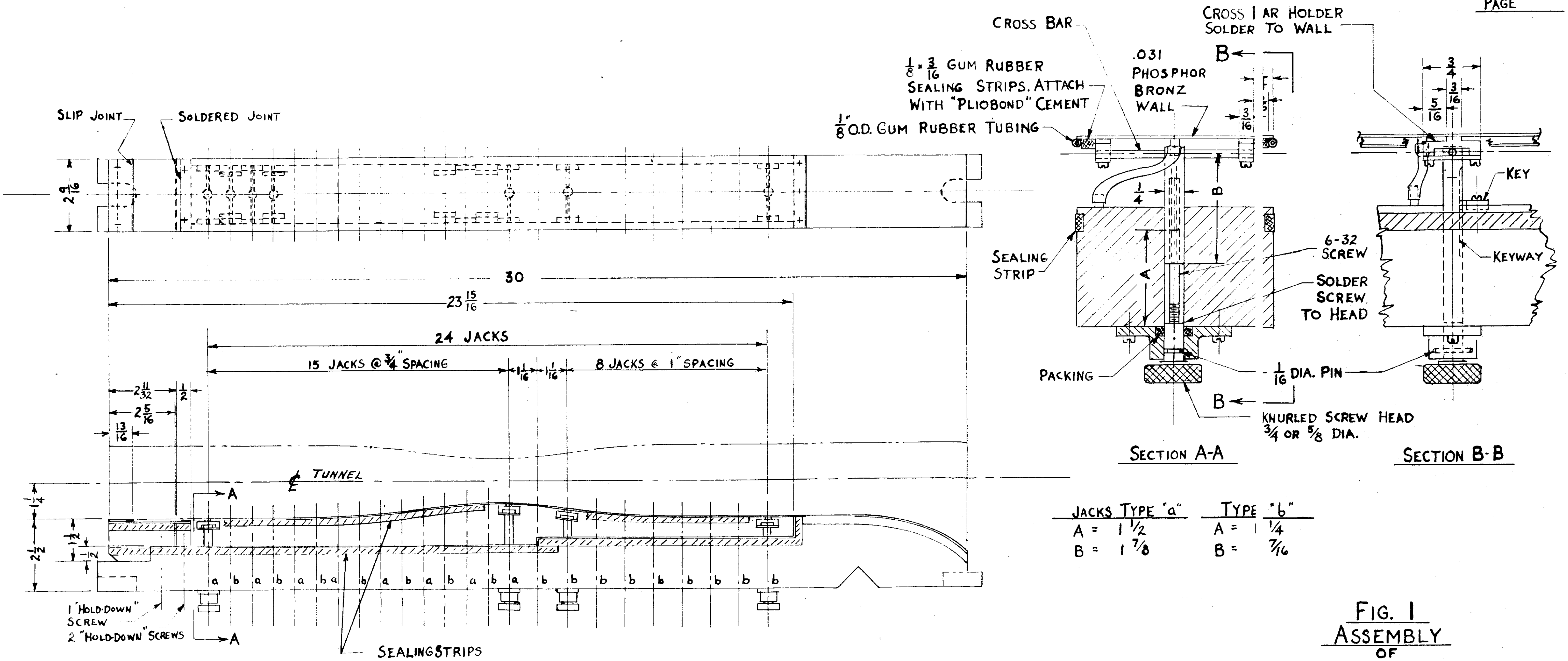

JACKS TYPE "a"	TYPE "b"
A = $1\frac{1}{2}$	A = $\frac{1}{4}$
B = $1\frac{7}{8}$	B = $\frac{7}{16}$

FIG. I
ASSEMBLY
OF
FLEXIBLE NOZZLE BLOCKS

J.H.G. 5-20-48

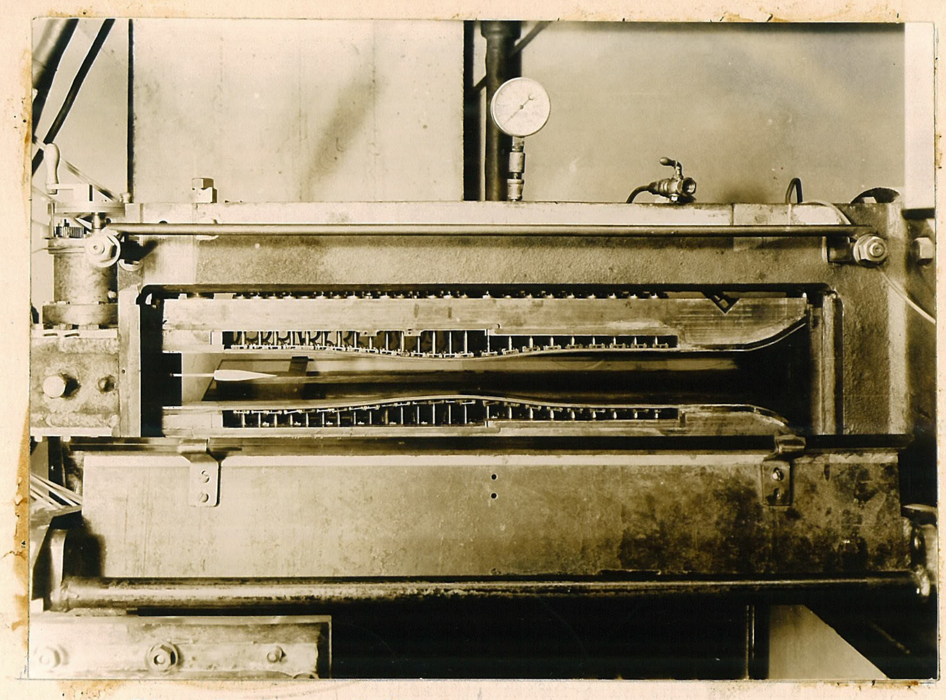

Fig. 2--General View of the Flexible Nozzle

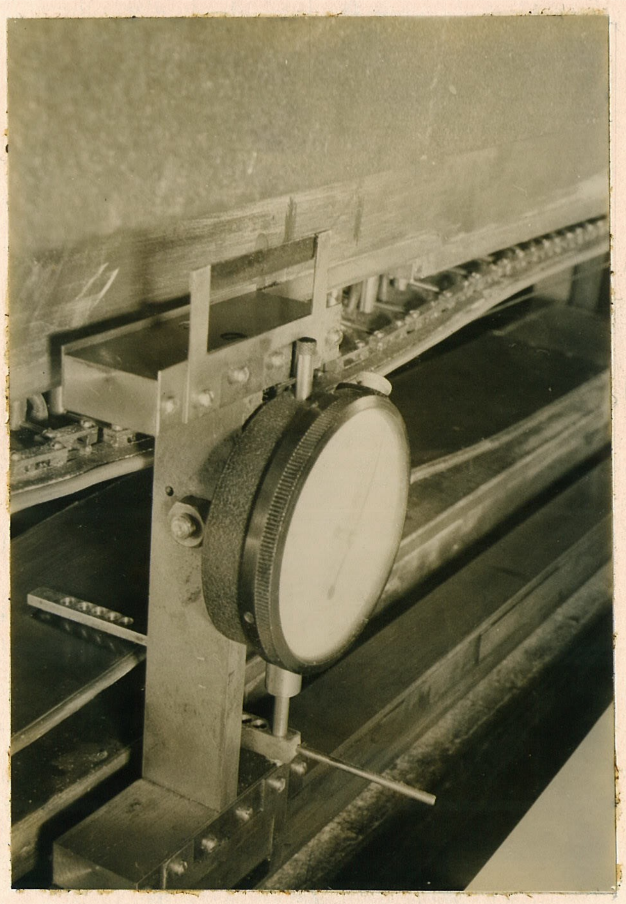

Fig. 3--The Nozzle Calibration Device

FIG. 4 CENTER LINE SURVEY M= 1.58

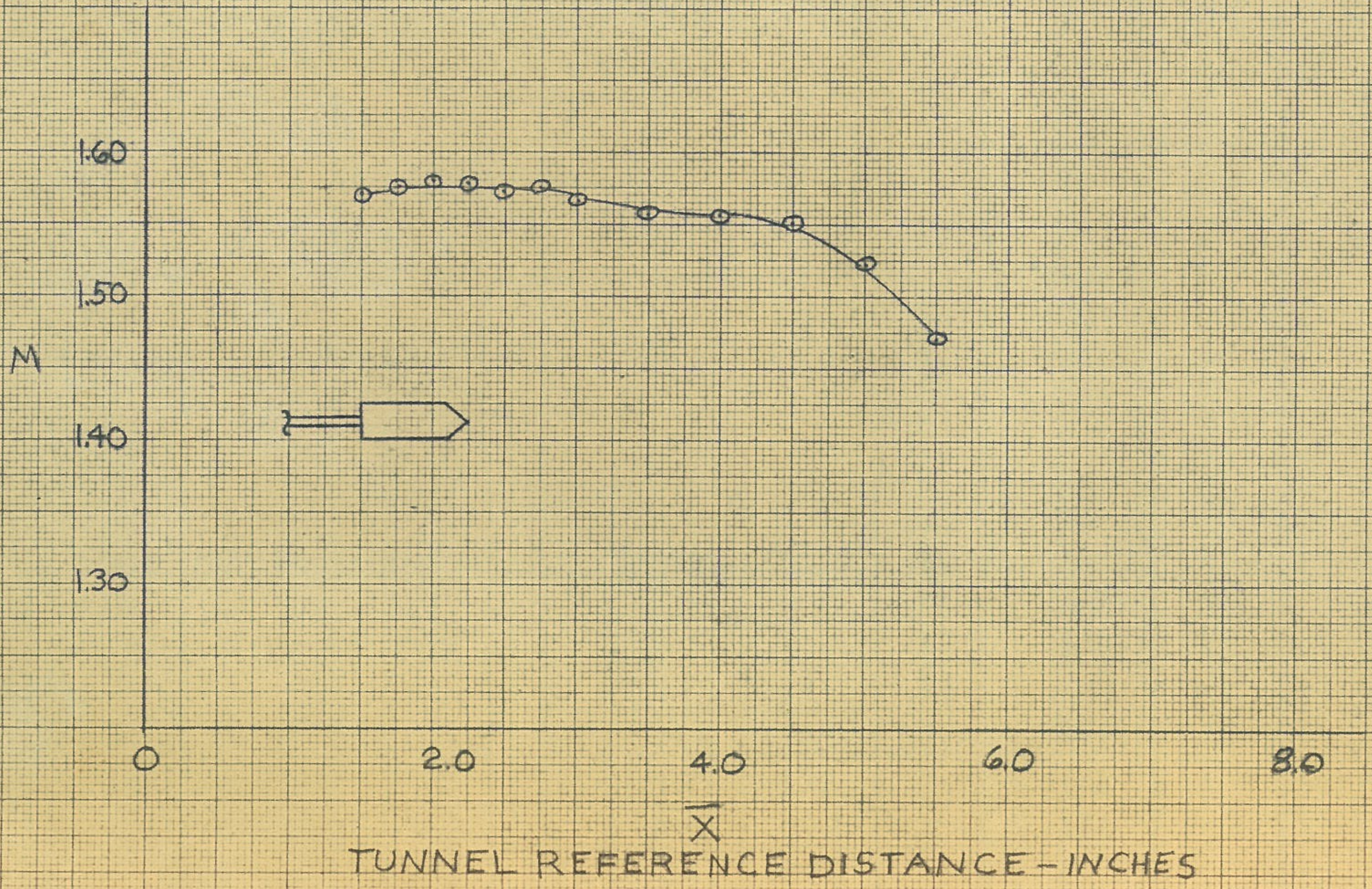

FIG. 5
CONE PRESSURE MODELS

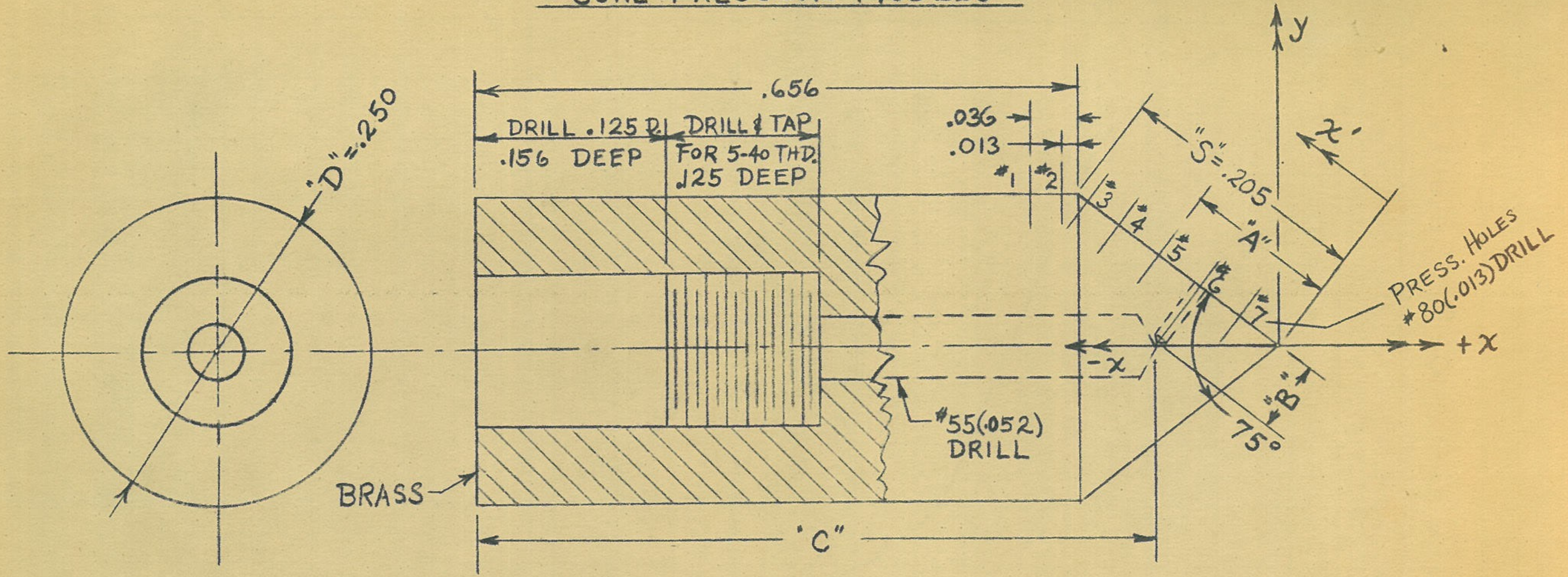

CONE NO.*	"A" (INCH)		"B" (INCHES)	"C" (INCHES)
	NOMINAL	ACTUAL		
1			.125	.656
2			.125	.656
3	.195	.197	.130	.656
4	.164	.159	.130	.666
5	.123	.122	.100	.712
6	.082	.078	.065	.750
7	.041	.042	.060	.773

* DRILL ONE PRESSURE PER CONE. I.E. CONE #1 HAS HOLE #1, ETC.

FIG. 6 : 75° CONE PRESSURE DISTRIBUTION

$M_1 = 1.41$

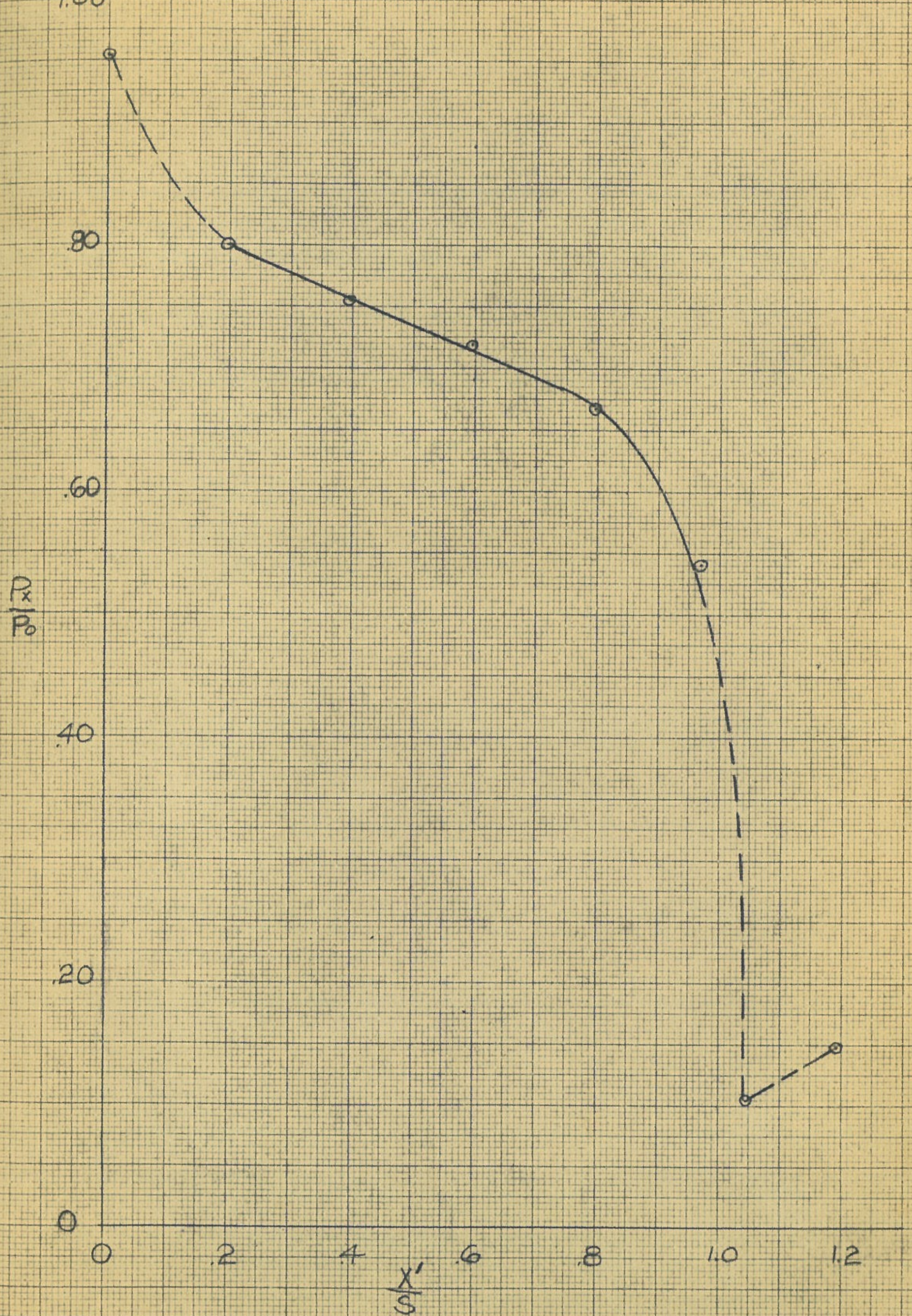

FIG. 7: 75° CONE PRESSURE DISTRIBUTION

$M_1 = 1.490$

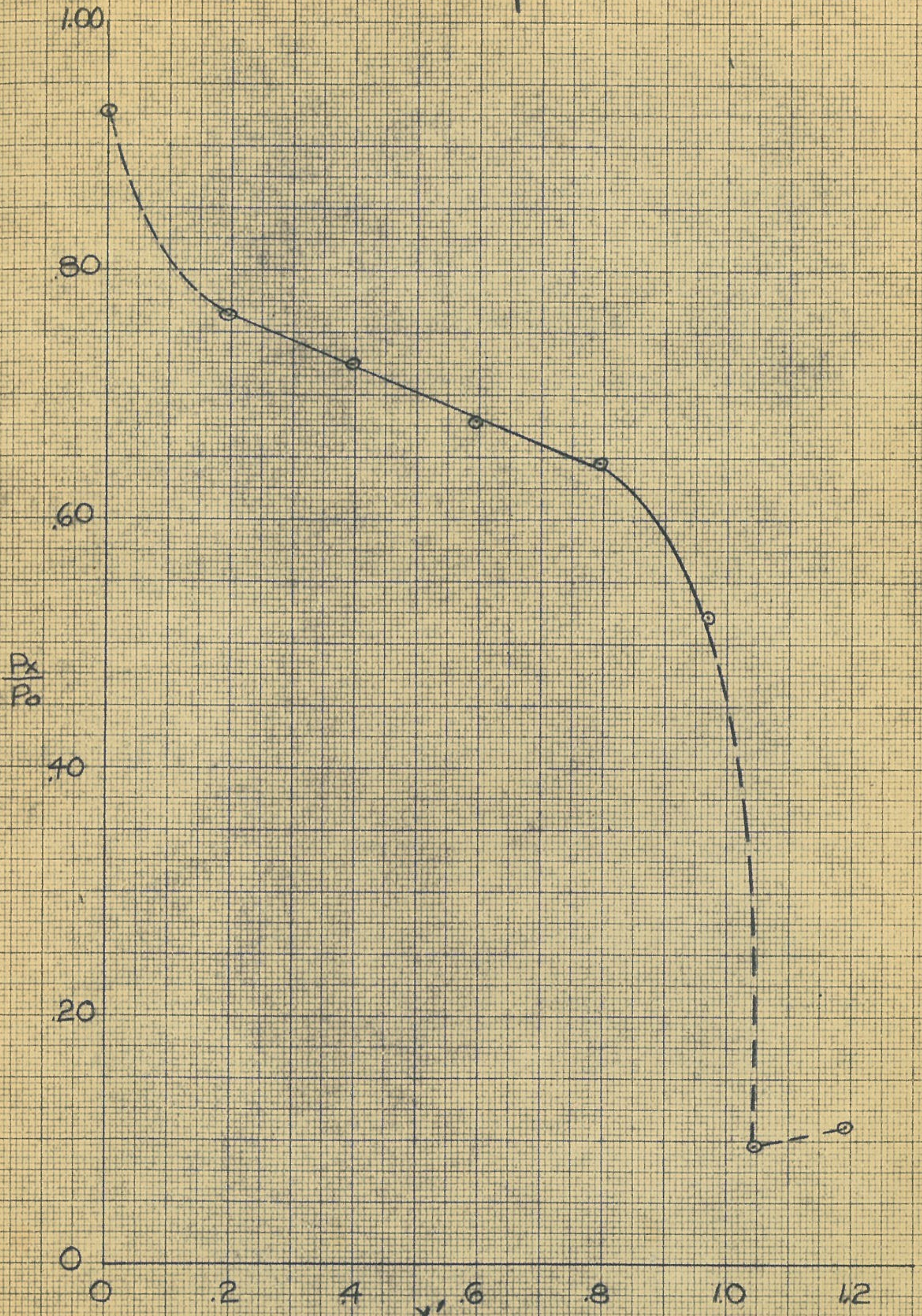

FIG. 8 75° CONE PRESSURE DISTRIBUTION
$M_1 = 1.58$

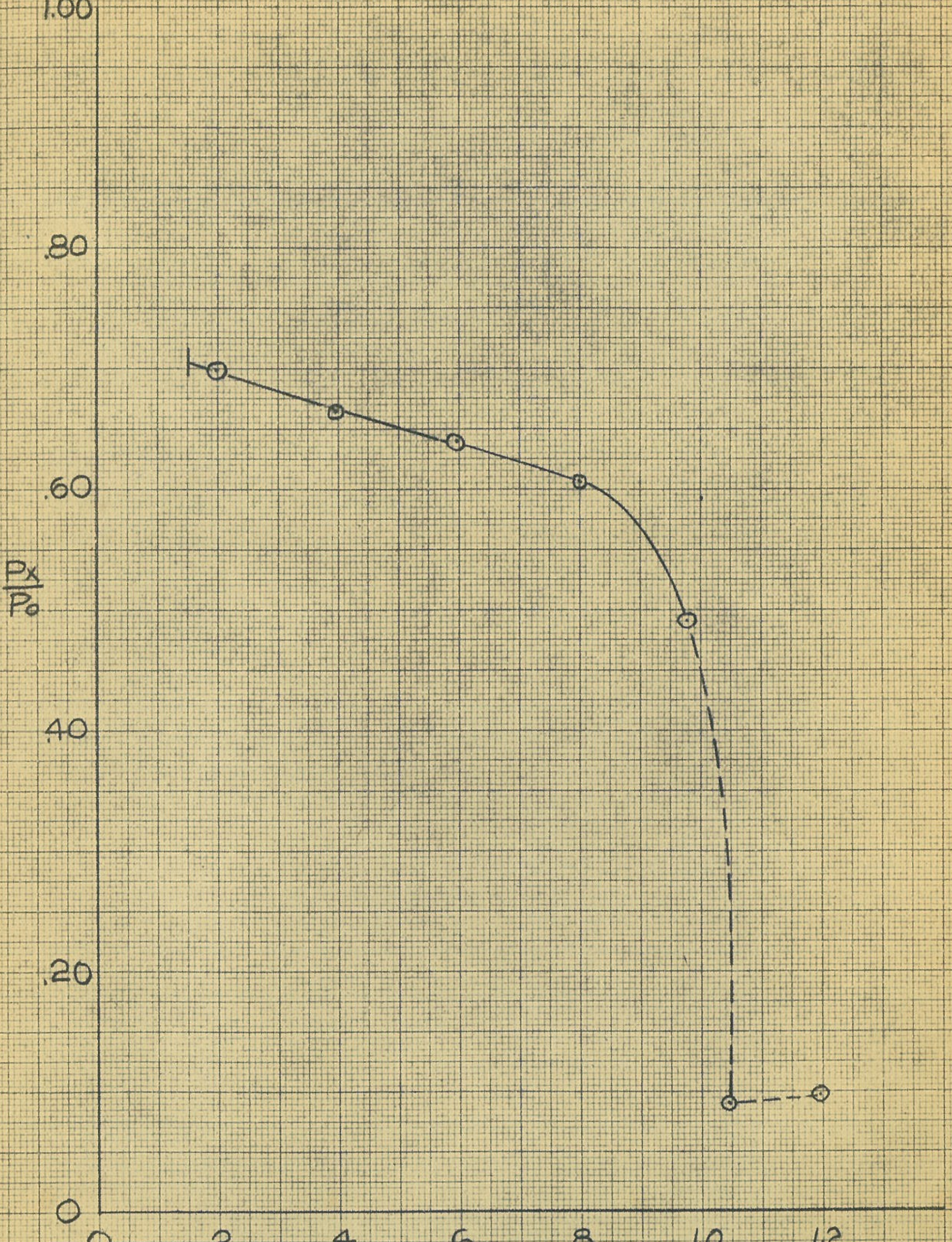

FIG. 9 75° CONE PRESSURE DISTRIBUTION
$M_1 = 1.71$

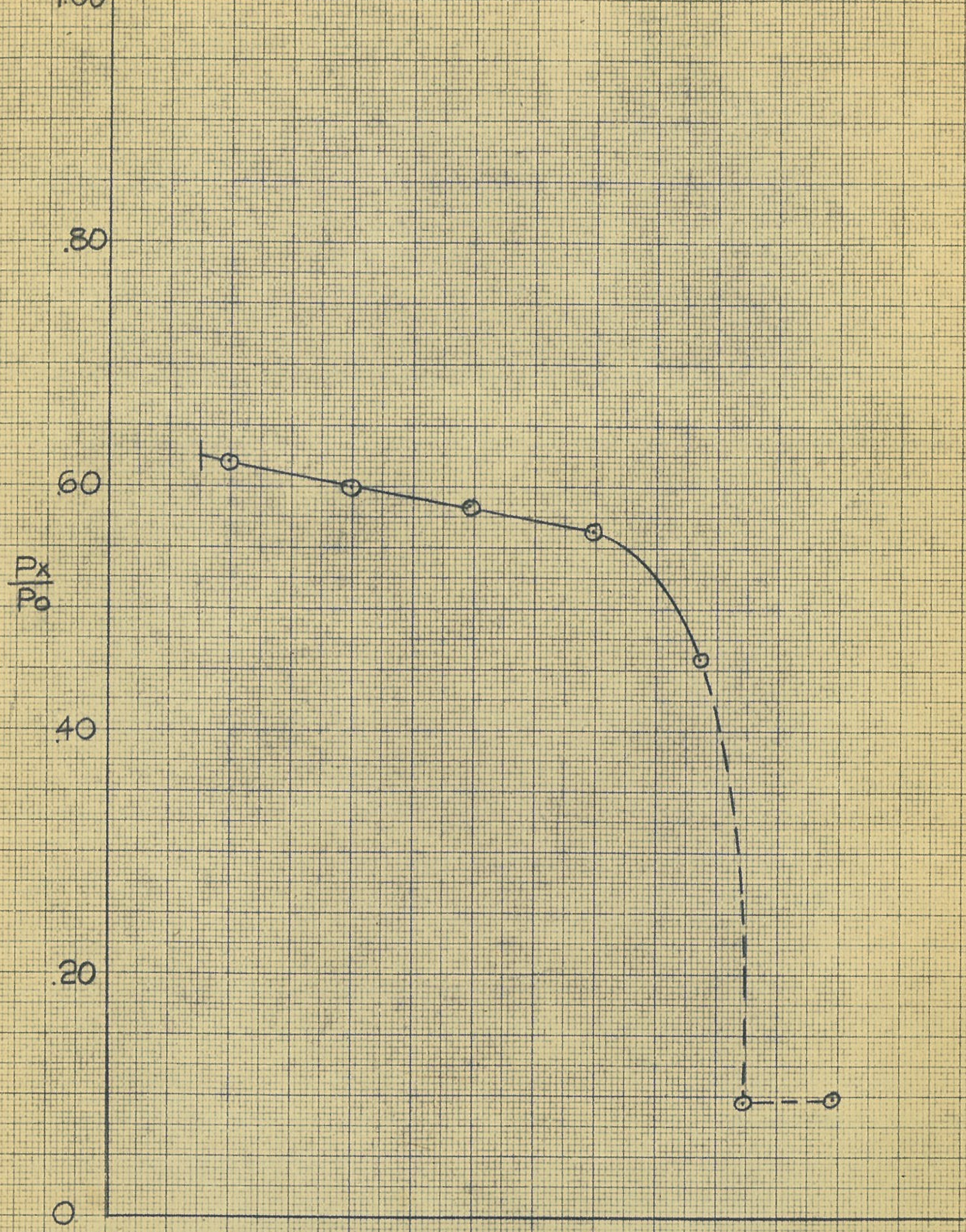

FIG. 10 75° CONE PRESSURE DISTRIBUTION

$M_1 = 1.83$

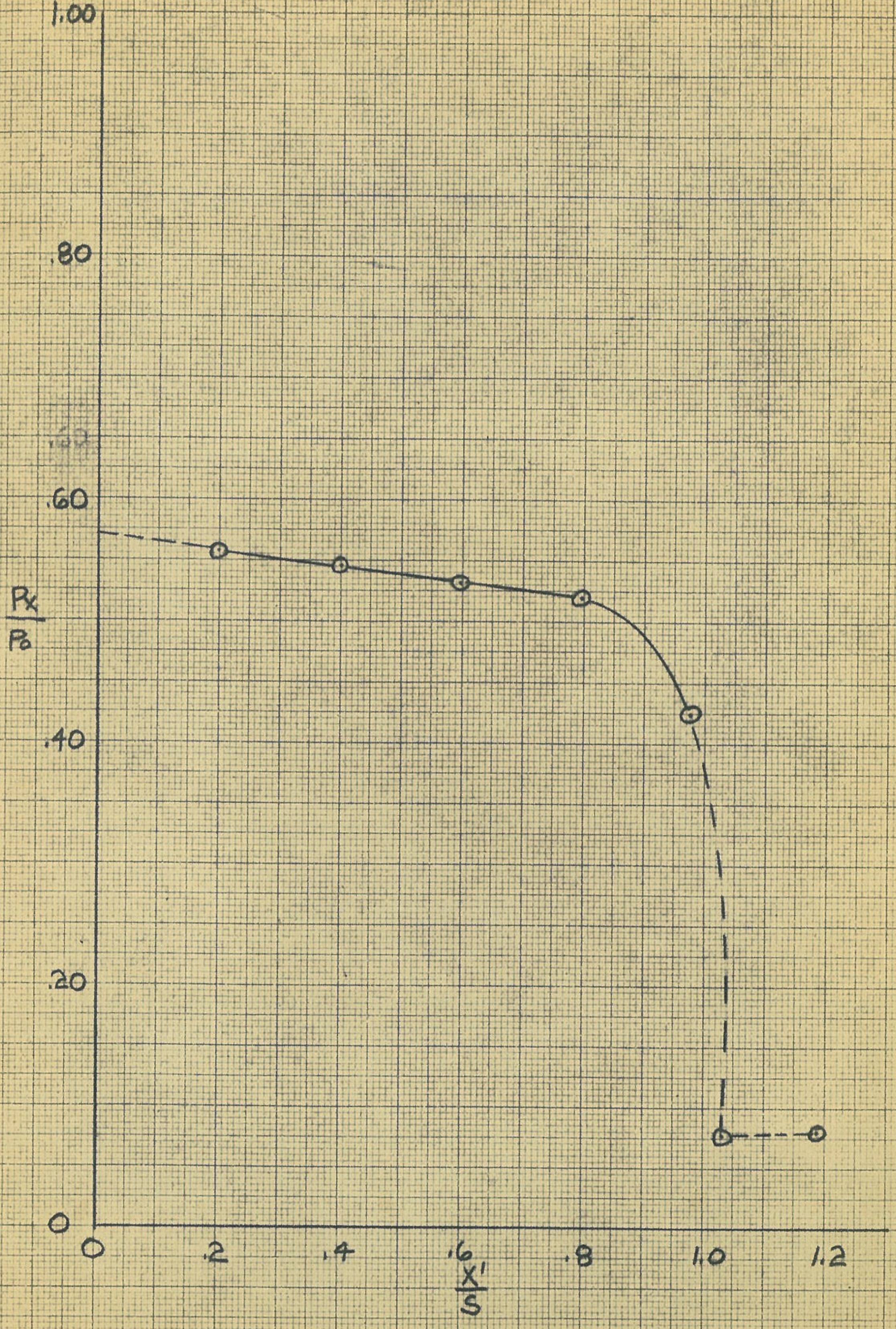

FIG. 11 75° CONE PRESSURE DISTRIBUTION

$M_1 = 1.99$

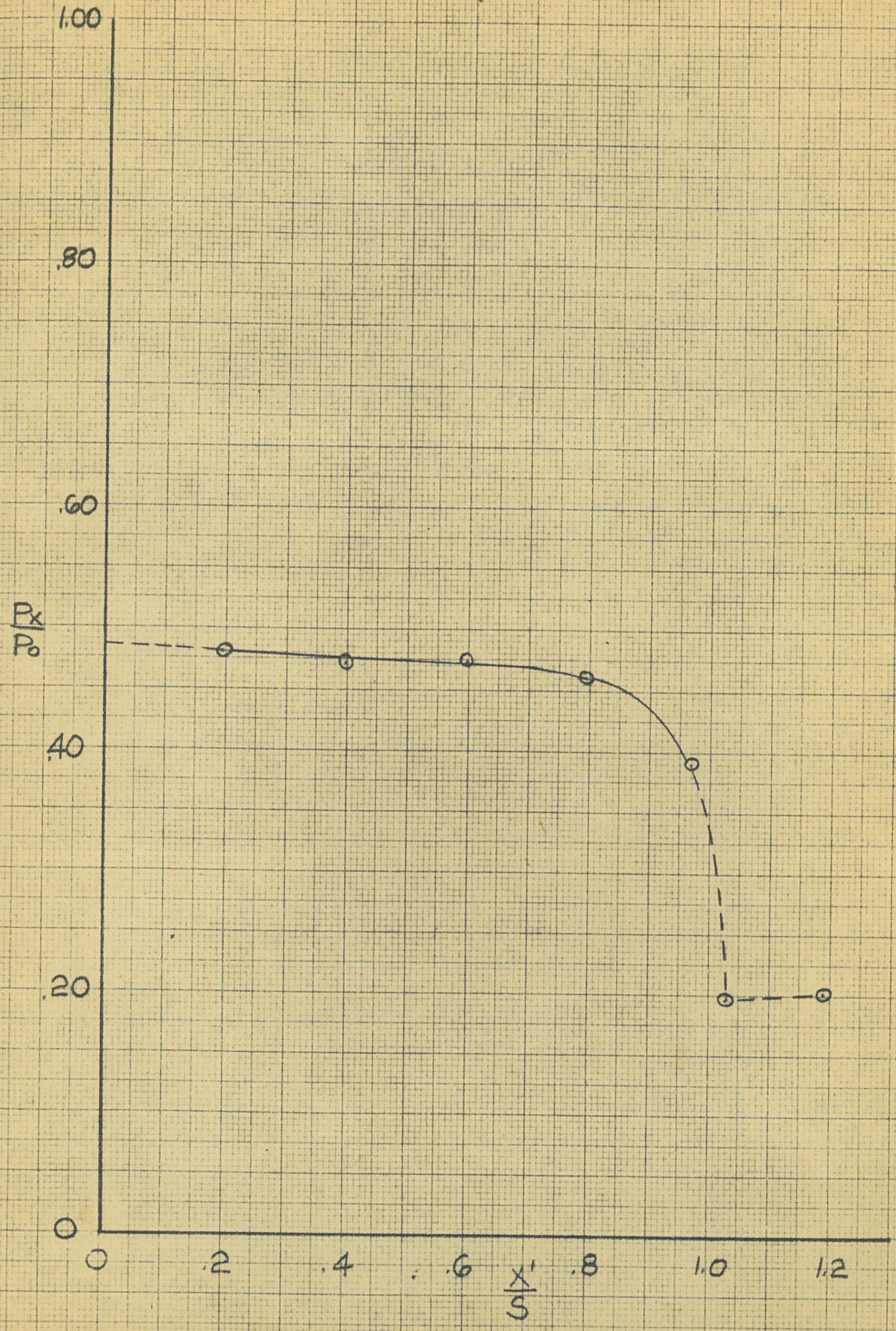

FIG 12 75° CONE PRESSURE DISTRIBUTION

SUMMARY

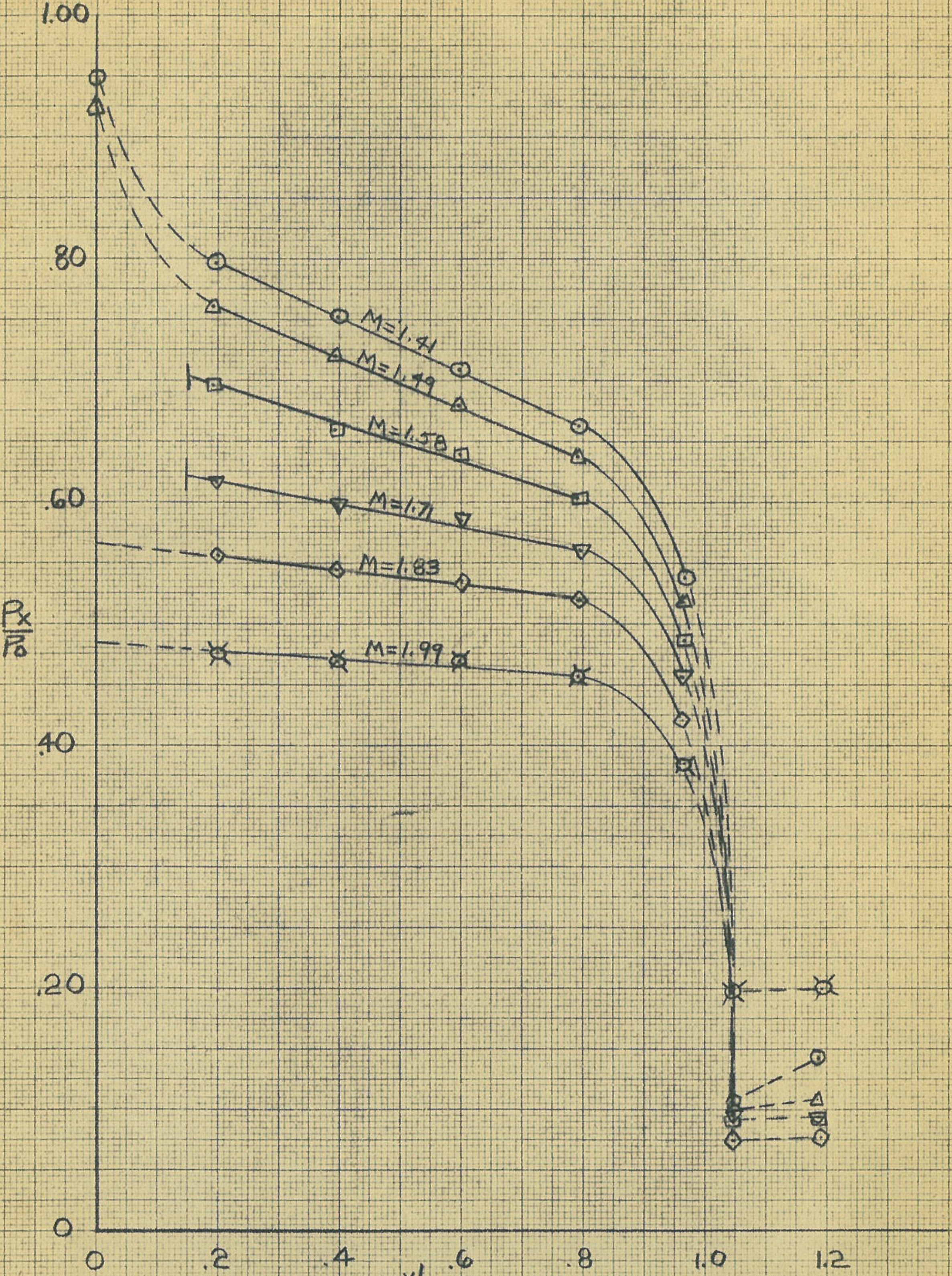

FIG. 13: 75° CONE PRESSURE DISTRIBUTION

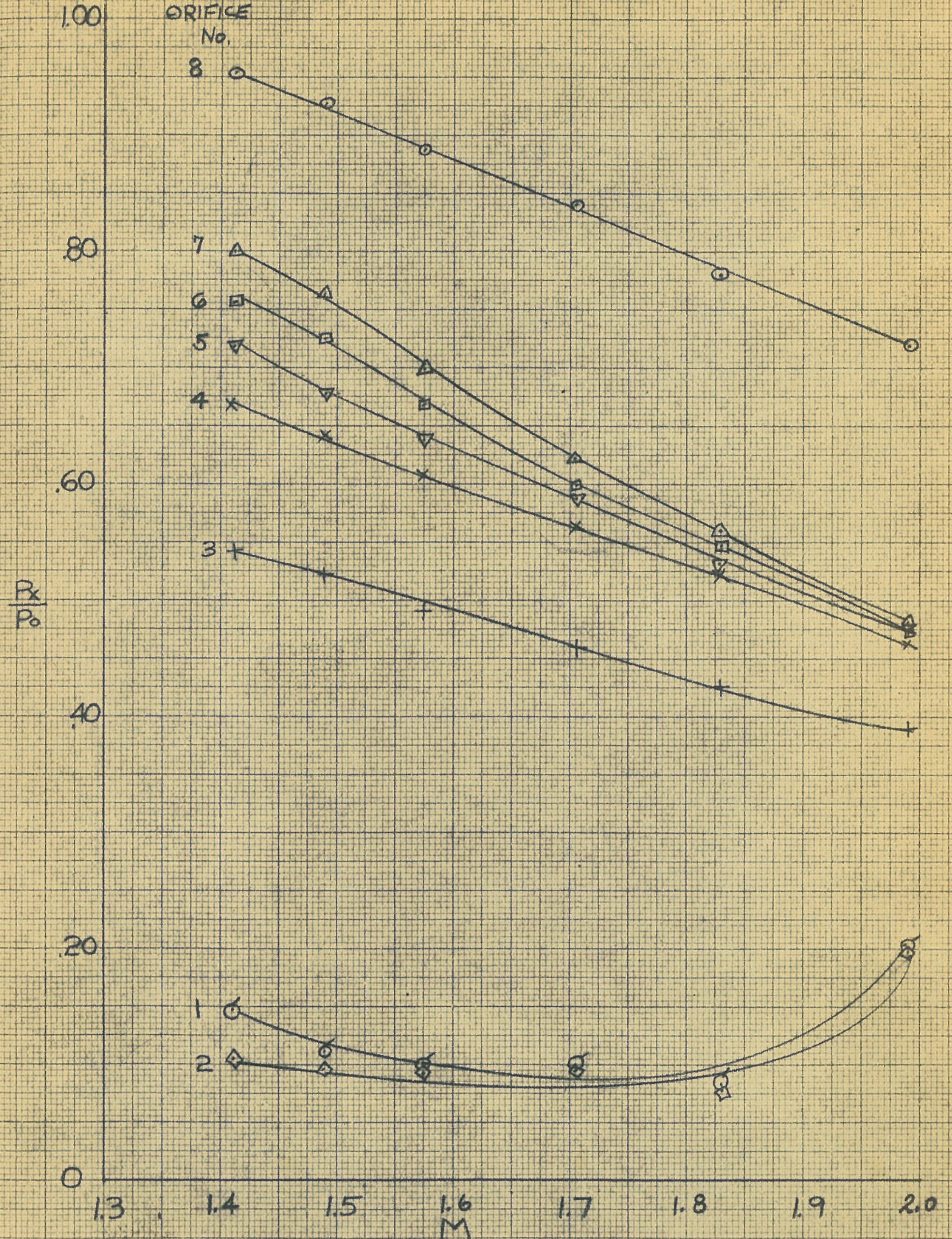

FIG. 14: 75° CONE PRESSURE DISTRIBUTION
$M_1 = 1.41$

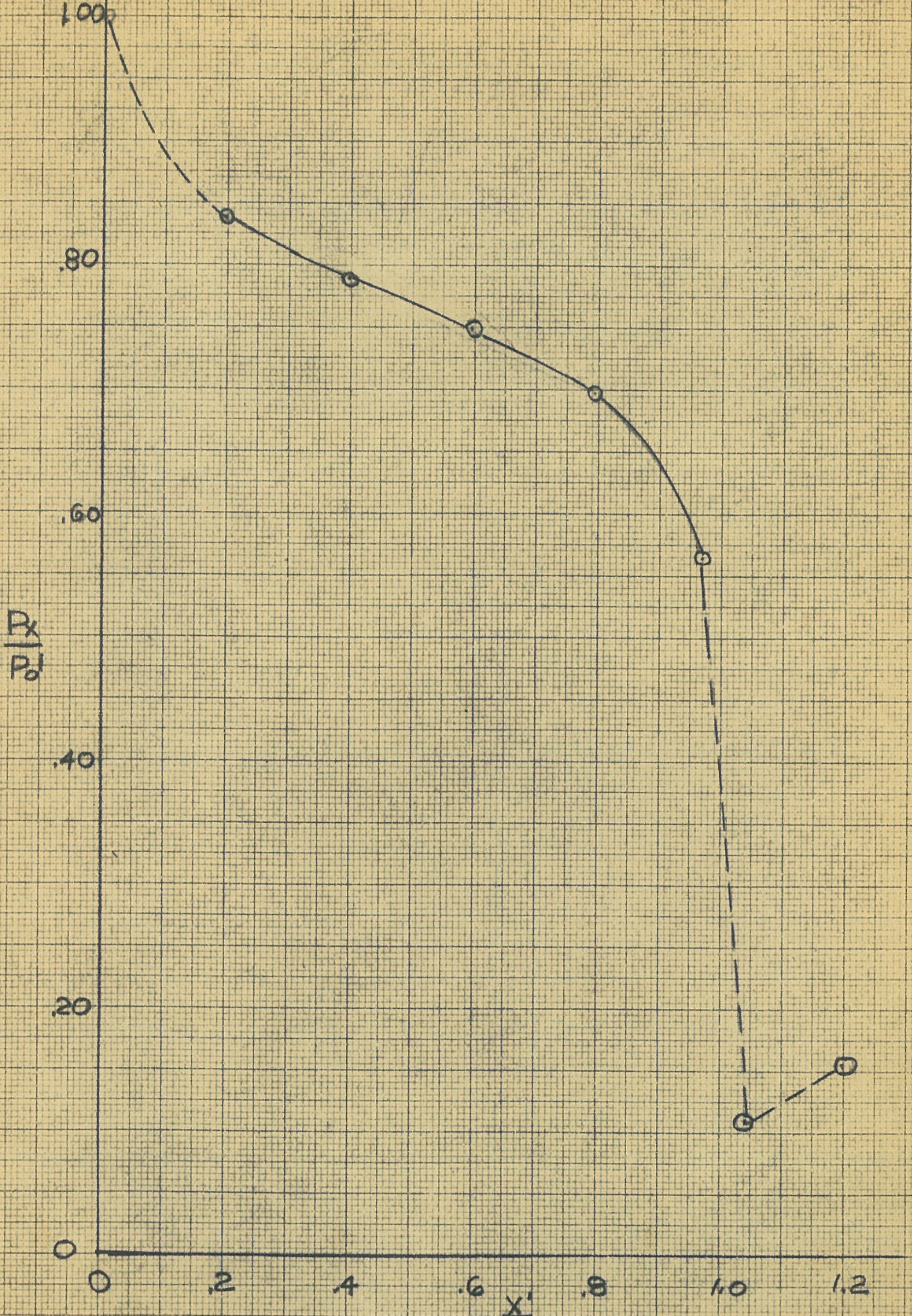

FIG. 15: 75° CONE PRESSURE DISTRIBUTION
$M_1 = 1.49$

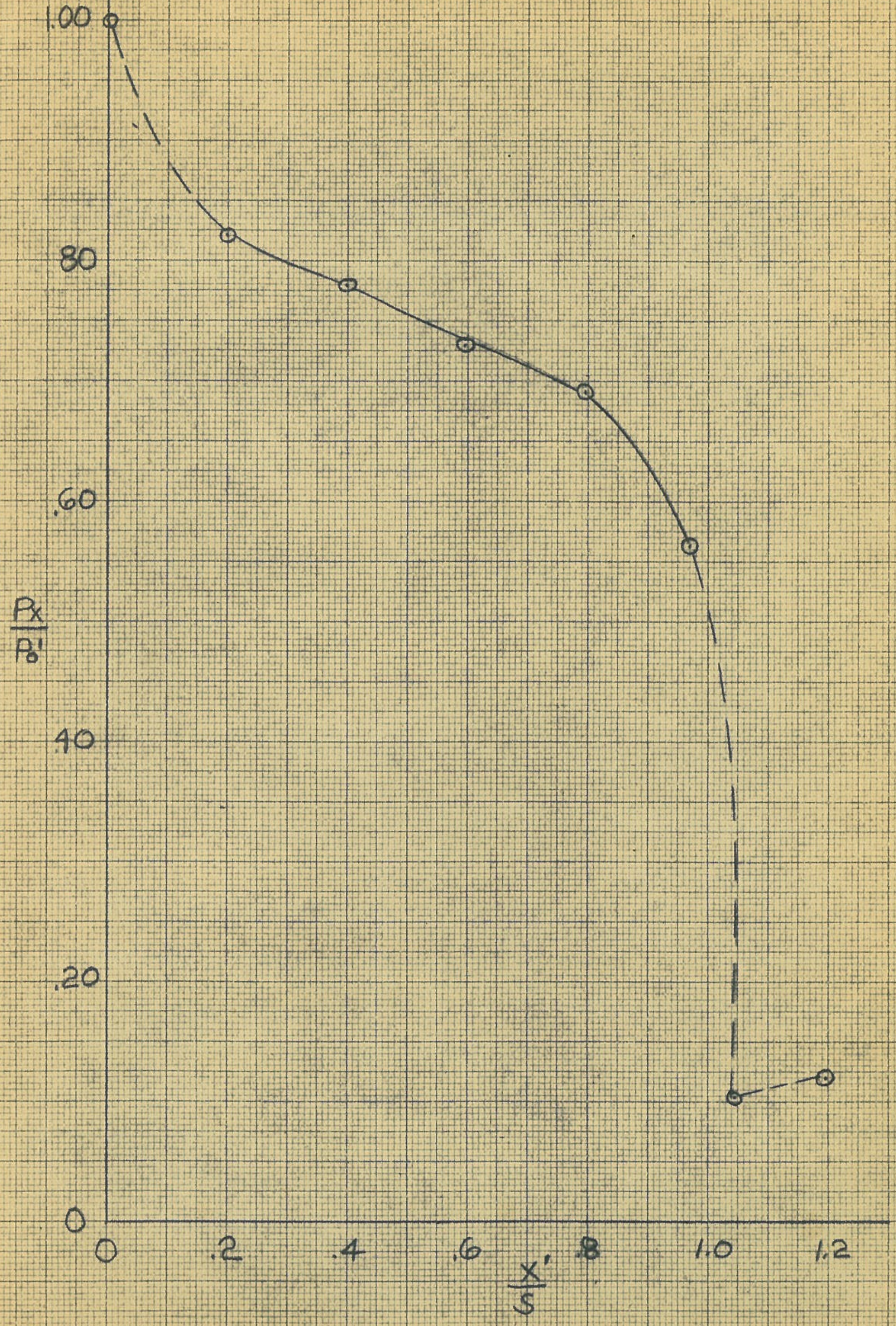

FIG. 16 75° CONE PRESSURE DISTRIBUTION
$M_1 = 1.58$

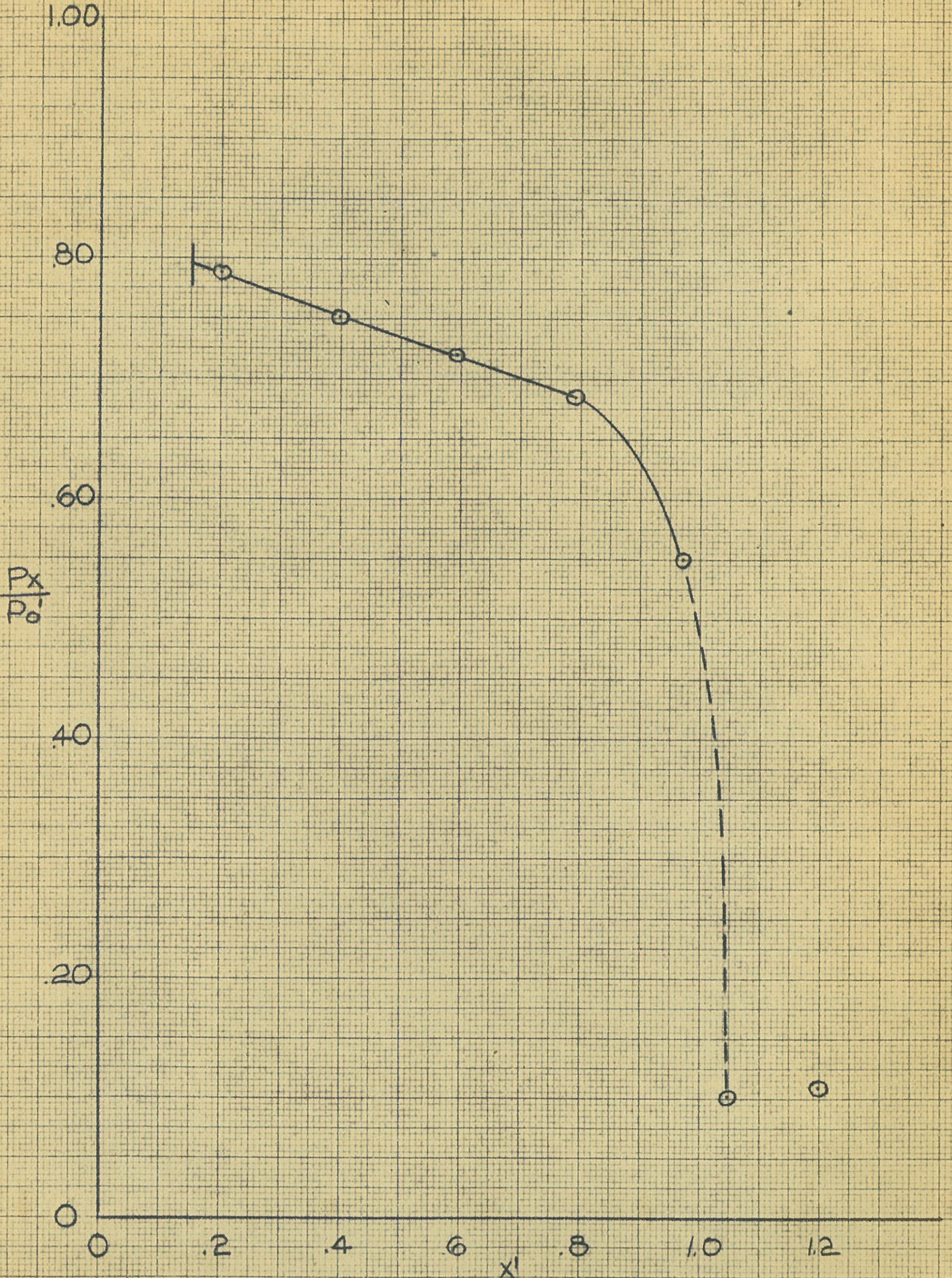

FIG. 17 75° CONE PRESSURE DISTRIBUTION
$M_1 = 1.71$

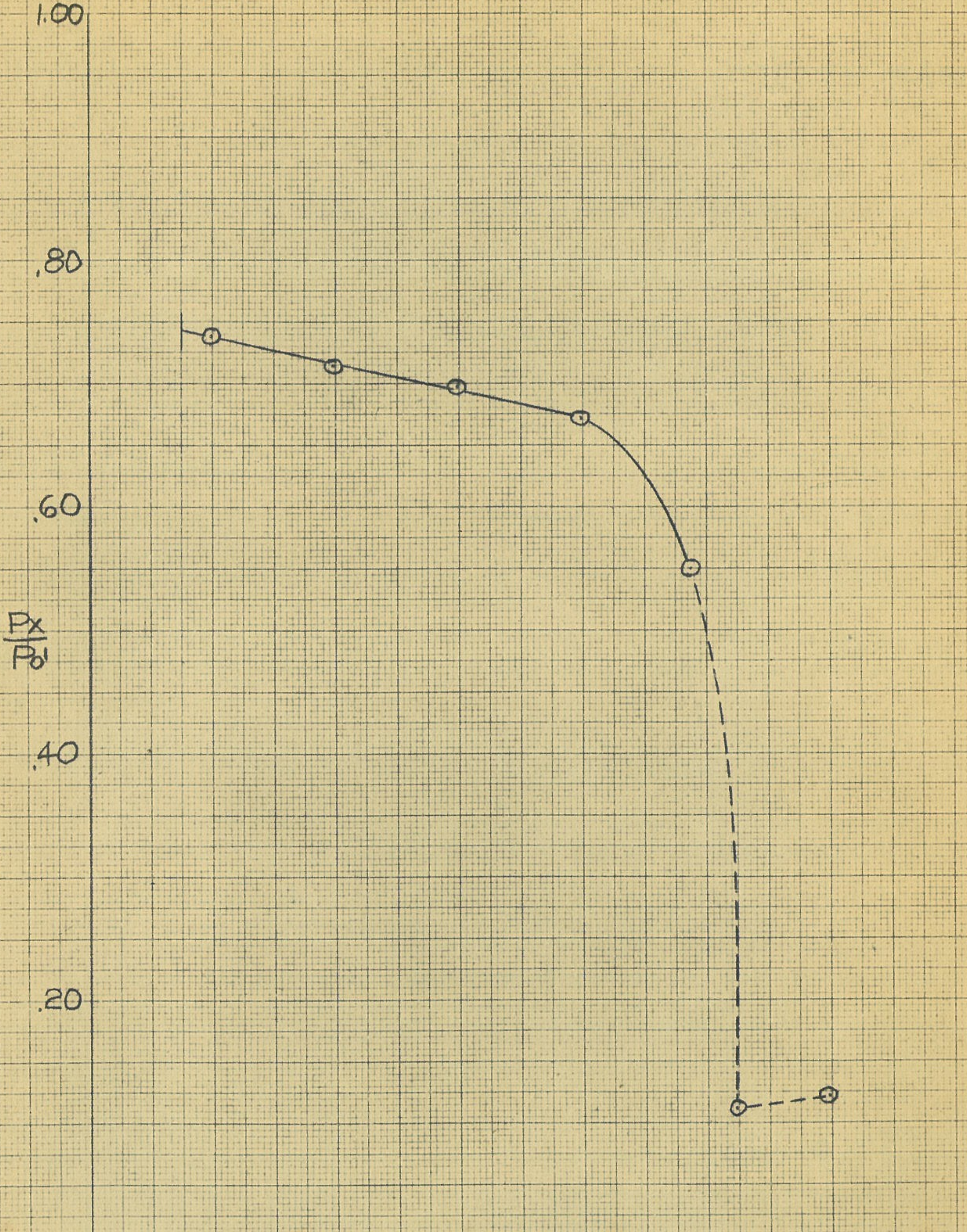

FIG. 18 75° CONE PRESSURE DISTRIBUTION

$M_1 = 1.83$

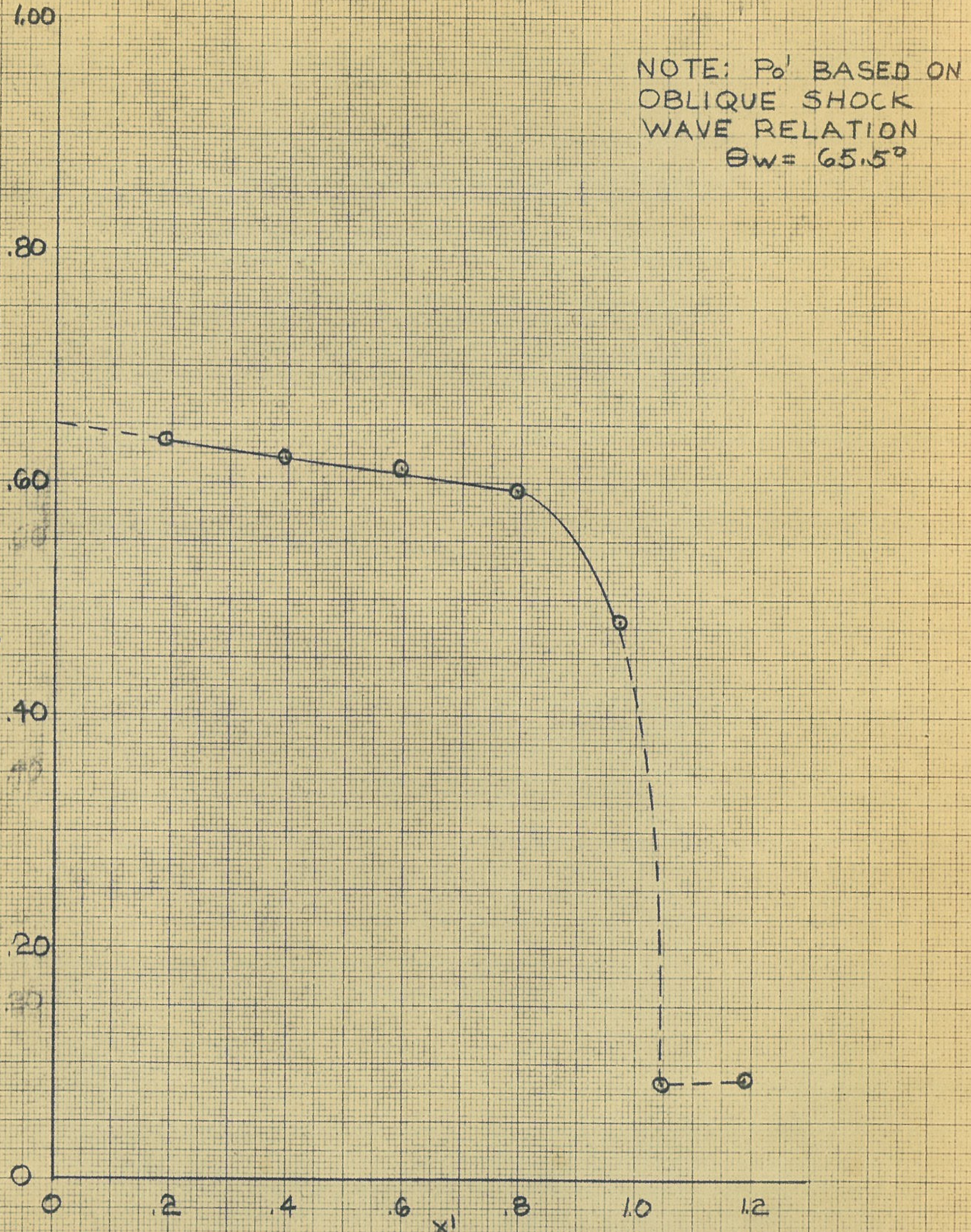

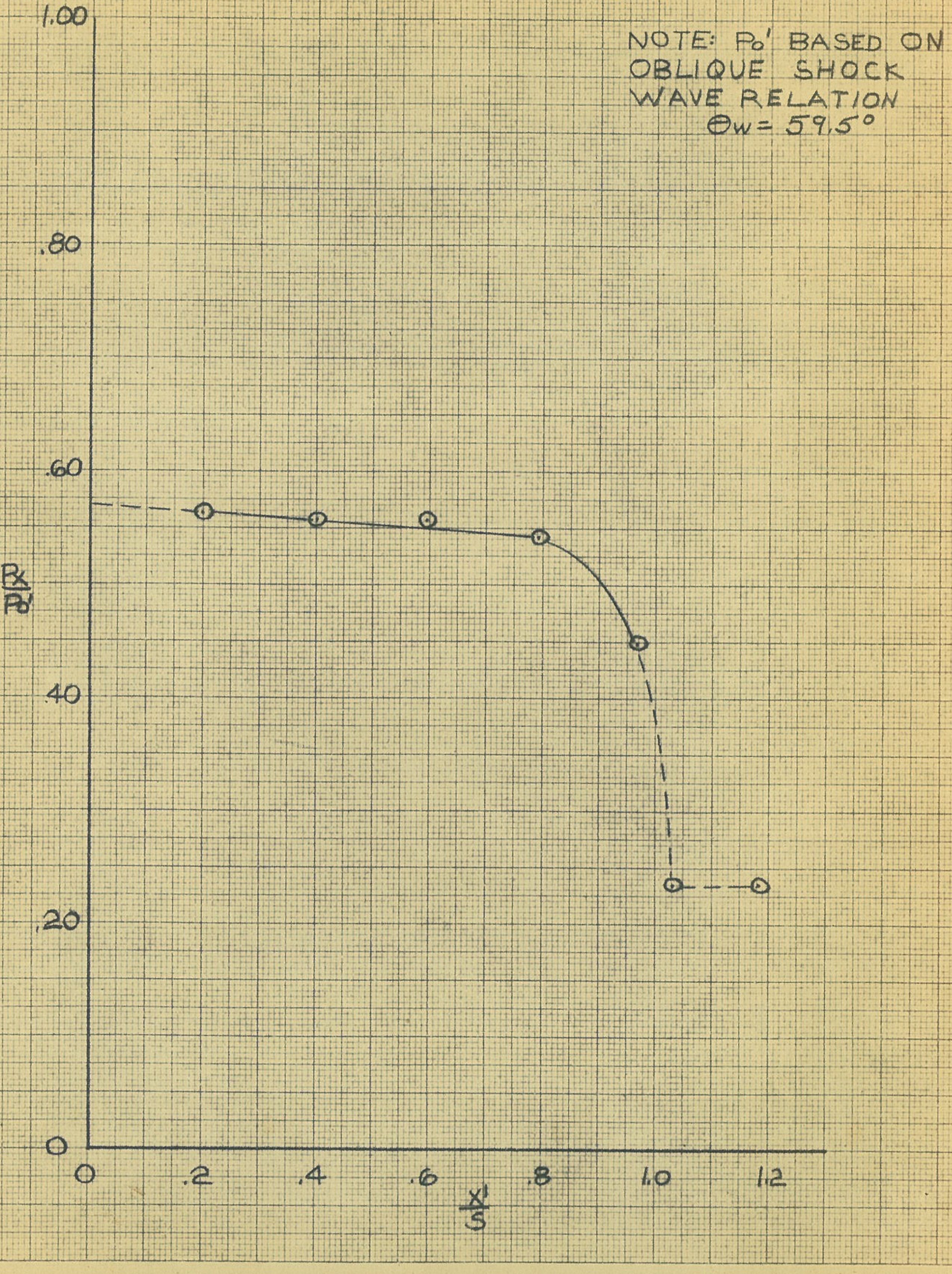

FIG. 19 75° CONE PRESSURE DISTRIBUTION

$M_1 = 1.99$

NOTE: P_o' BASED ON OBLIQUE SHOCK WAVE RELATION $\theta_w = 59.5°$

FIG 20 75° CONE PRESSURE DISTRIBUTION SUMMARY

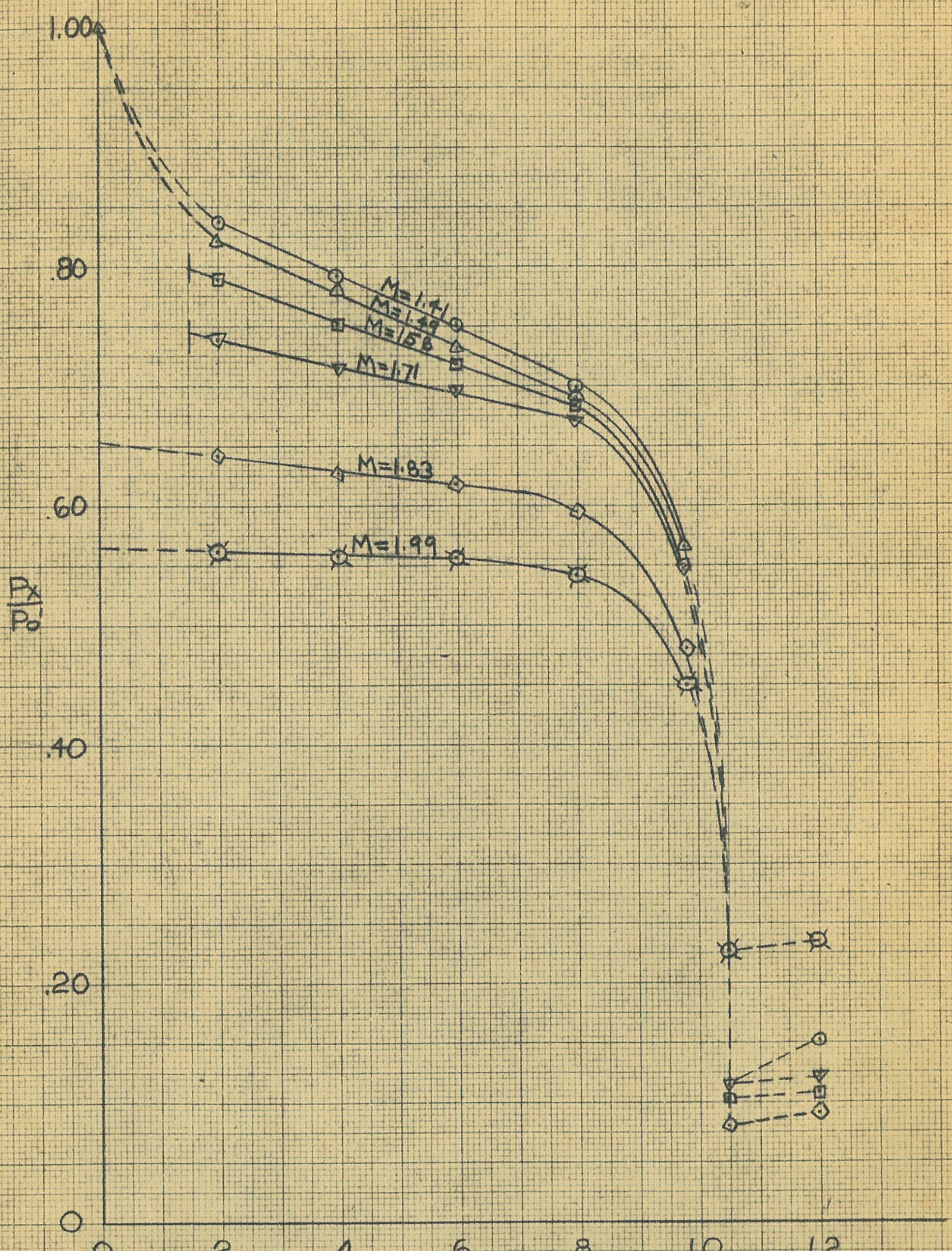

FIG. 21 75° CONE PRESSURE DISTRIBUTION

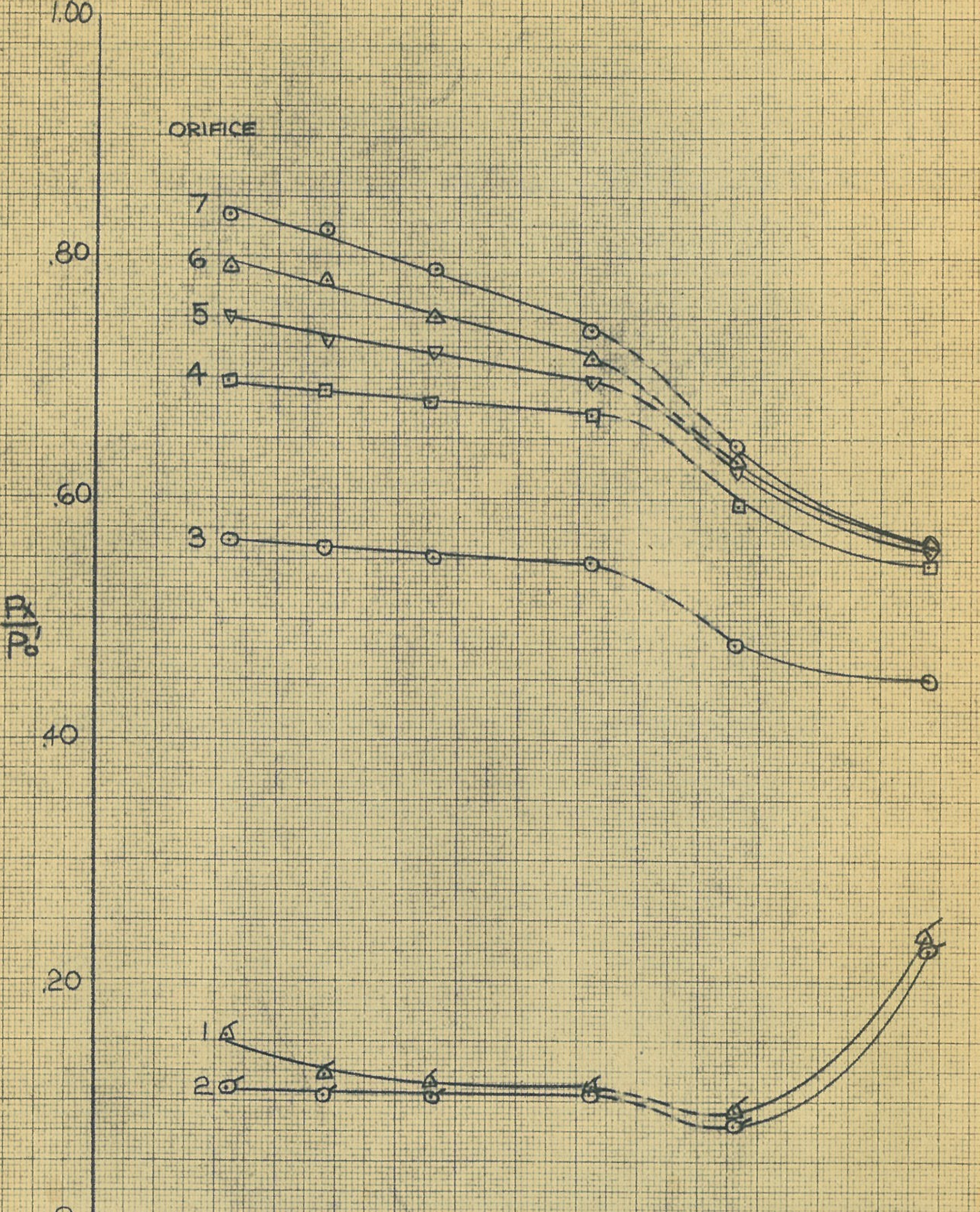

FIG. 22

COMPARISON
TOTAL HEAD RATIOS
CALCULATED VS. BLUNT CYLINDER

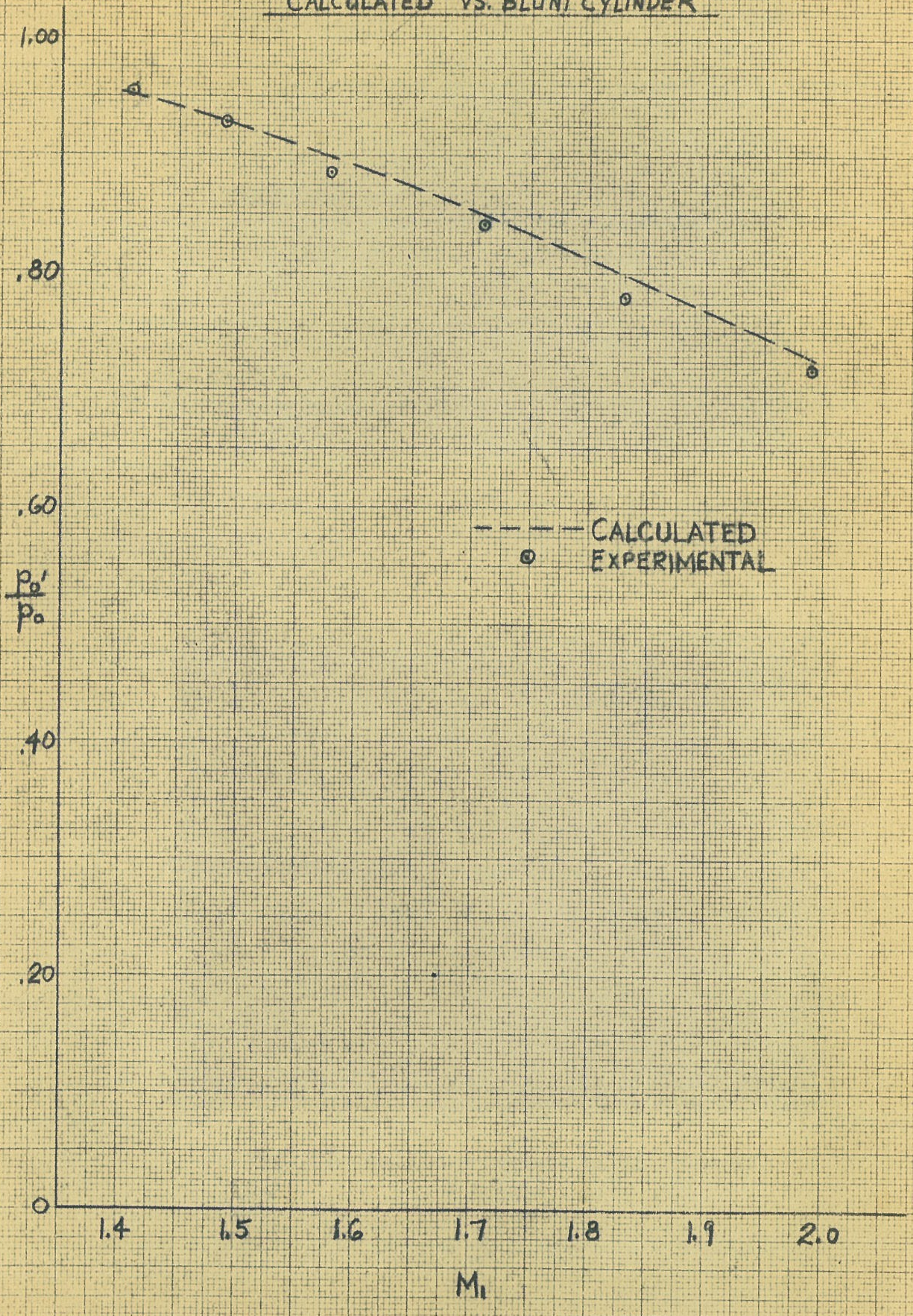

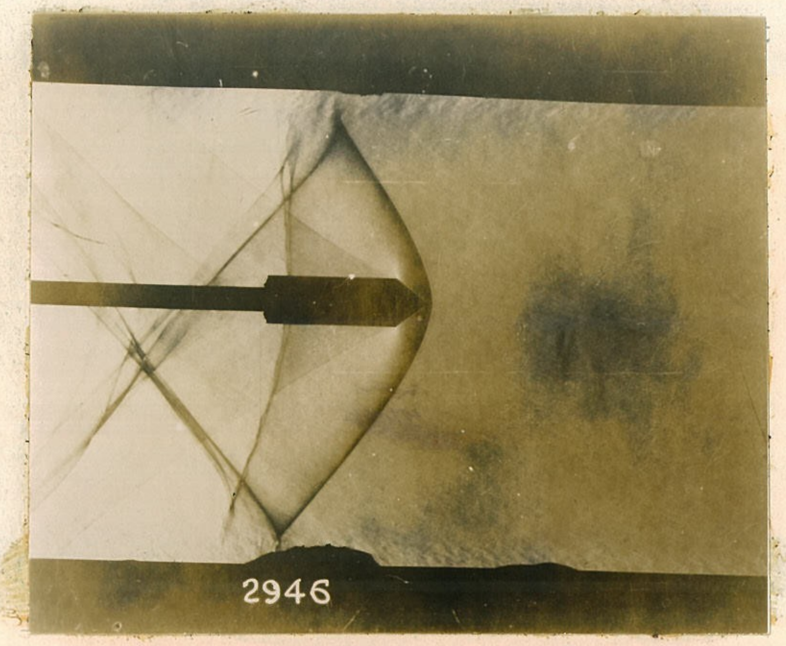

Fig. 23--Schlieren Picture of 75° cone at
M = 1.41

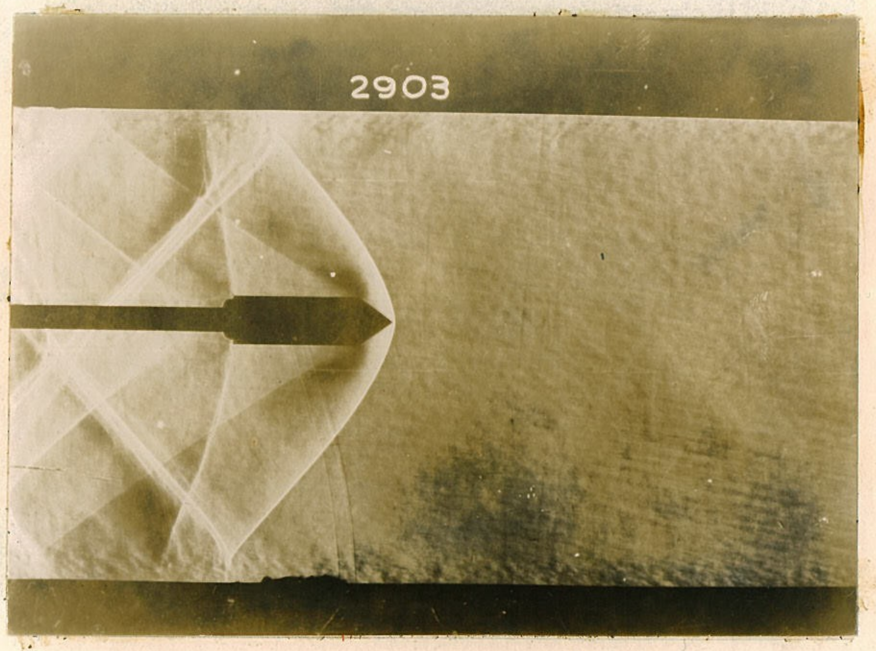

Fig. 24--Schlieren Picture of 75° cone at
M = 1.49

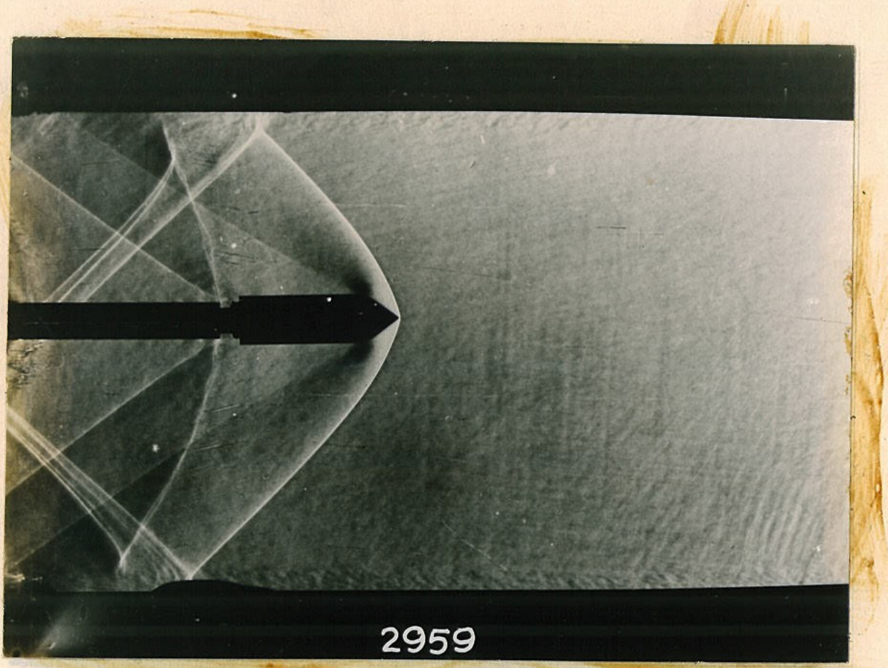

Fig. 25--Schlieren Picture of 75° cone at
M = 1.58

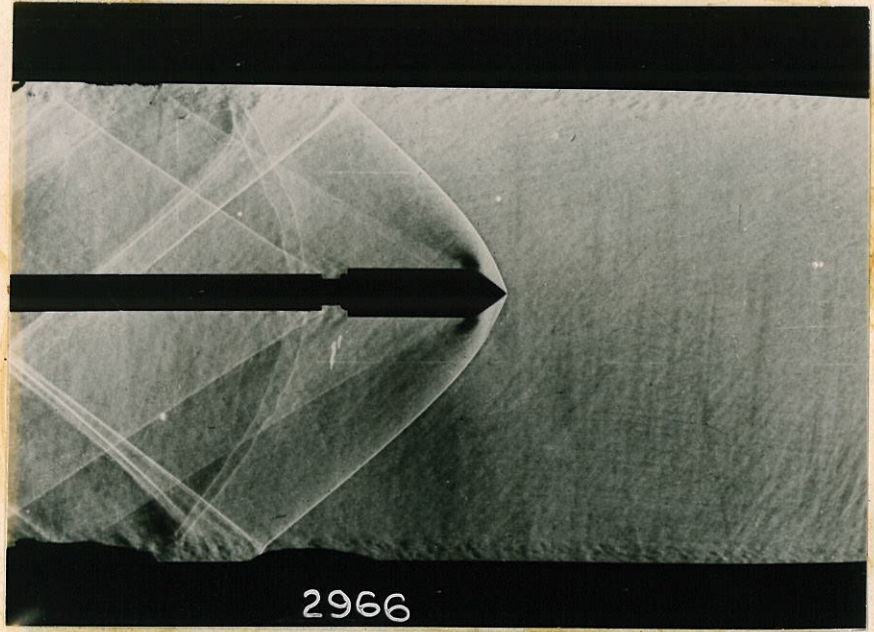

Fig. 26--Schlieren Picture of 75° cone at
M = 1.71

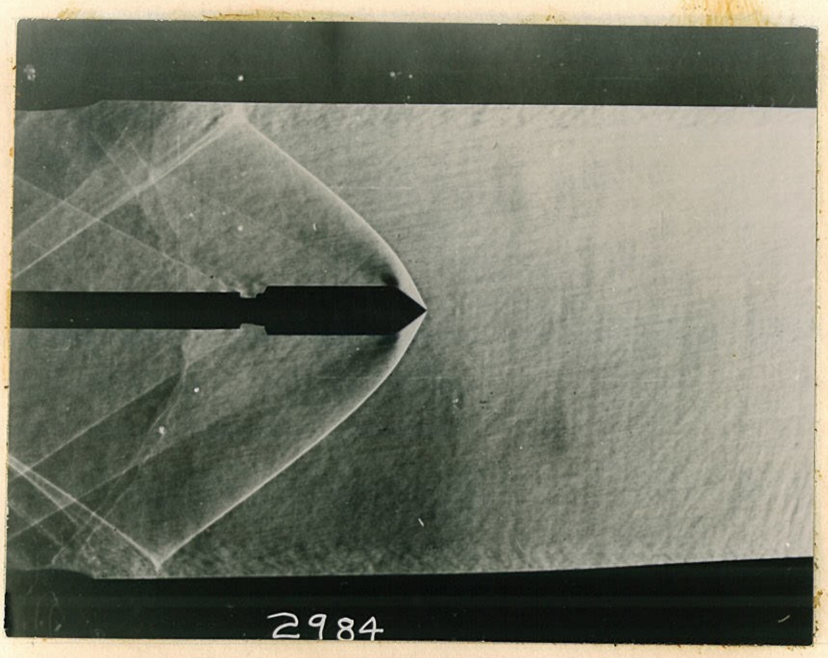

Fig. 27--Schlieren Picture of 75° cone at $M = 1.83$

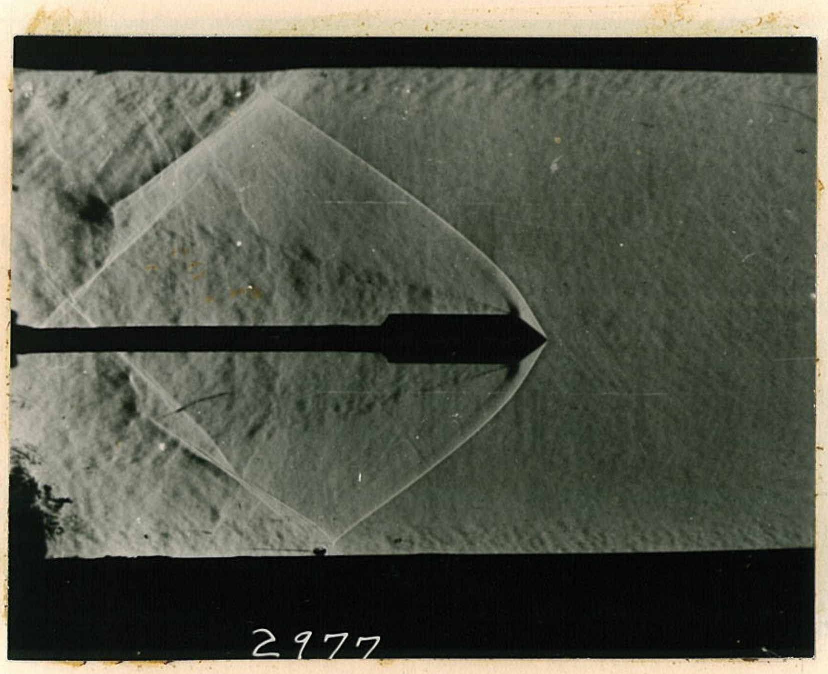

Fig. 28--Schlieren Picture of 75° cone at $M = 1.99$

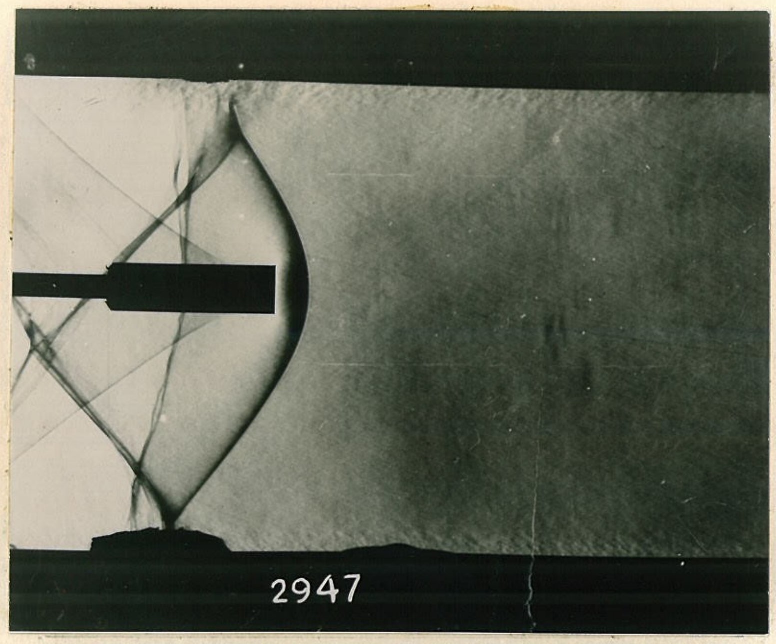

Fig. 29--Schlieren Picture of Blunt Cylinder at
M = 1.41

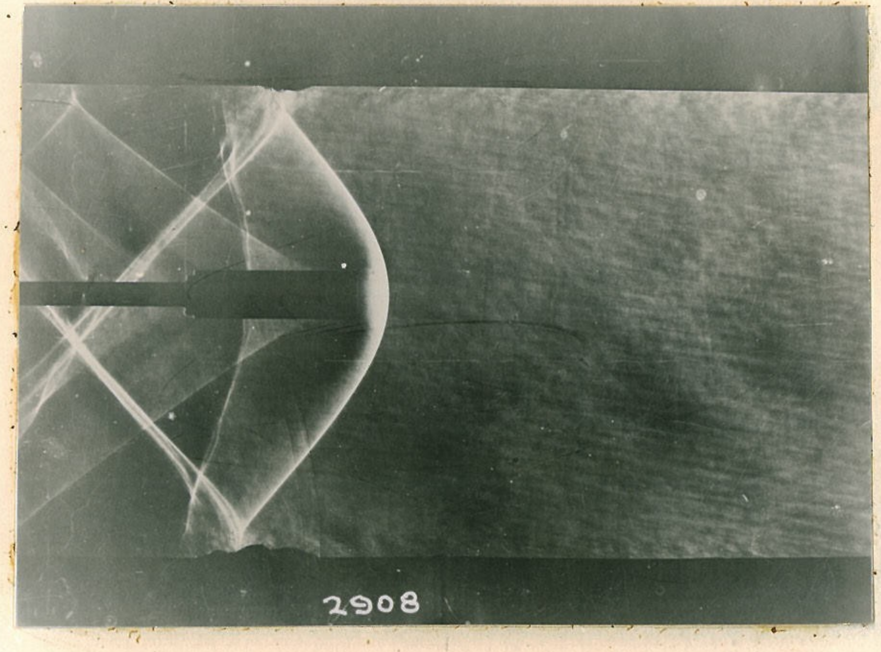

Fig. 30--Schlieren Picture of Blunt Cylinder at
M = 1.49

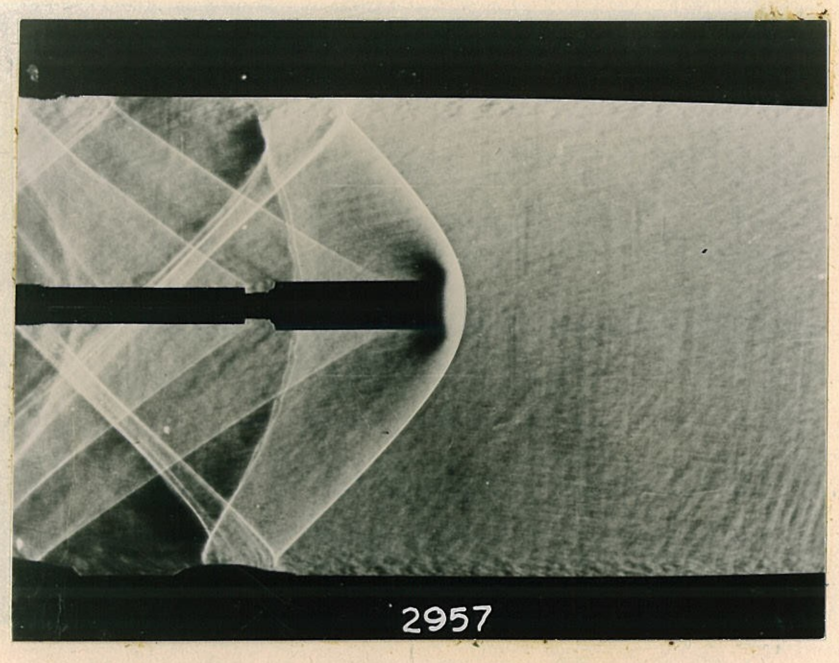

Fig. 31--Schlieren Picture of Blunt Cylinder at
M = 1.58

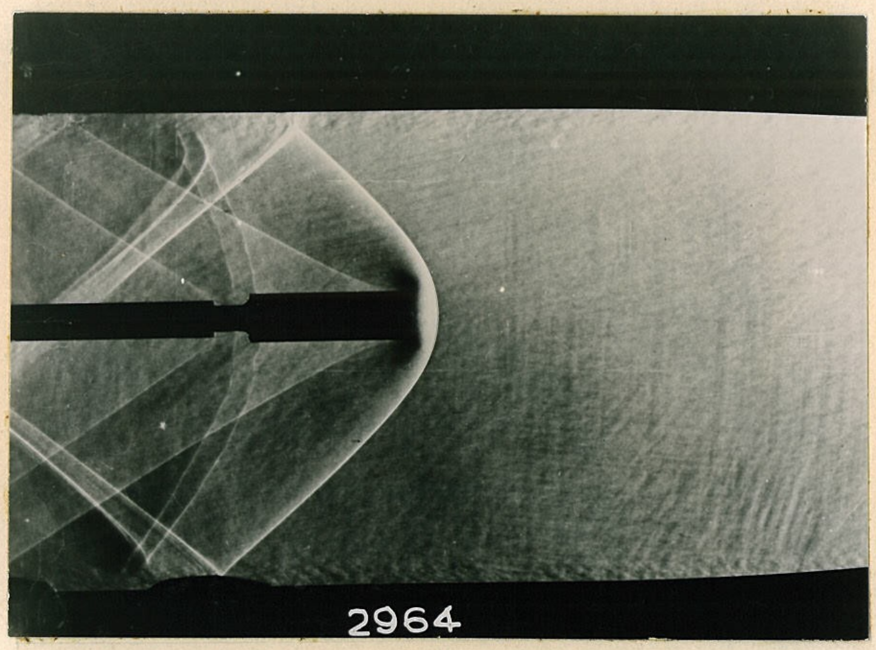

Fig. 32--Schlieren Picture of Blunt Cylinder at
M = 1.71

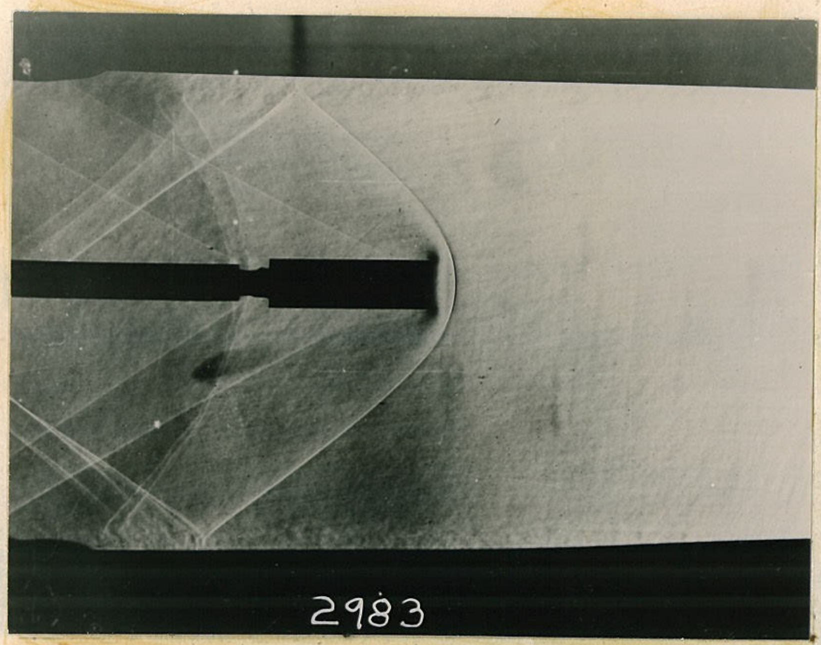

Fig. 33--Schlieren Picture of Blunt Cylinder at
M = 1.83

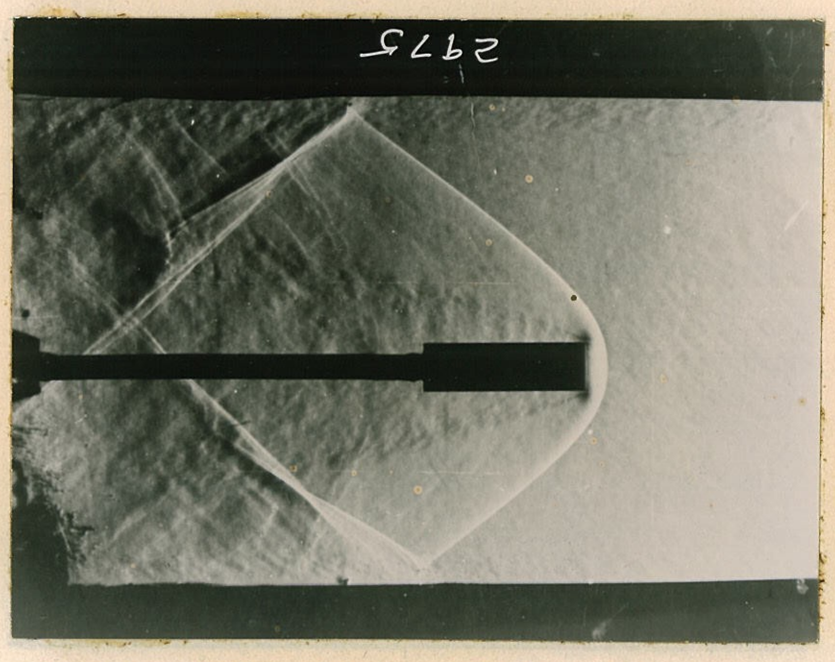

Fig. 34--Schlieren Picture of Blunt Cylinder at
M = 1.99

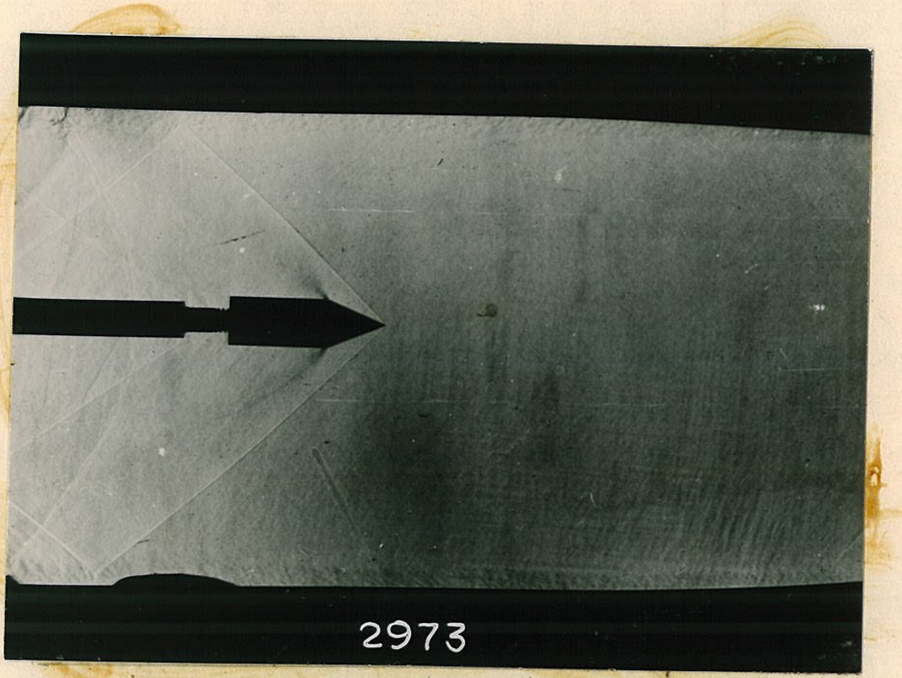

Fig. 35--Schlieren Picture of 45° cone at M = 1.71

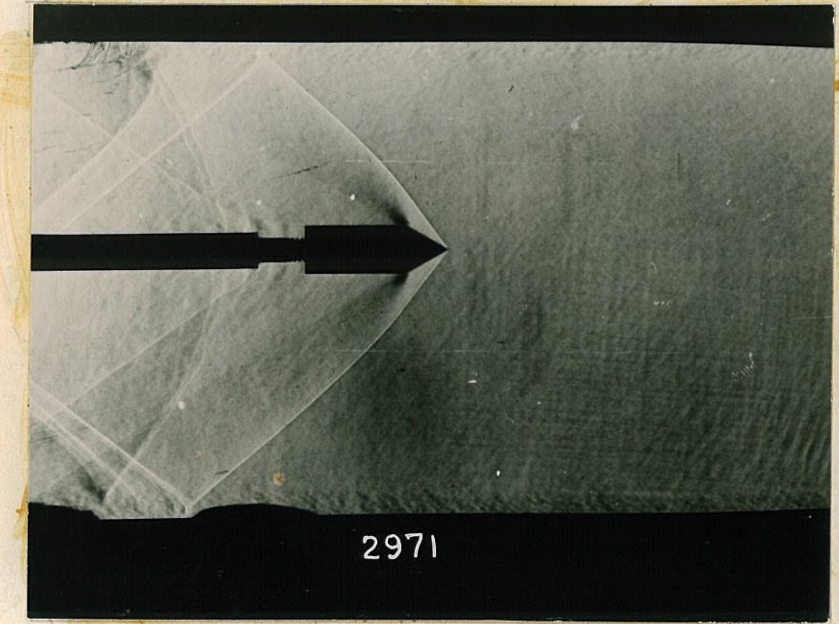

Fig. 36--Schlieren Picture of 60° cone at M = 1.71

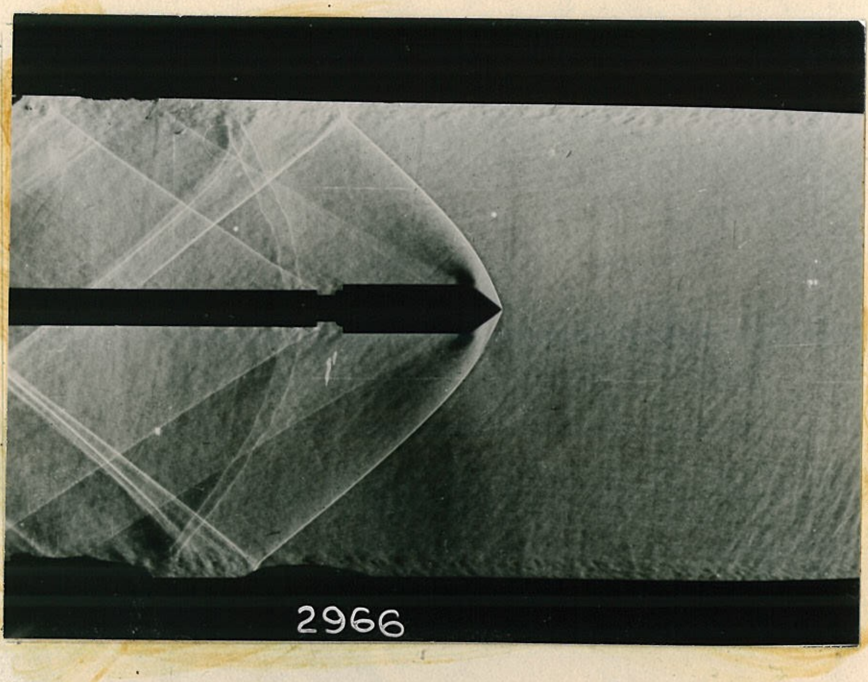

Fig. 37--Schlieren Picture of 75° cone at M = 1.71

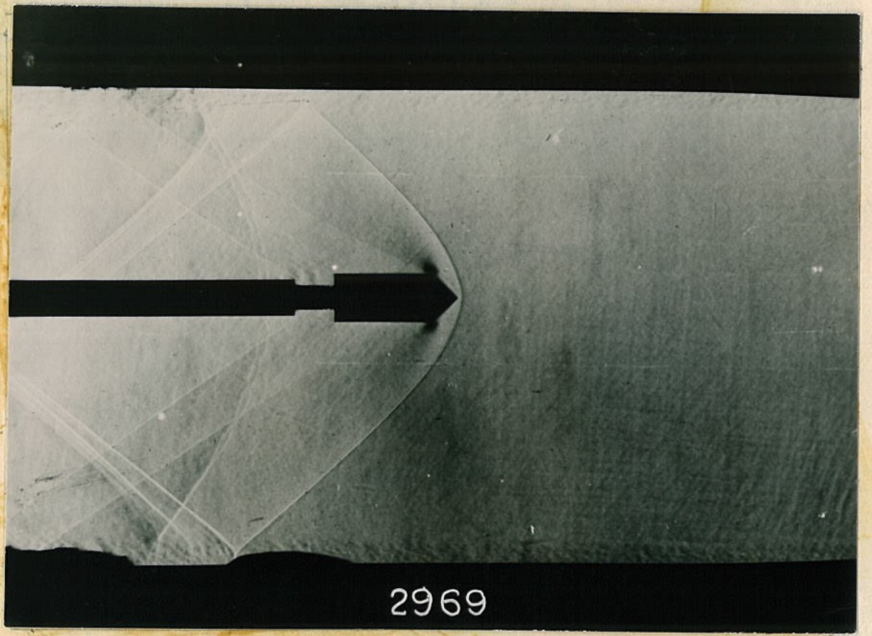

Fig. 38--Schlieren Picture of 90° cone at M = 1.71

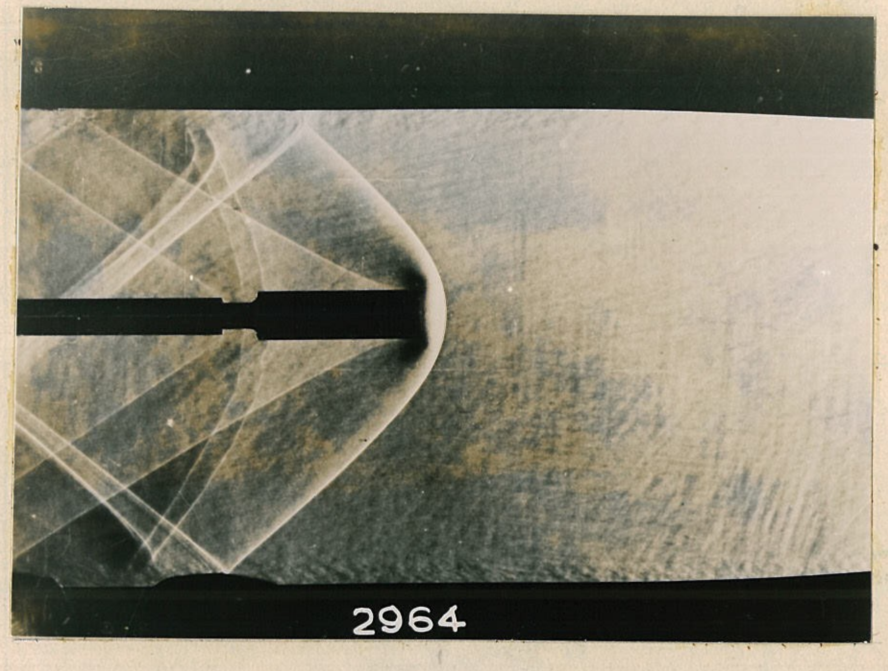

Fig. 39--Schlieren Picture of Blunt Cylinder at
M = 1.71

FIG. 40: 75° CONE $M_1 = 1.41$

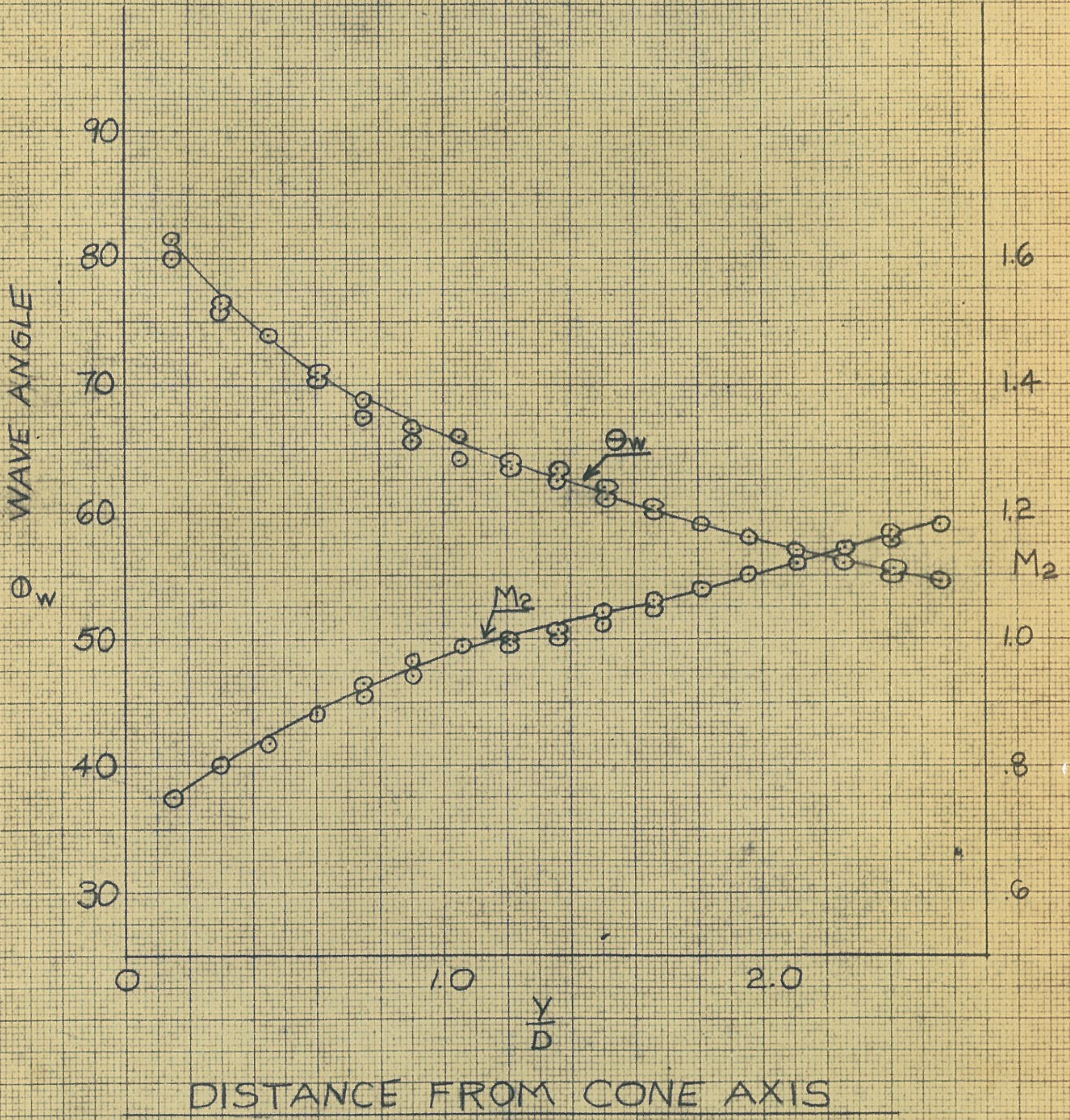

FIG. 41: 75° CONE $M_1 = 1.49$

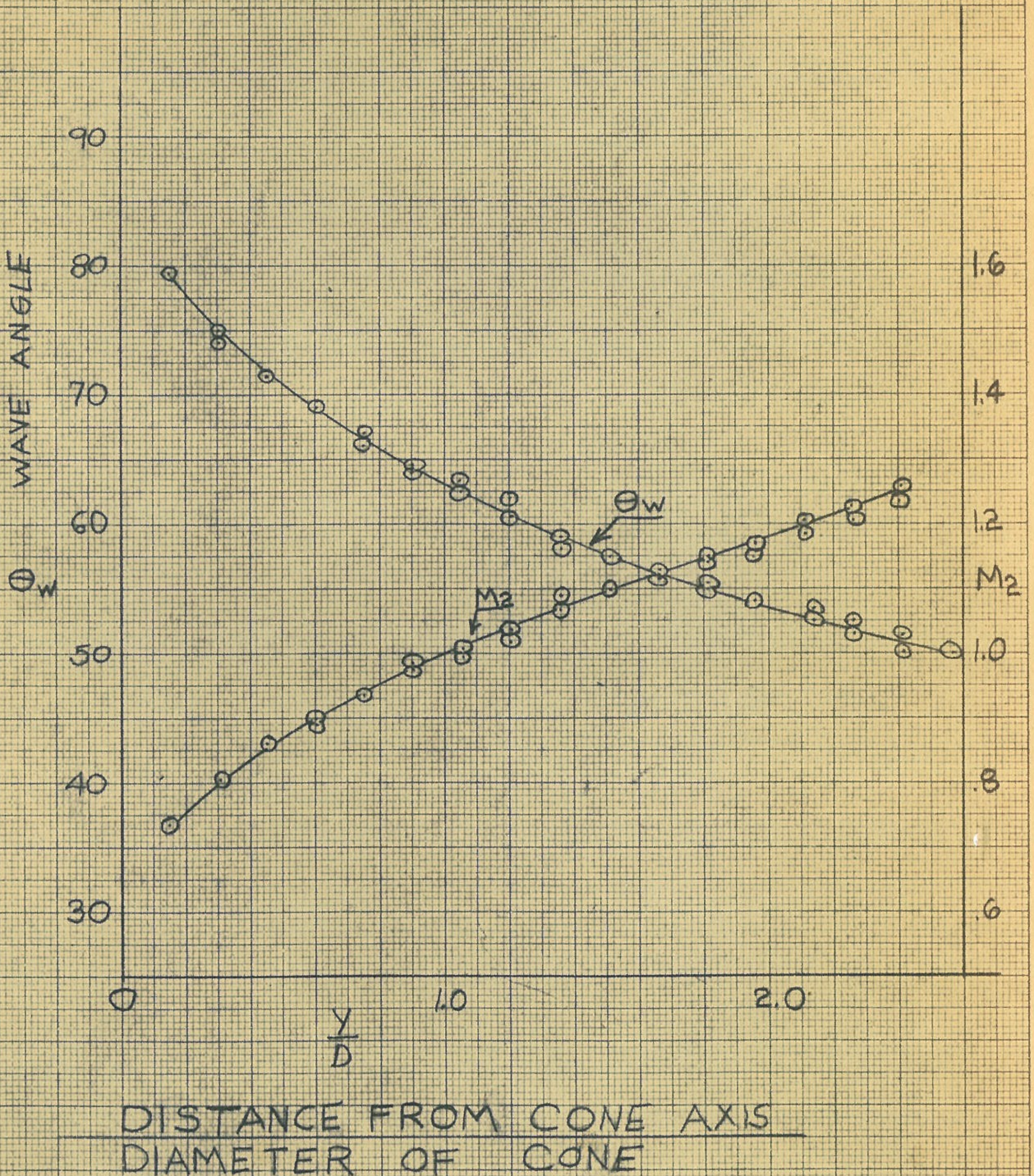

FIG. 42: 75° CONE $M_1 = 1.58$

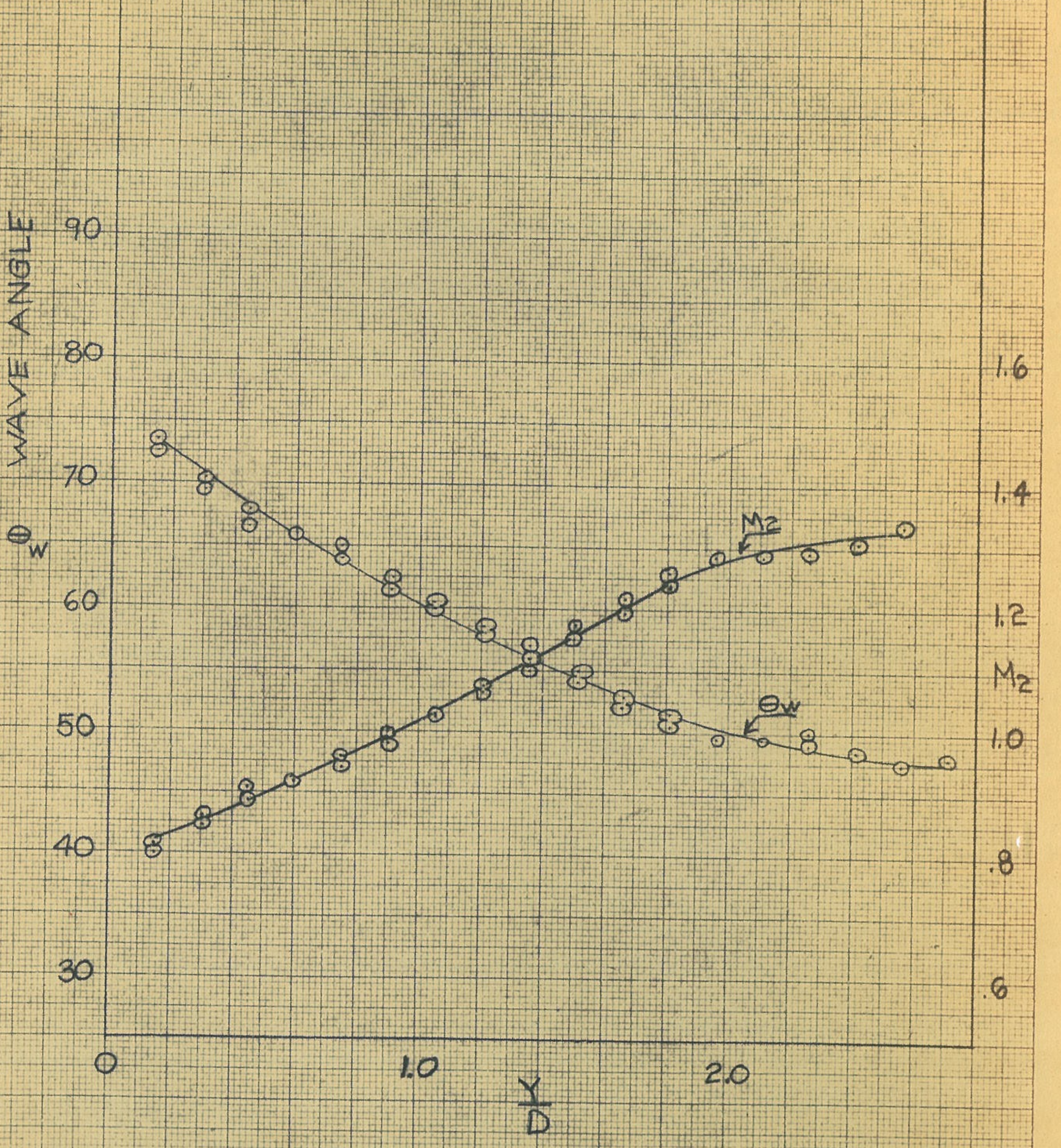

DISTANCE FROM CONE AXIS / DIAMETER OF CONE

FIG. 43: 75° CONE $M_1 = 1.71$

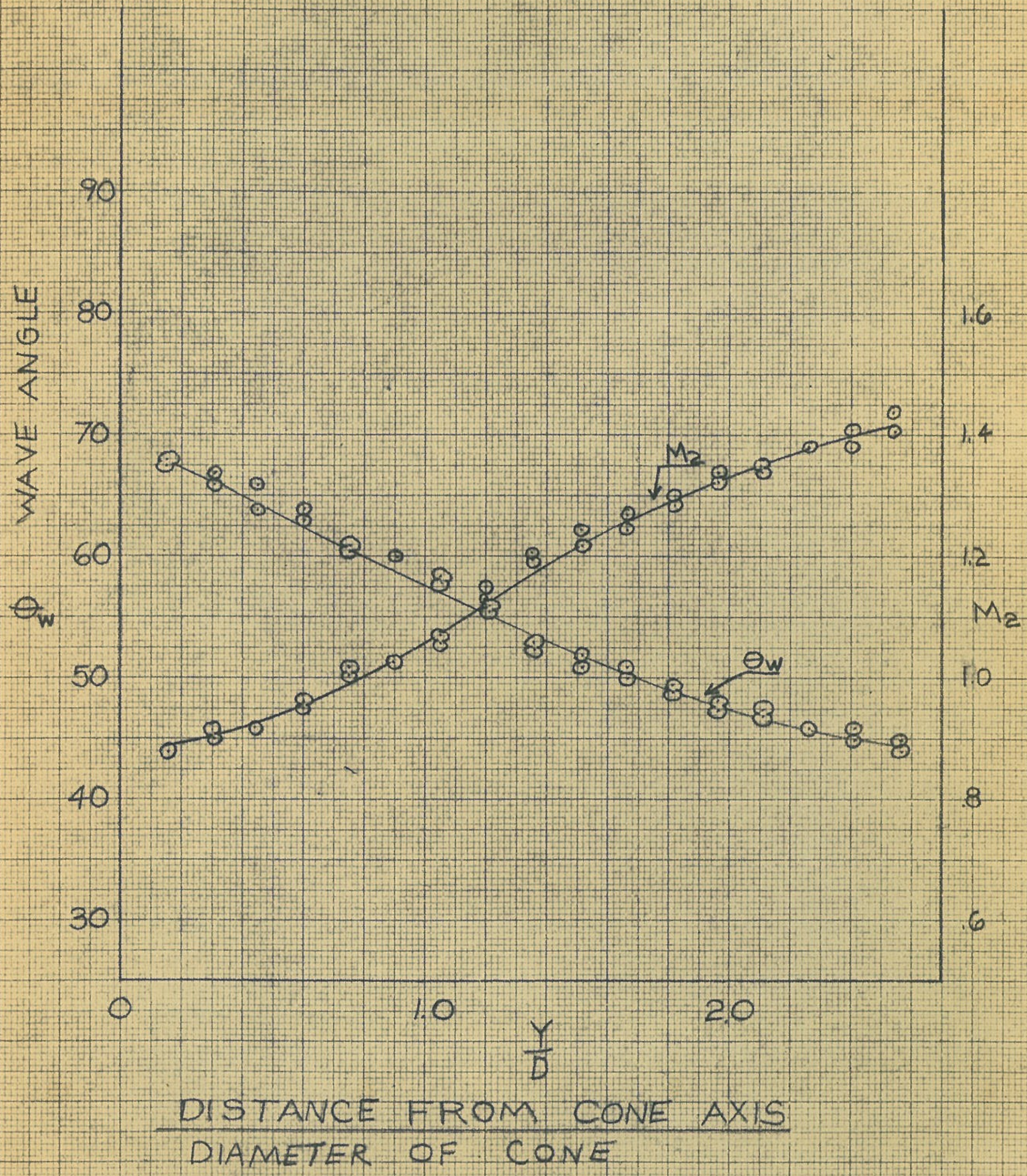

FIG. 44

75° CONE

$M_1 = 1.83$

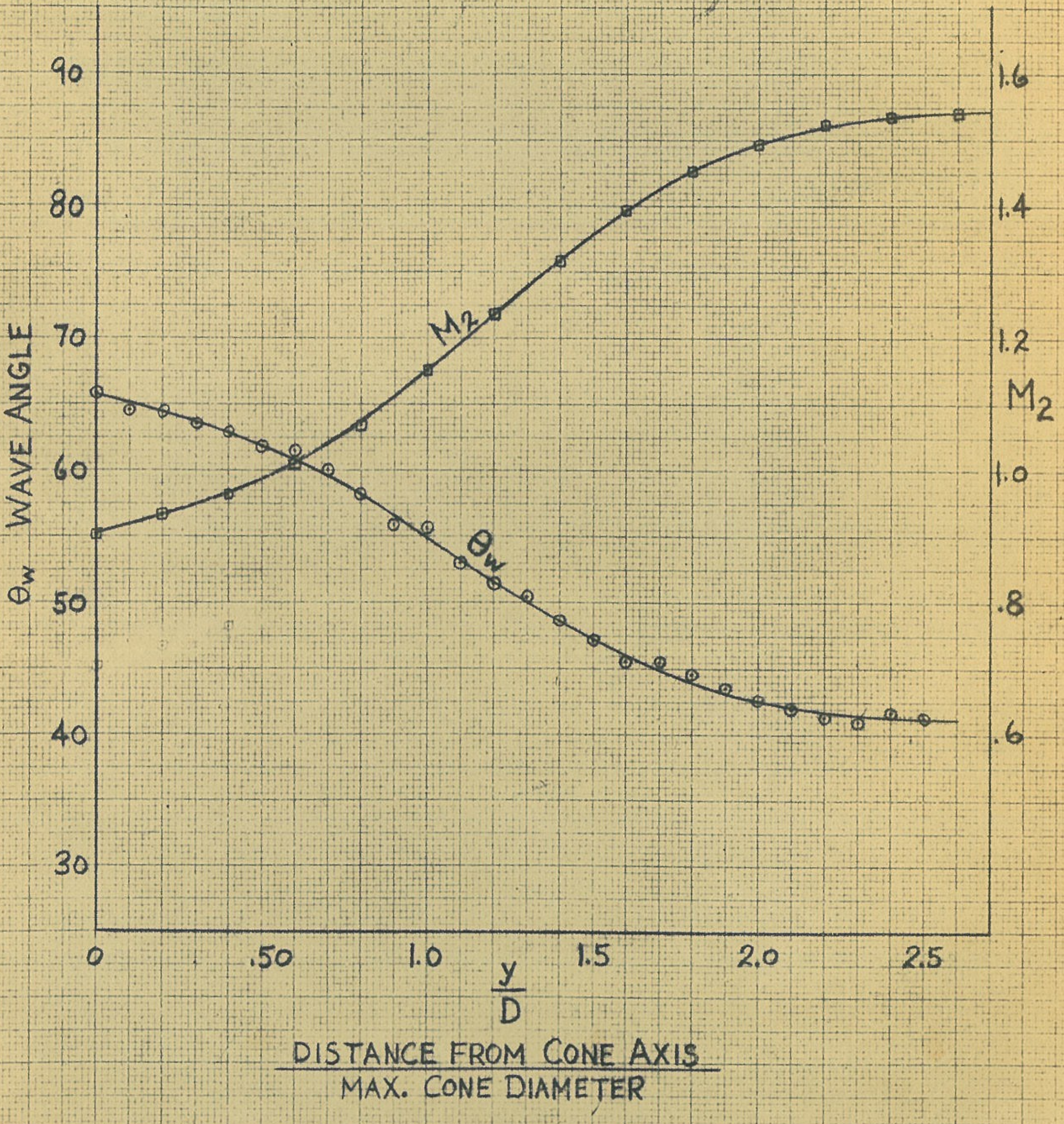

FIG. 45: 75° CONE $M_1 = 1.99$

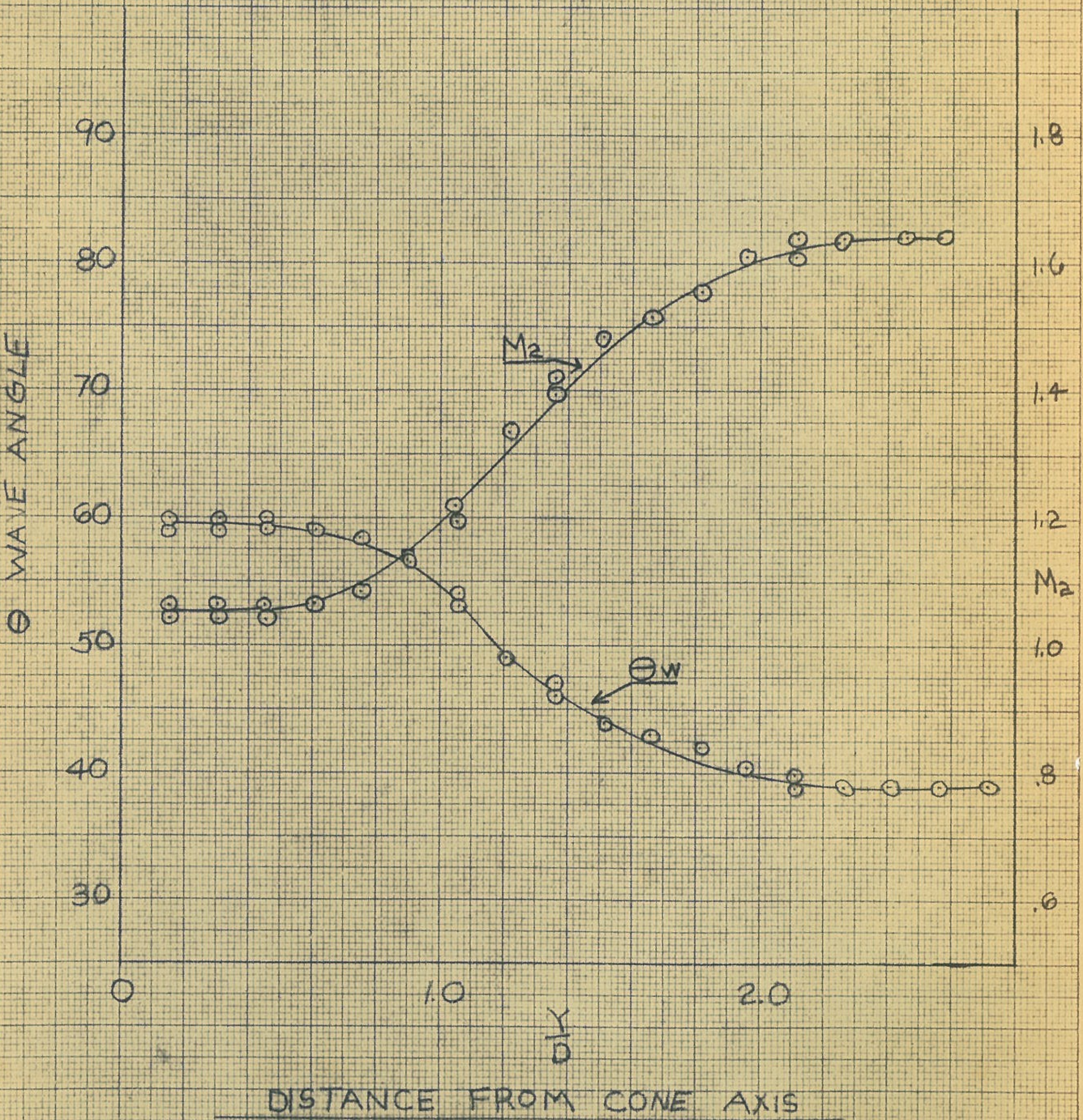

$\frac{\text{DISTANCE FROM CONE AXIS}}{\text{DIAMETER OF CONE}}$

FIG. 46 M_2 SUMMARY FOR 75° CONE

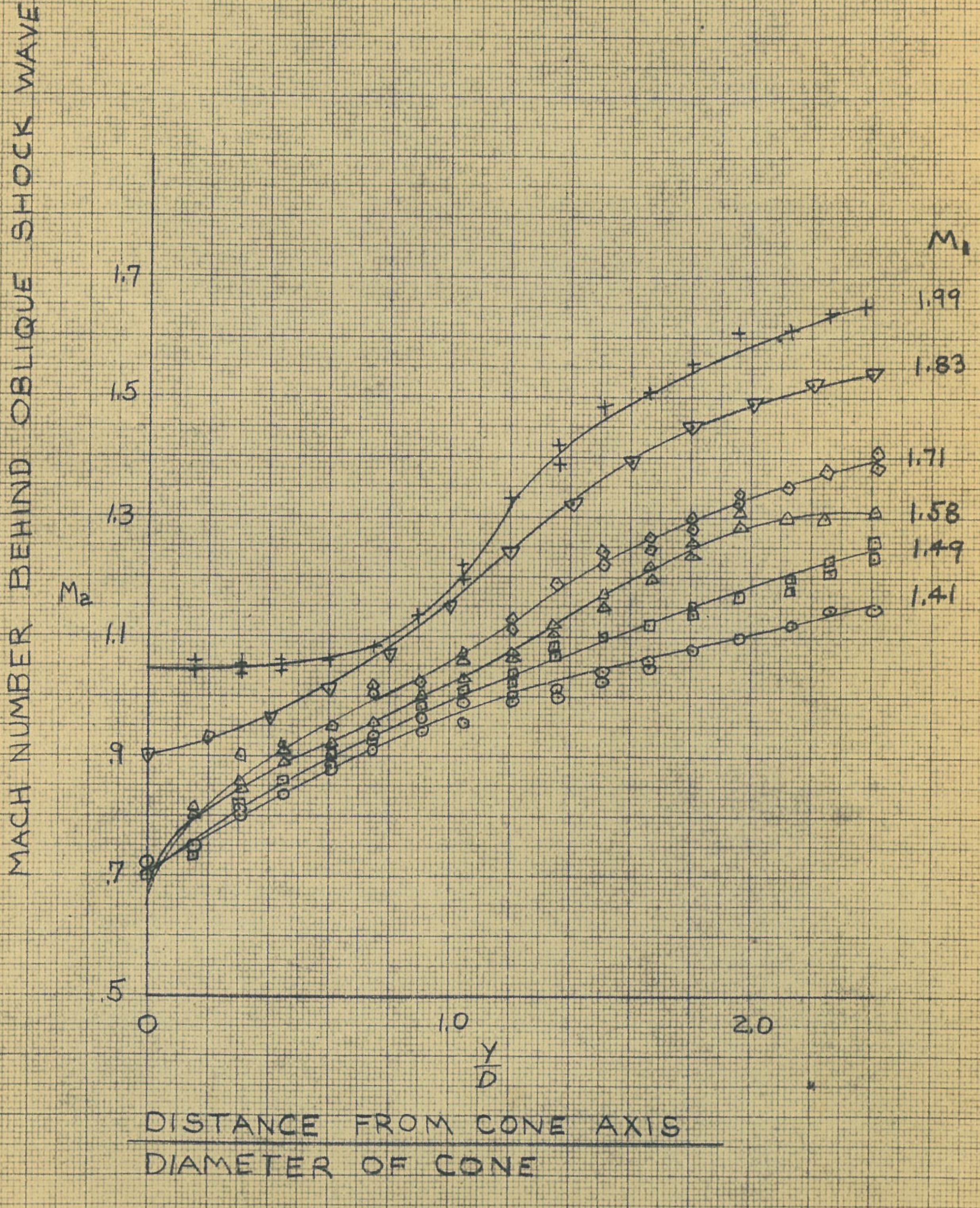

FIG.47 BLUNT CYLINDER $M_1 = 1.41$

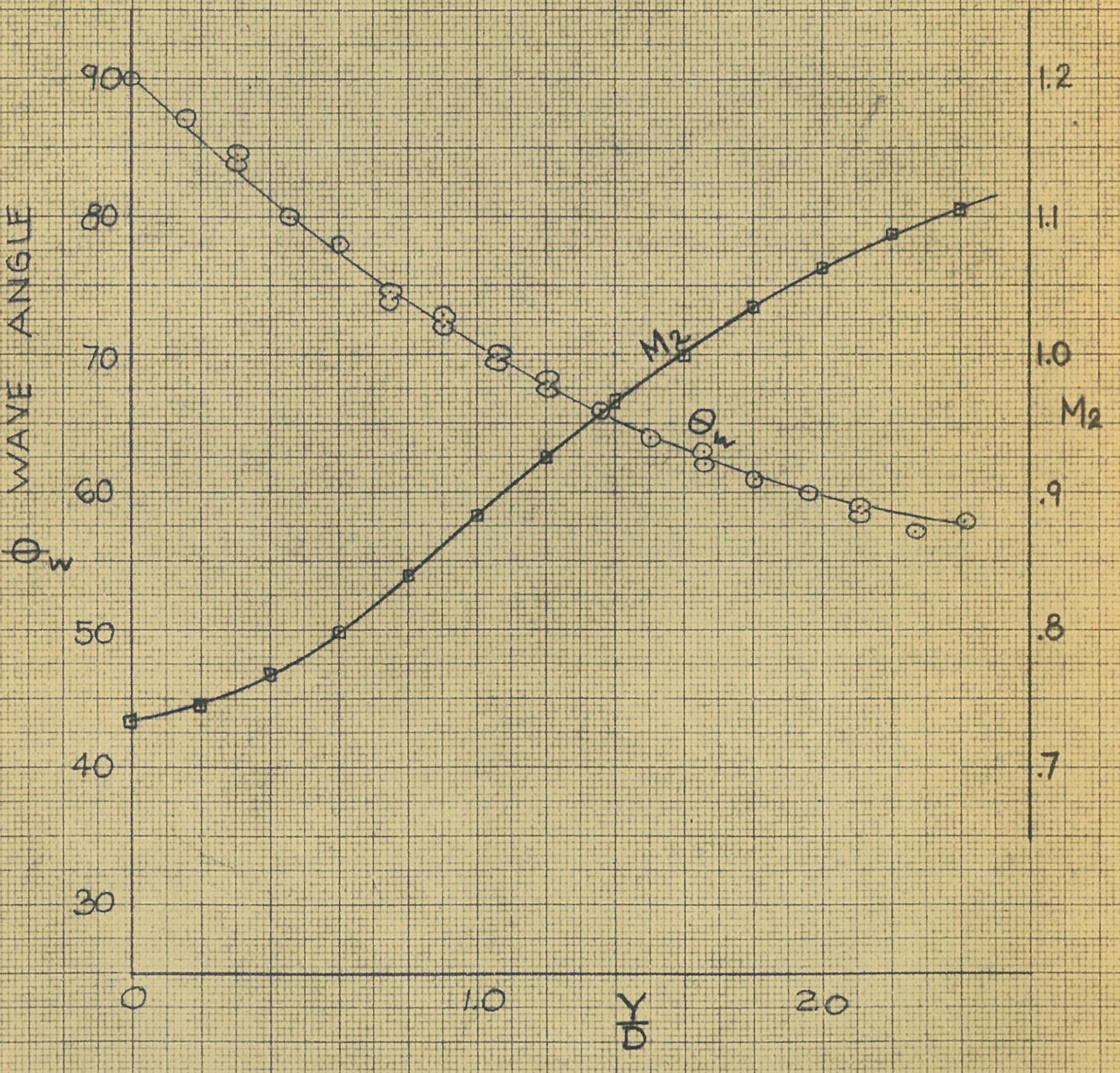

DISTANCE FROM CYLINDER AXIS
DIAMETER OF CYLINDER

FIG. 48 BLUNT CYLINDER $M_1 = 1.49$

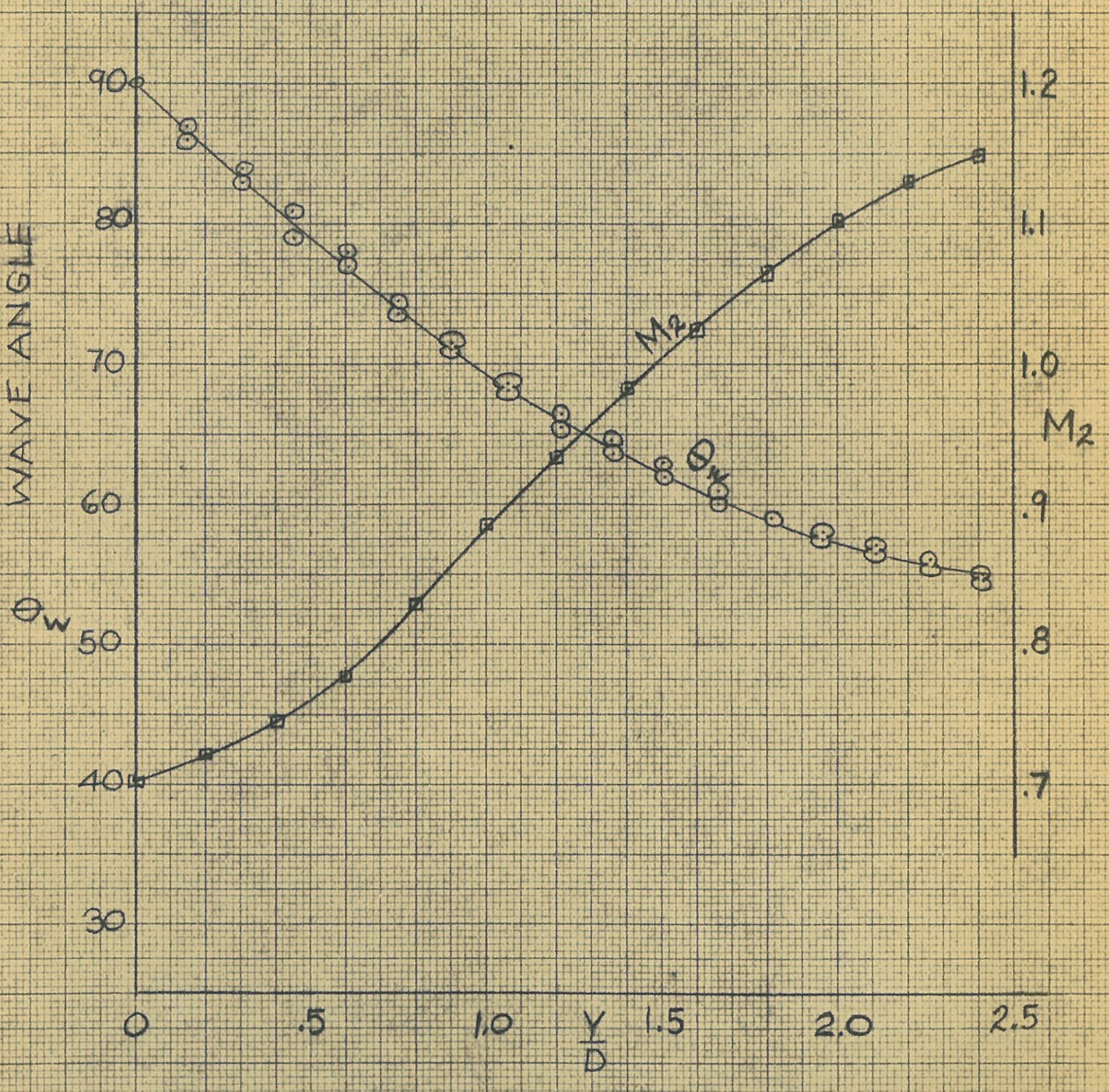

$\frac{\text{DISTANCE FROM CYLINDER AXIS}}{\text{DIAMETER OF CYLINDER}}$

FIG. 49 BLUNT CYLINDER $M_1 = 1.58$

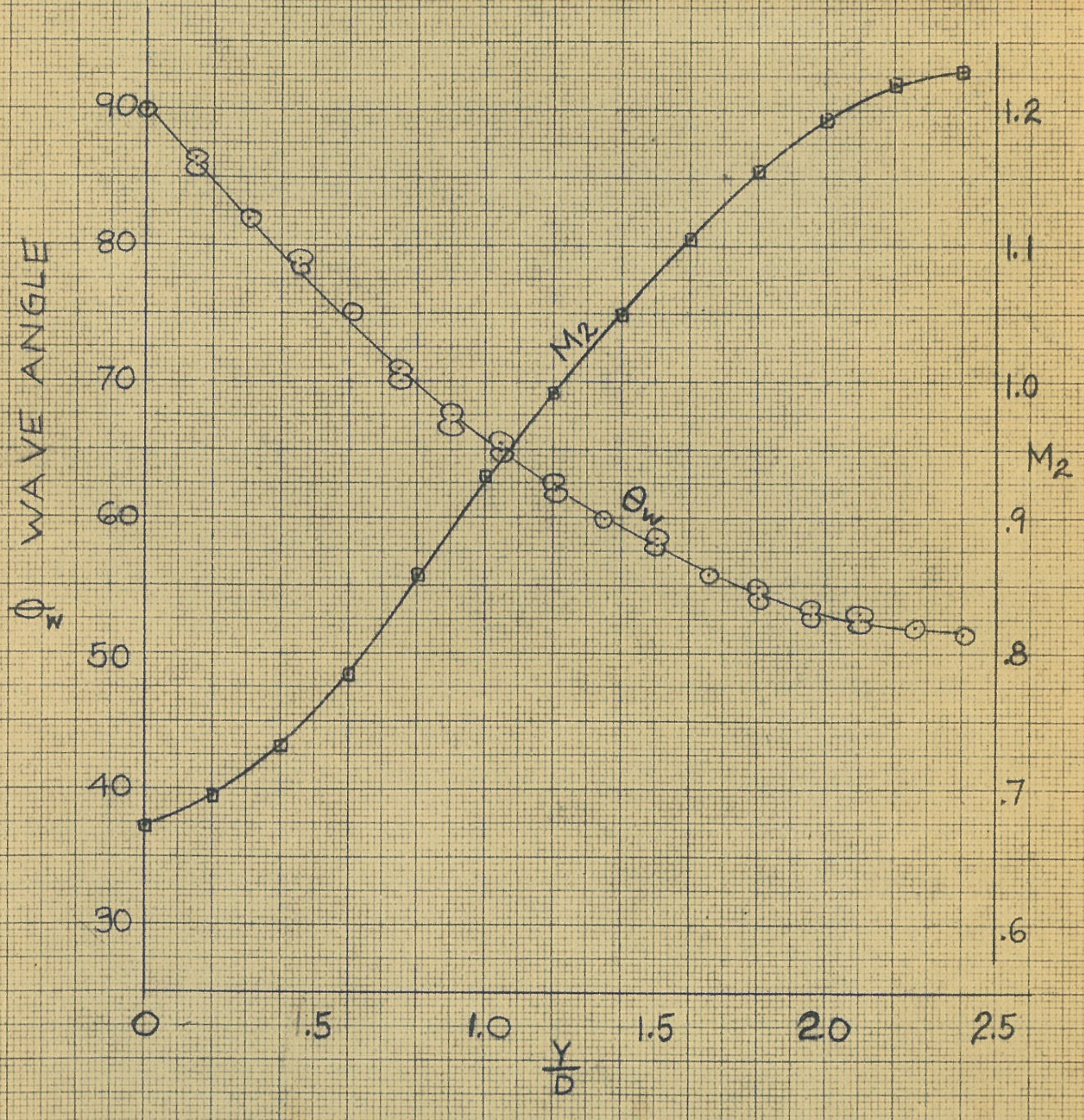

DISTANCE FROM CYLINDER AXIS / DIAMETER OF CYLINDER

FIG. 50 BLUNT CYLINDER $M_1 = 1.71$

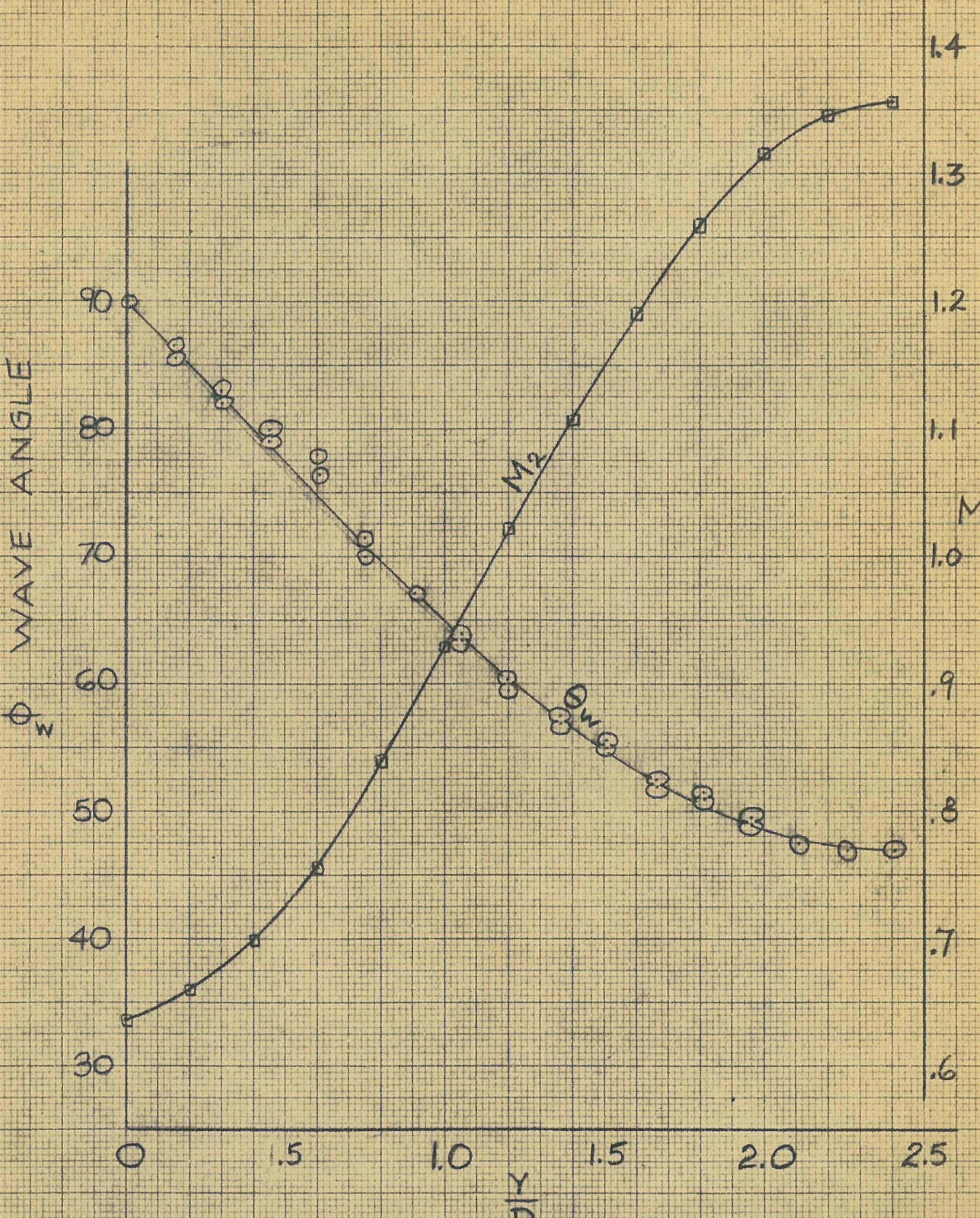

FIG. 51
BLUNT CYLINDER
$M_1 = 1.83$

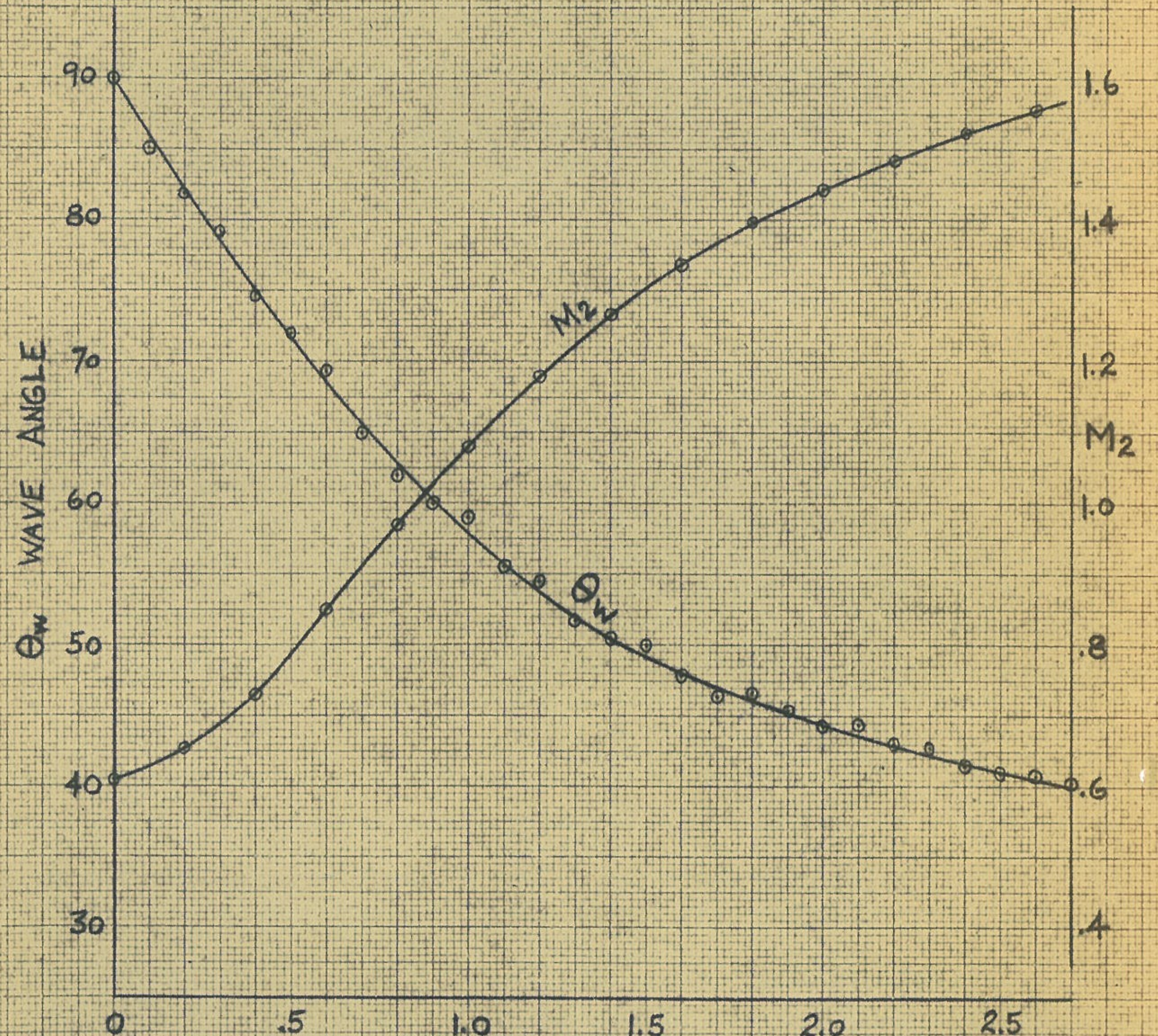

FIG. 52 BLUNT CYLINDER $M_1 = 1.99$

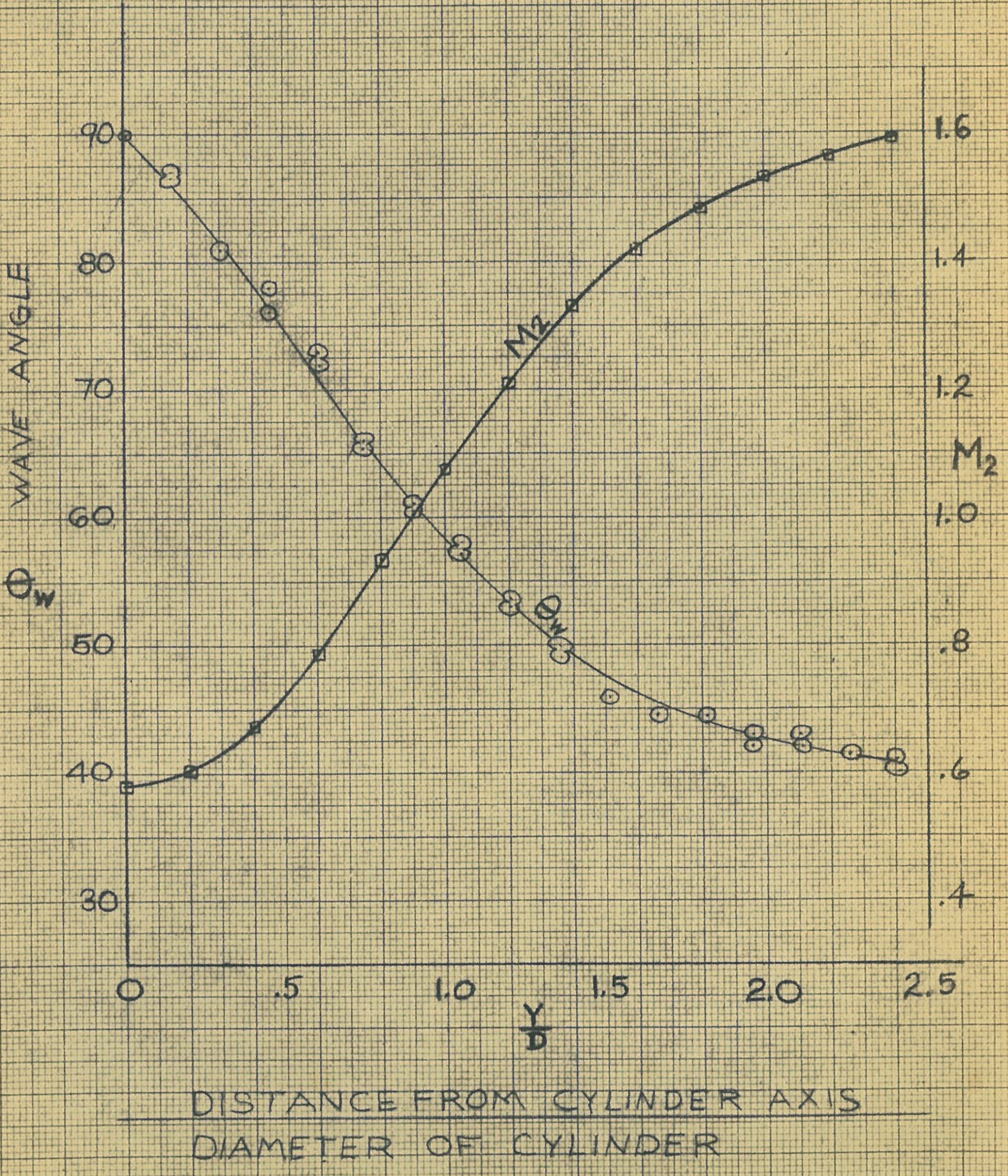

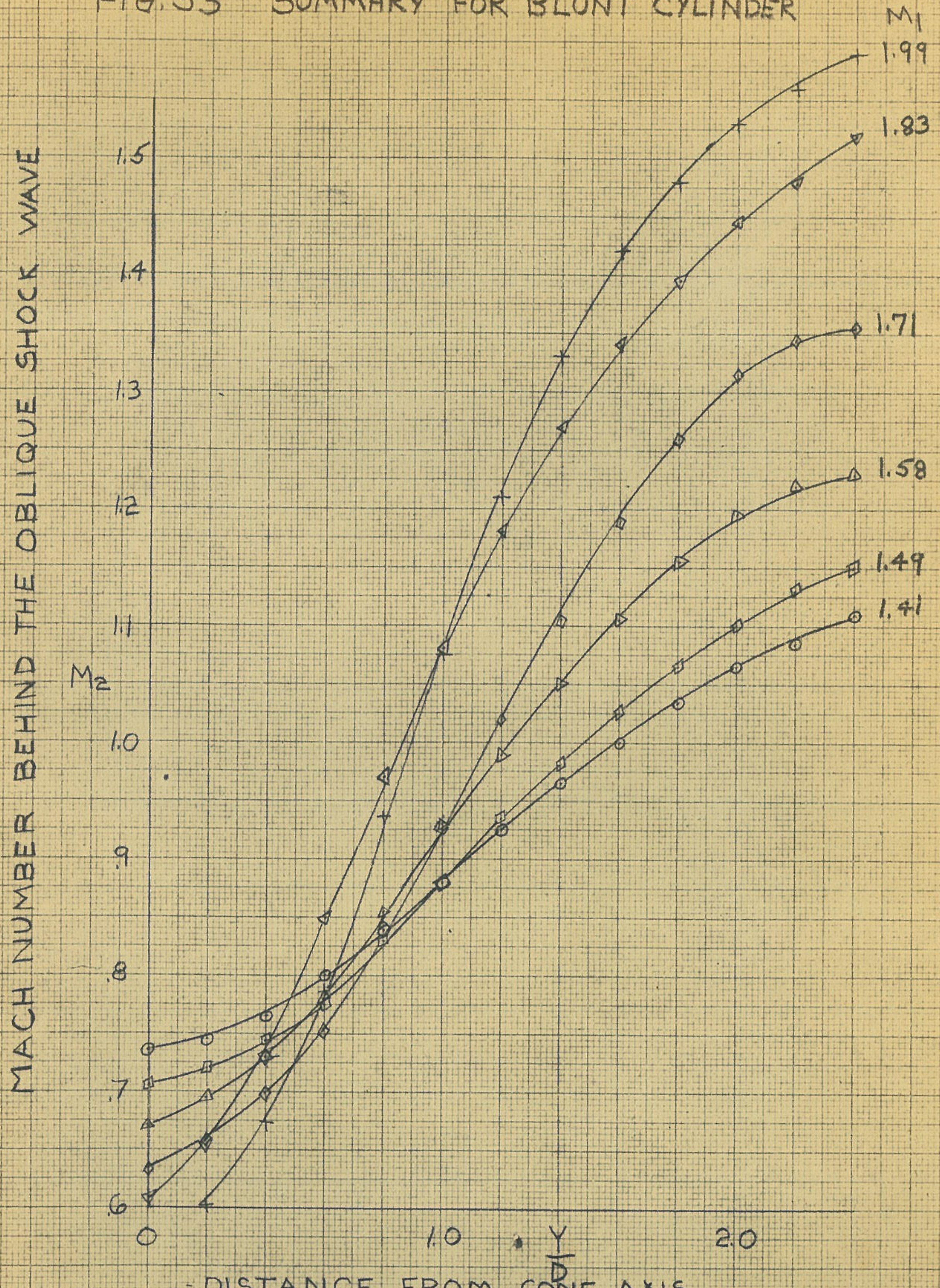

FIG. 53 SUMMARY FOR BLUNT CYLINDER

FIG. 54: SHOCK WAVE PATTERN 75° CONE

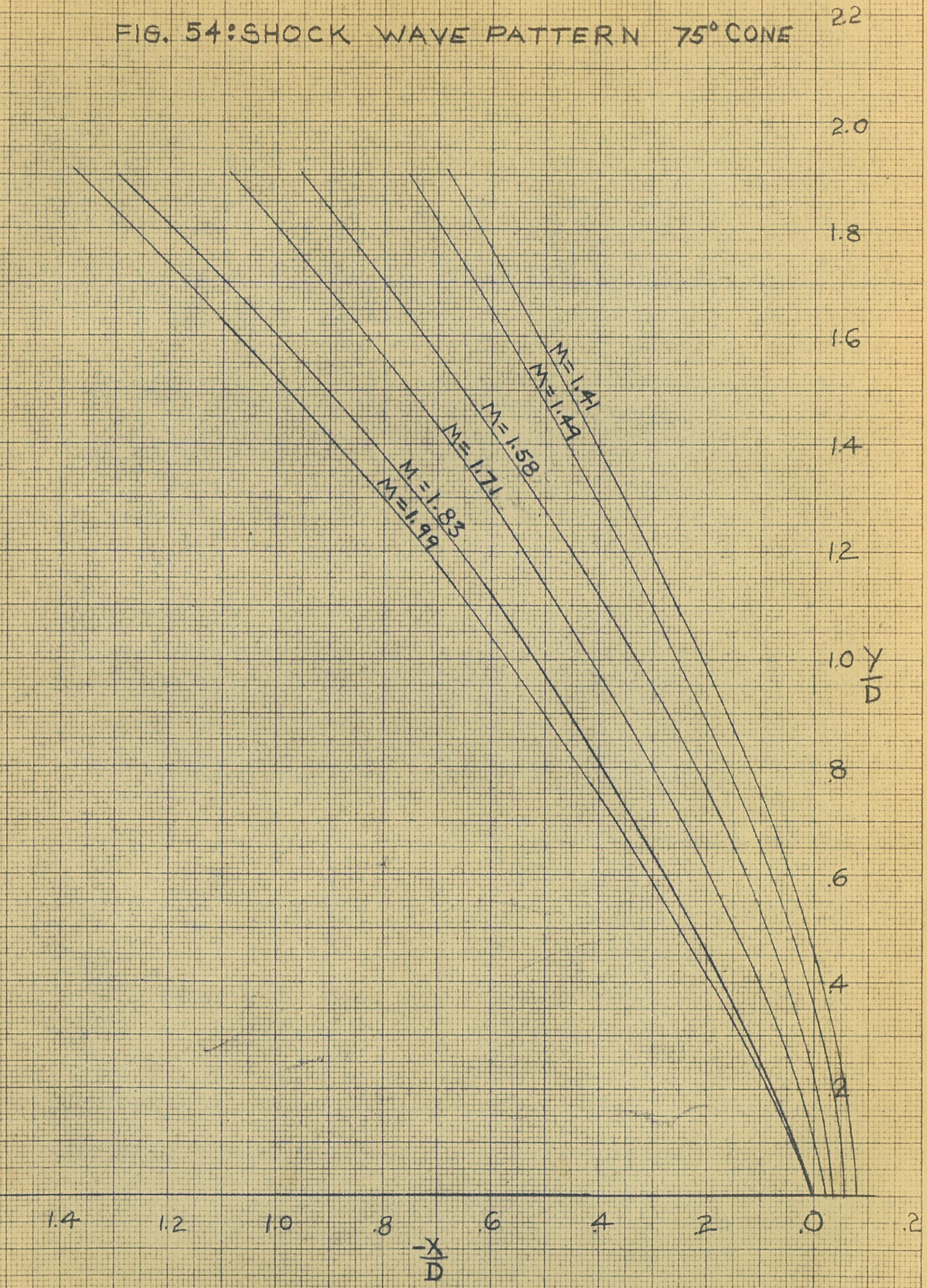

FIG. 55: SHOCK WAVE PATTERN BLUNT CONE

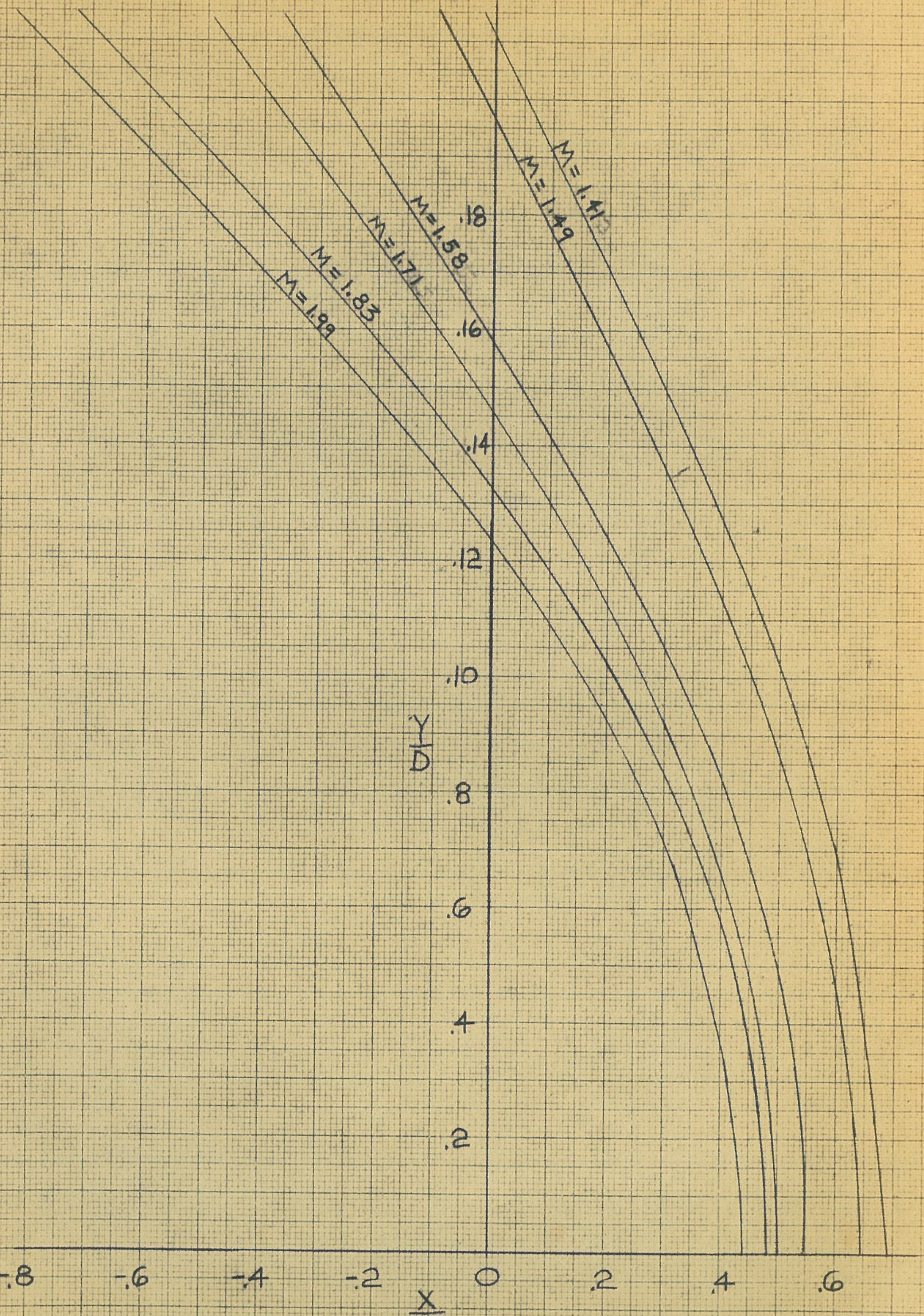

FIG. 56: SHOCK WAVE PATTERN
$M_1 = 1.71$

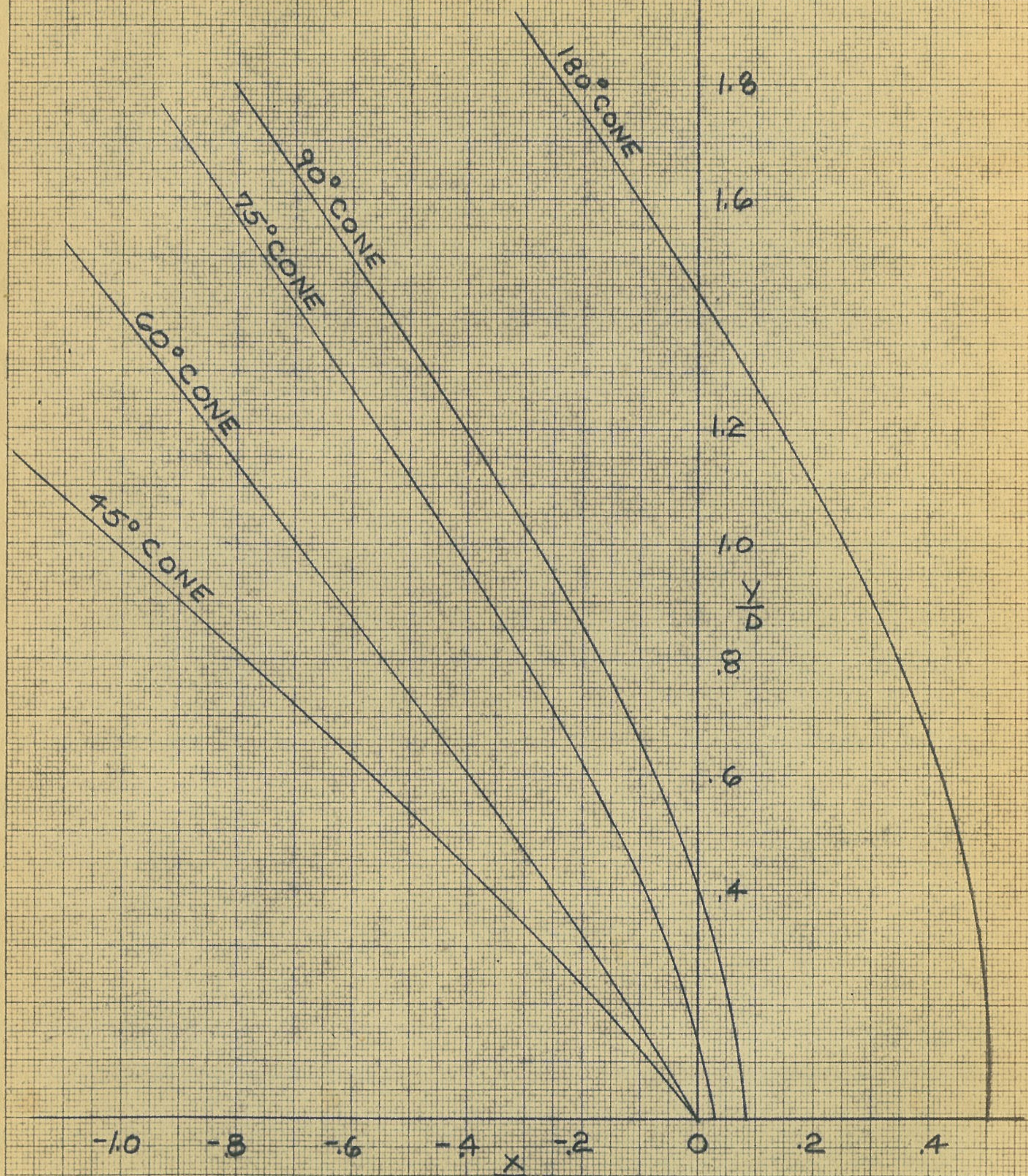

FIG. 57

SHOCK WAVE PATTERN

M = 1.83

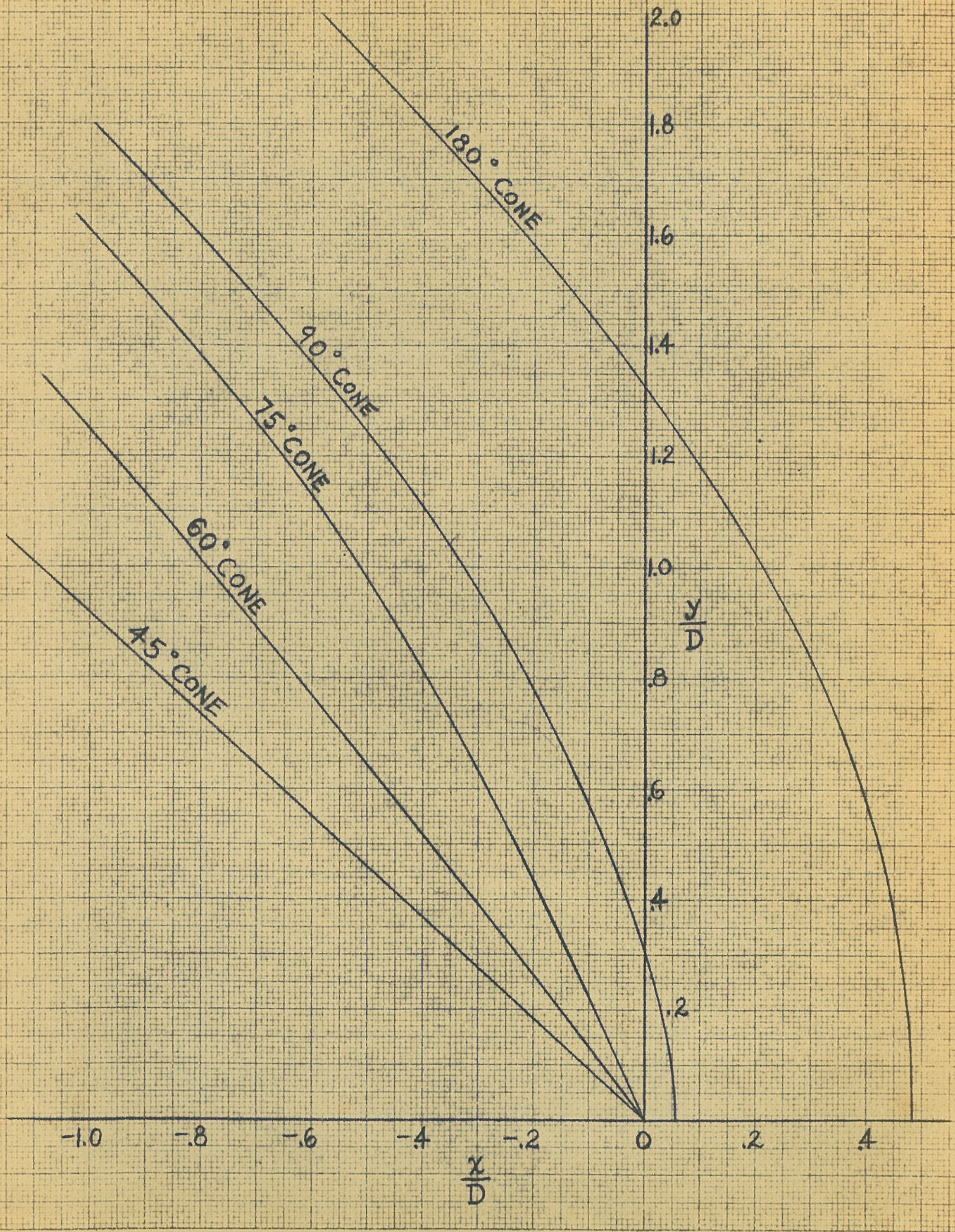

FIG.58 SHOCK WAVE PATTERN
$M_1 = 1.99$

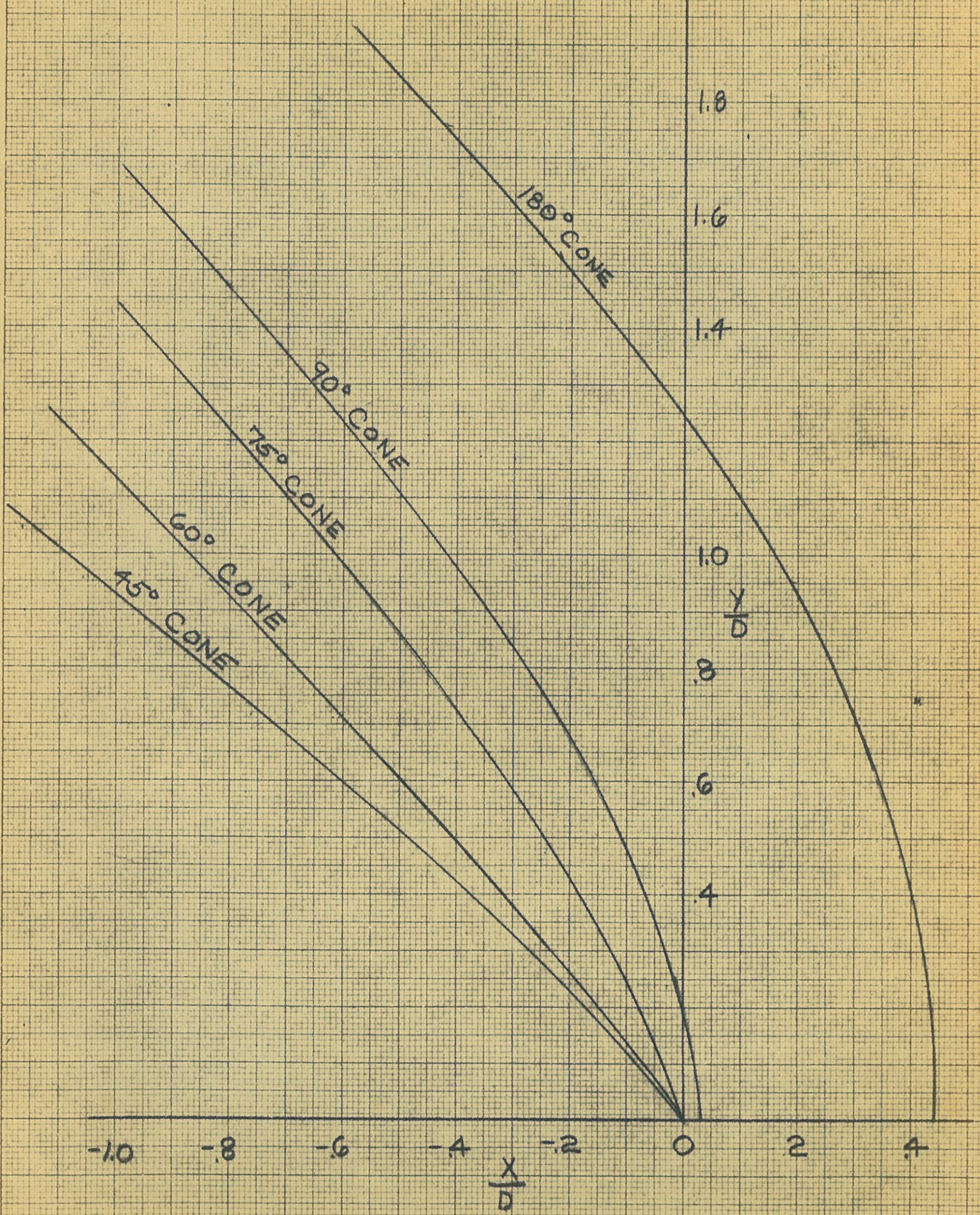

FIG. 59: DETACHED SHOCK WAVE DISTANCE
75° CONE

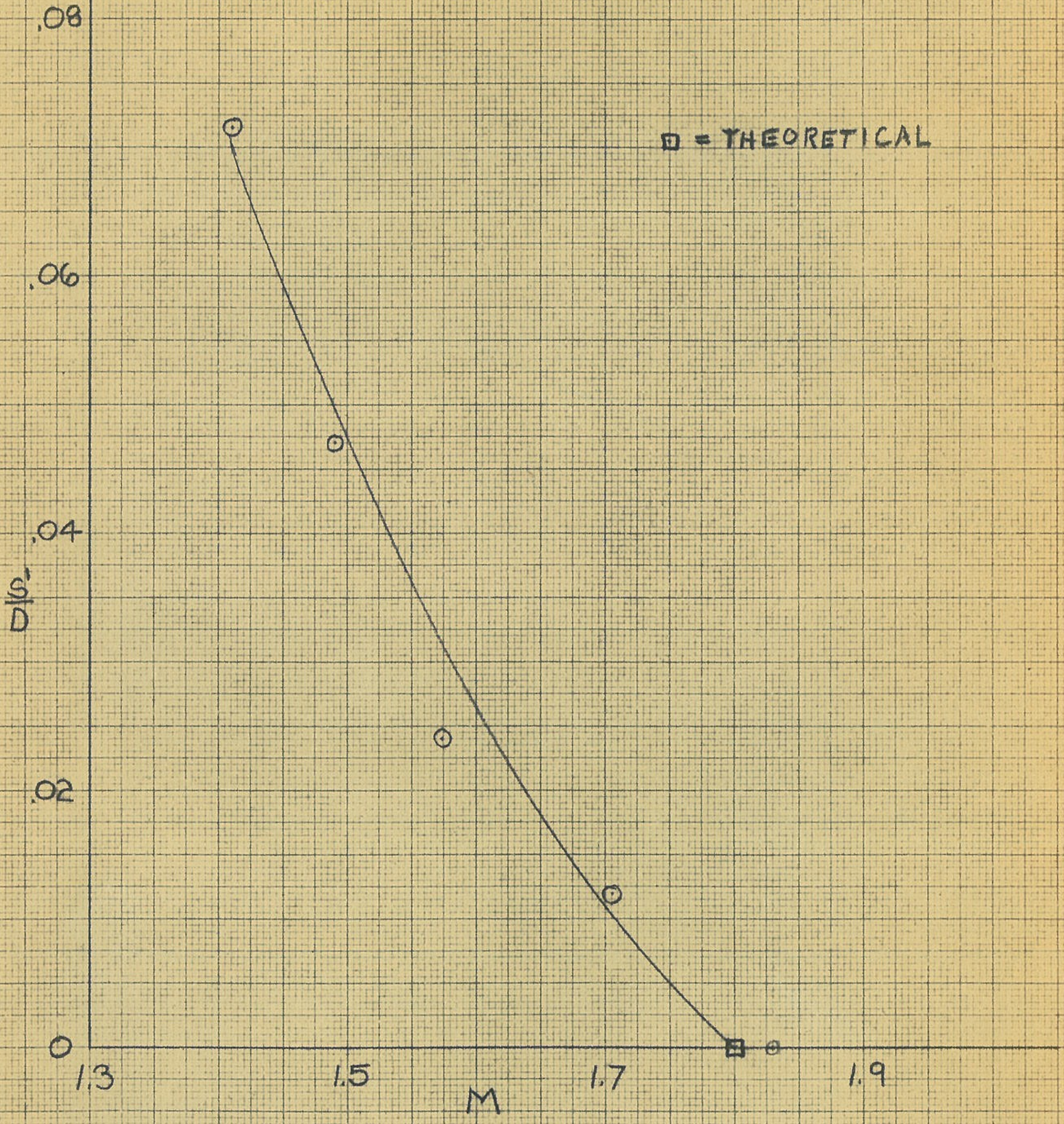

FIG. 60: DETACHED SHOCK WAVE DISTANCE
BLUNT CYLINDER

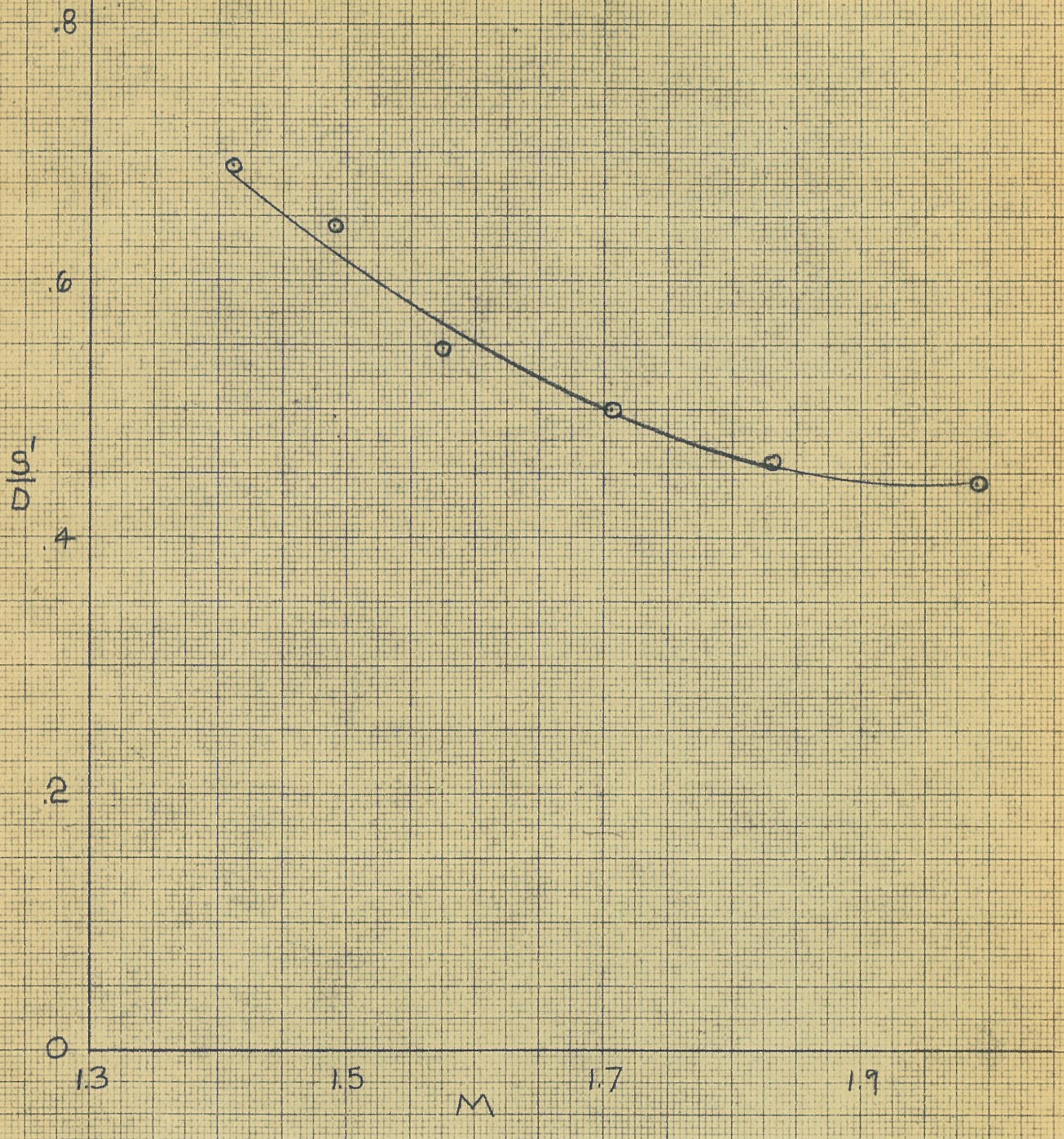

FIG. 61 LOCATION OF $M_2 = 1.00$

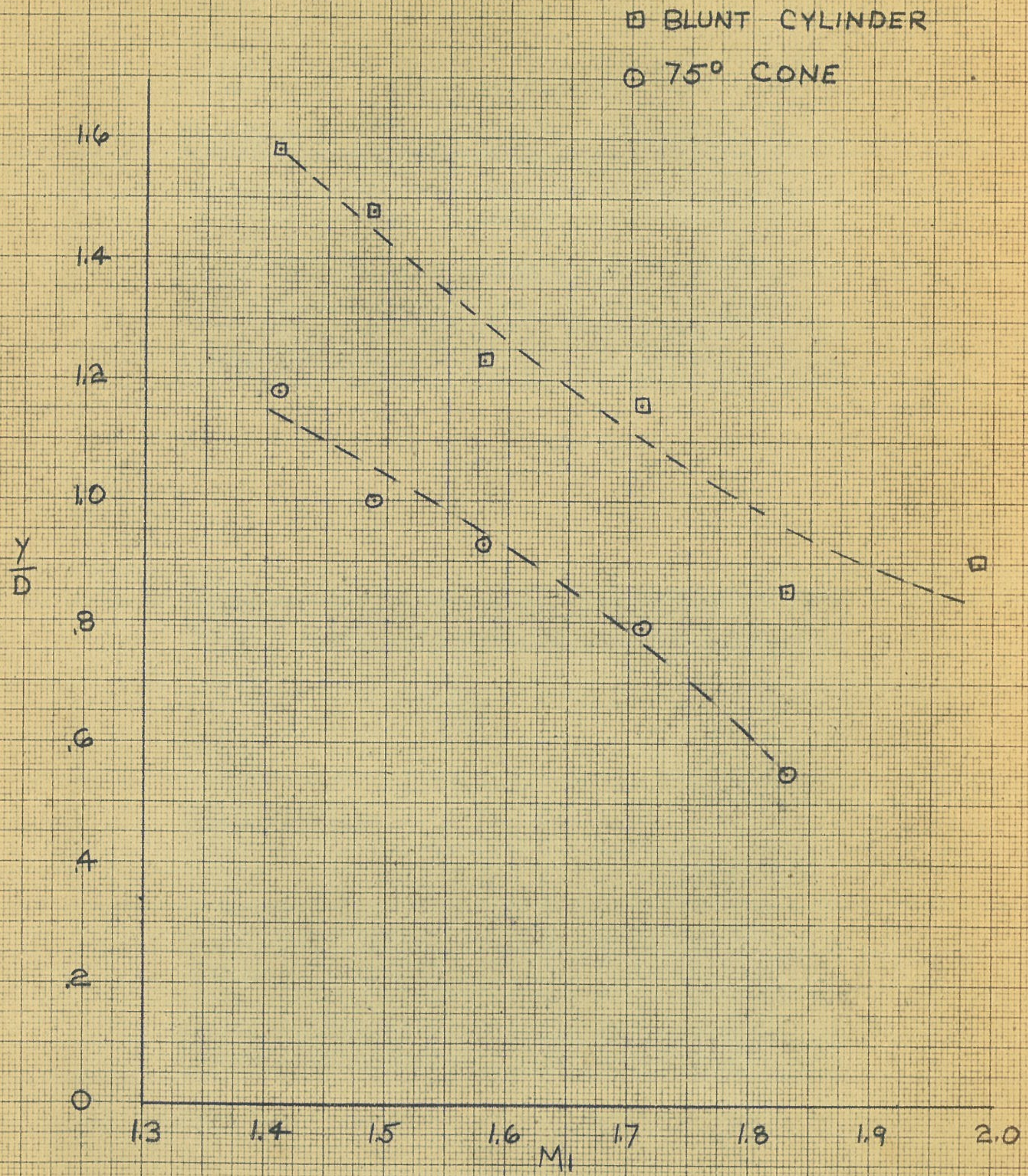

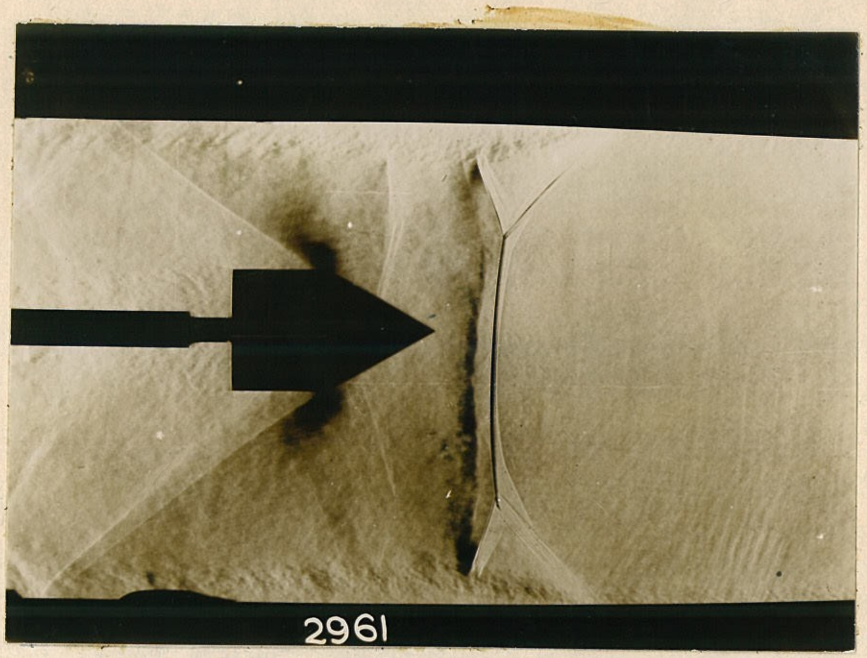

Fig. 62--Schlieren Picture of Flow Prior to Blocking at M = 1.58

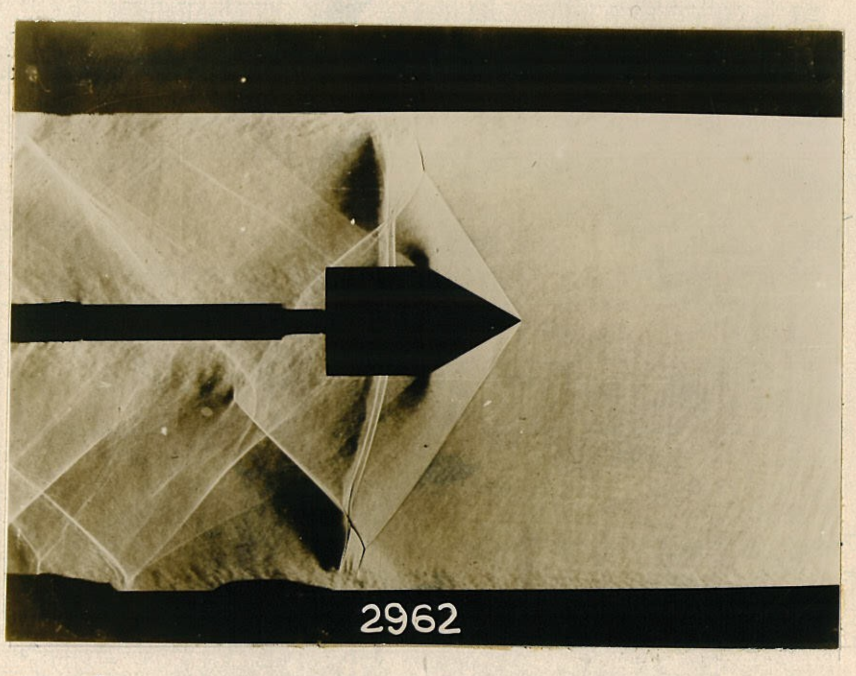

Fig. 63--Schlieren Picture of Flow with Blockage at M = 1.58

FIG. 64

TEST SECTION BLOCKING AREA
2 1/2" SUPERSONIC TUNNEL

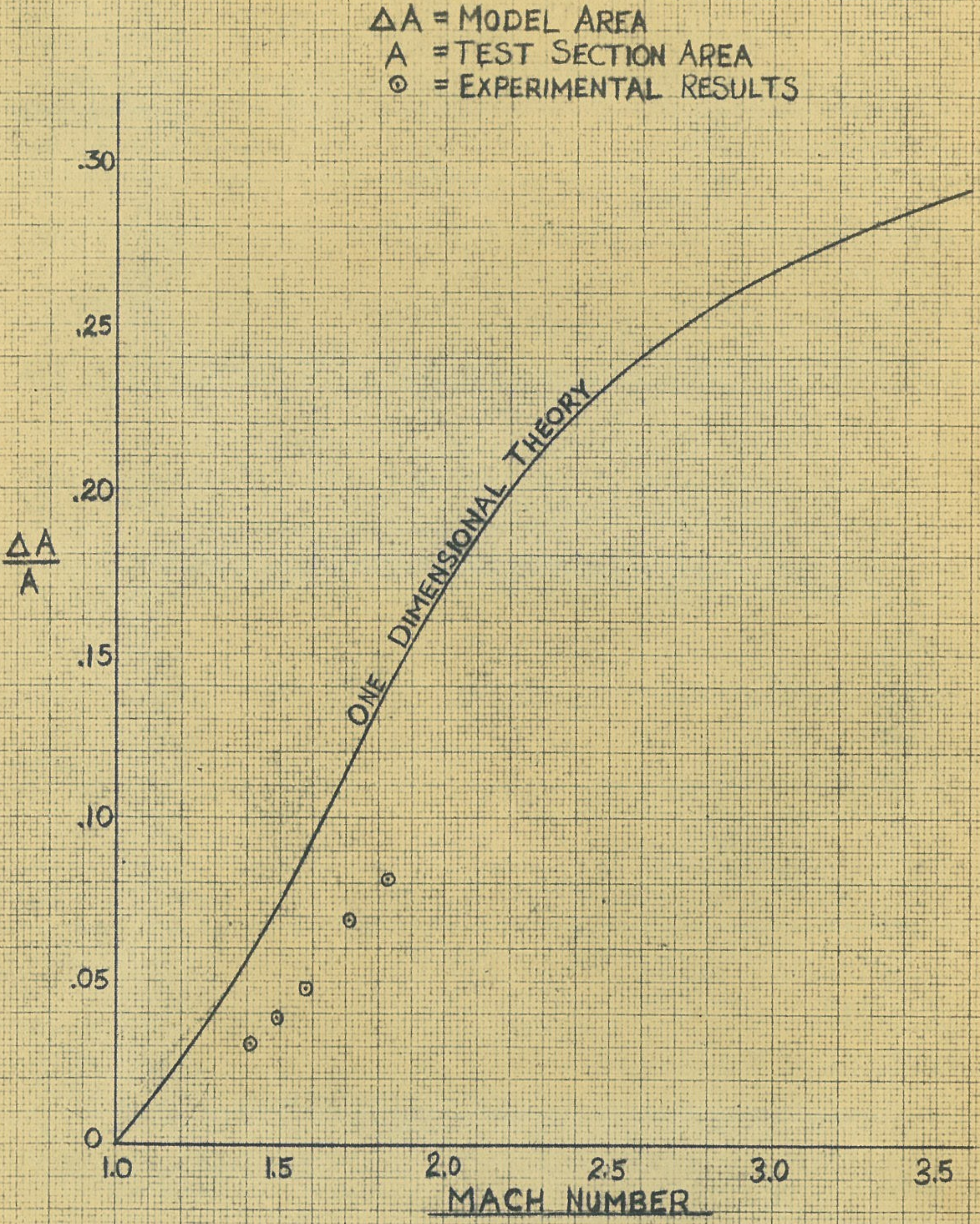

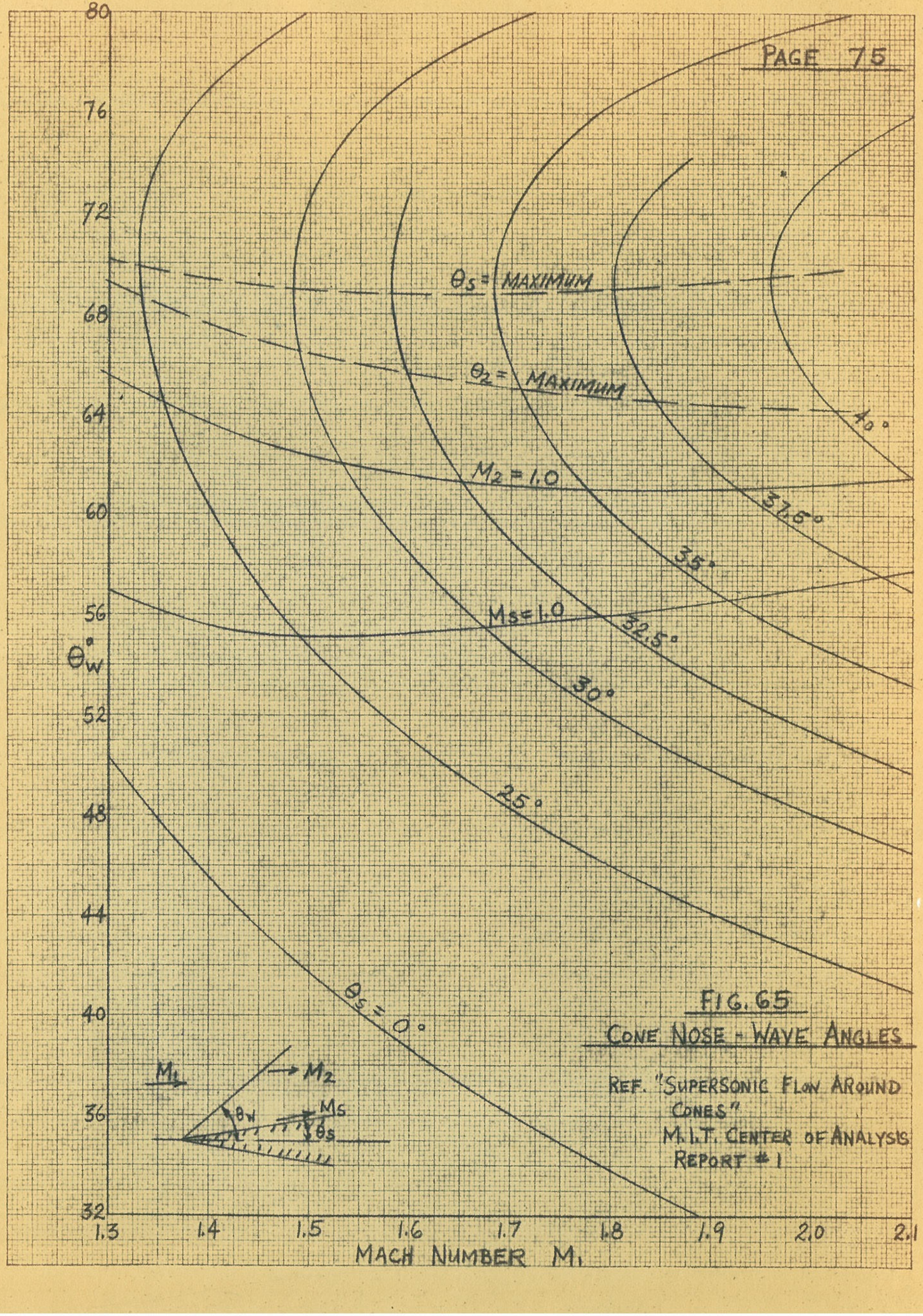

FIG. 65

CONE NOSE - WAVE ANGLES

REF. "SUPERSONIC FLOW AROUND CONES"
M.I.T. CENTER OF ANALYSIS
REPORT #1